Karlsruher Mineralogische und Geochemische Hefte
Schriftenreihe des Instituts für Mineralogie und Geochemie
30

Frédéric Pujol

Chemostratigraphy of some key European Frasnian-Famennian boundary sections (Germany, Poland, France)

universitätsverlag karlsruhe

Frédéric Pujol

Chemostratigraphy of some key European Frasnian-Famennian boundary sections (Germany, Poland, France)

Karlsruher Mineralogische und Geochemische Hefte

Schriftenreihe des Instituts für Mineralogie und Geochemie,

Universität Karlsruhe (TH)

Band 30

Chemostratigraphy of some key European Frasnian-Famennian boundary sections (Germany, Poland, France)

von
Frédéric Pujol

universitätsverlag karlsruhe

Dissertation, Universität Karlsruhe (TH),
Fakultät für Bauingenieur-, Geo- und Umweltwissenschaften, 2005
Referenten: Prof. Dr. D. Stüben, Prof. Dr. G. Racki

Anschrift des Autors:
Frédéric Pujol
140 route du polygone
67100 Strasbourg

Anschrift der Schriftleitung:
Karlsruher Mineralogische und Geochemische Hefte
Institut für Mineralogie und Geochemie
Universität Karlsruhe (TH)
D – 76128 Karlsruhe

Impressum

Universitätsverlag Karlsruhe
c/o Universitätsbibliothek
Straße am Forum 2
D-76131 Karlsruhe

www.uvka.de

ISSN 1618-2677
ISBN 3-937300-89-9

Chemostratigraphy of some key European Frasnian-Famennian boundary sections (Germany, Poland, France)

Zur Erlangung des akademischen Grades eines

DOKTORS DER NATURWISSENSCHAFTEN

von der Fakultät für

Bauingenieur-, Geo- und Umweltwissenschaften
der Universität Fridericiana zu Karlsruhe (TH)

genehmigte

DISSERTATION

von

Res. Ing. Pujol Frédéric

aus Orthez (Frankreich)

2005

Tag der mündlichen Prüfung:	13 Juli
Hauptreferent:	Prof. Dr. D. Stüben
Korreferent:	Prof. Dr. G. Racki

Zusammenfassung

Die vorliegende Arbeit untersucht unter Anwendung multipler geochemischer Indikatoren die globalen Umweltveränderungen während der Frasne/Famenne-Grenze (Kellwasser Bioevent).

Die Untersuchung ausgewählter europäischer Profile der Frasne/Famenne-Grenze (Coumiac und la Serre, Montagne Noire, Frankreich; Steinbruch Schmidt/Branau und Büdesheimer Bach/Prümer Mulde, Deutschland; Kowala Profil, Holy Cross Mountains, Polen) erbrachte neue geochemische Hinweise für tektono-magmatische Prozesse wie Vulkanismus und hydrothermale Aktivität, die eine maßgebliche Rolle während der Ablagerung der Kellwasser-Horizonte zwischen der südlichen Küste von Laurussia und dem nördlichen Gondwana gespielt haben. Der hier angewandte geochemische Multi-Indikator Ansatz offenbart zum ersten einen relativen Meeresspiegelsanstieg gekoppelt mit verstärktem Nährstoff-Eintrag, zum zweiten eine Zunahme der magmatischen Aktivität (angedeutet durch eine Zunahme von hydrothermalem und vulkanischem Einfluss), und zum dritten die generelle Entwicklung eines sauerstoffarmen Milieus während der Ablagerung der Kellwasser-Horizonte. Unter den Änderungen der Umweltbedingungen, die zu einer Veränderung der Geochemie in den Kellwasser-Horizonten führten, scheint der schnelle Anstieg des Meeresspiegels der wichtigste Parameter zu sein. Allerdings muss zwischen langfristigen (wie der halb-geschlossenen Struktur der Paläothetys im Späten Devon) und kurzfristigen Prozessen unterschieden werden.

Desweiteren zeigen die Ergebnisse, dass konventionelle Indikatoren wie der Gehalt natürlichen organischen Materials oder der Sauerstoffgehalt des Bodenwassers nicht immer hilfreich sind die Kellwasser-Horizonte zu identifizieren. Darüber hinaus offenbaren einige verbreitet eingesetzte Indikatoren wie etwa die Verhältnisse V/Cr und Ni/Co, dass sie nicht immer repräsentative Paläoumwelt-Parameter darstellen. Der in dieser Arbeit angewandte geochemische Multiparameter-Ansatz ermöglicht es, verlässlichere Schlussfolgerungen bezüglich der Paläo-Umweltbedingungen zu ziehen, da er zwischen verschiedenen Prozessen unterscheiden kann. Letzendlich muss die beobachtete Anreicherung von Metallen, Nährstoffen und die Abnahme des gelösten Sauerstoffgehalts verbunden mit einer erhöhten bakteriellen Aktivität während der Ablagerung der Kellwasser-Horizonte, eine entscheidende

Rolle für die große biotische Krise (Massenaussterben) während des Frasne-Famenne Übergangs gespielt haben.

Parallel zu diesem klassischen Ansatz wurden die Veränderungen der Spurenelementkonzentrationen in authigenen Pyriten entlang des Profils Büdesheimer Bach aufgenommen, um deren ergänzende Aussagekraft für das jeweilige Ablagerungsmilieu zu prüfen.

Diese Methode erwies sich für die Frasne/Famenne-Grenze in den untersuchten Profilen als kaum anwendbar. Die Hauptursache dafür war das Fehlen von geeigneten Frasne/Famenne-Profilen mit langandauernden sauerstoffarmen Bedingungen, die eine ausreichend hohe Auflösung der Probennahme von authigenen Pyriten ergeben hätte, um eine detaillierte vergleichende Untersuchung hinsichtlich des Gehalts an Spurenelementen in Pyrit zuzulassen.

Dennoch betonen die Ergebnisse, dass Studien an Pyriten umsichtig zwischen den verschiedenen Mechanismen der Pyrit-Genese unterscheiden müssen, um relevante Informationen über die Paläo-Umweltbedingungen zu bekommen. Der Gehalt an Elementen wie Ni, Co oder Cu in Pyriten kann nützlich sein, um den Bildungsmechanismus der Pyrite und die Natur des Ausgangsmaterials bestimmen zu können.
Nach dem Entfernen von epigenetischen Pyriten und solchen, die durch Pyritisierung von organischen Resten gebildet wurden, besteht ein positiver Zusammenhang zwischen As_{pyrite}, Cd_{pyrite} und DOP, was mit früheren Arbeiten überstimmt (Huerta-Diaz and Morse, 1992; Sternbeck et al., 2000). In Anbetracht der geringen Zahl von Publikationen über den Spurenelementgehalt von Pyriten als ein Indikator für Änderungen der Redox-Bedingungen können die vorliegenden Ergebnisse für weitere Arbeiten auf diesem Gebiet hilfreich sein.

Abstract

This study aimed to put constraints on regional and/or global environmental changes, which took place during the Frasnian-Famennian transition by using a geochemical multiproxy approach.

The investigation of several key European Frasnian-Famennian boundary sections (Coumiac and la Serre, Montagne Noire, France; Steinbruch Schmidt/Branau, the drilling Büdesheimer Bach/Prümer Mulde, Germany; Kowala Section, Holy Cross Mountains, Poland) brings new geochemical evidences which emphasize the role of tectono-magmatic processes, like volcanism, hydrothermalism and major tectonic movements in the development of the particularities of the Kellwasser Horizons deposited close to the southern shores of Laurussia and the northern parts of Gondwana. The adopted geochemical multiproxy approach revealed a relative sea-level rise coupled with higher nutrient input, the intensification of magmatic activity (as indicated by increased hydrothermal and volcanic influence) as well as the development of a generally more oxygen deficient depositional environment during the deposition of the Kellwasser Horizons. Among the environmental changes at the origin of the geochemical variations recorded in the Kellwasser Horizons, the rapid sea-level fluctuation seems to be the most important parameter. Indeed, long-term (like the semi-closed configuration of the Paleotethys in the late Devonian) and short-term processes must be distinguished.

The results also show that conventionally used indicators like the organic matter content or the oxygenation level of bottom waters does not have always-diagnostic values for recognizing the Kellwasser Horizons. Moreover, some of the proxies, like the V/Cr and Ni/Co ratios, turned out to be not representative in the Kellwasser Horizons for the environmental conditions to which they are generally associated. By its ability to discern among different processes, a multiparametric geochemical approach, as used in the present study, allows to draw more reliable paleo-environmental conclusions.

Finally the observed enrichment in metals, in nutrients and the lowering of the oxygen level in the seawater during the deposition of the Kellwasser Horizons, coupled with an enhanced bacterial activity, must have played a decisive role in the major biotic crisis occurring at the Frasnian – Famennian transition.

In parallel to this classical approach, the trace element contents in authigenic pyrites along the Büdesheimer Bach core were recorded in order to test the capability of this method as a source for supplementary information on depositional conditions.

This method proved to be hardly applicable in the sections studied. The main reason was the lack of appropriate Frasnian-Famennian sections with continuous and long lasting anoxic conditions, which would have yielded a sufficiently high sampling resolution of authigenic pyrites to permit a detailed comparative study in terms of trace element contents in pyrite.

However, the results of this work emphasize that studies on pyrite geochemistry, including such on isotope composition of sulphur, should cautiously discriminate among pyrites formed at different sites and different mechanisms in order to obtain reliable paleoenvironmental information. The content of elements like Ni, Co or Cu in pyrites may be a useful tool to identify the mechanism of pyrite formation and the nature of its precursor. After eliminating epigenetic pyrites and those formed by pyritization of organic rests, there is a positive correlation between As_{pyrite}, Cd_{pyrite} and DOP, which is in agreement with previous works (Huerta-Diaz and Morse, 1992; Sternbeck et al., 2000). The importance of this study also includes, its contribution to the small number of existing publications dealing with the potential of trace element pattern of pyrite as an indicator of depositional environments.

Résumé

Ce travail a pour objectif la recherche de possibles variations environmentales communes aux Horizons Kellwasser déposés au Sud du continent Laurussia et au Nord du continent Gondwana à l'aide de multiples indicateurs géochimiques.

L'étude de plusieurs profils de la limite Frasnien/Famennien d'Europe (Coumiac et la Serre, Montagne Noire, France; Steinbruch Schmidt/Branau, Büdesheimer Bach/Prümer Mulde, Allemagne; Kowala, Montagne de la Sainte-Croix, Pologne) apporte de nouvelles données géochimiques soulignant le rôle des processus tectoniques et magmatiques, comme le volcanisme, l'hydrothermalisme dans le développement des particularités des Horizons Kellwasser déposés au Sud du continent Laurussia et au Nord du continent Gondwana. L'approche à partir de multiples indicateurs géochimiques adoptée dans cette étude a révélé en effet une augmentation du niveau marin couplée avec un apport plus important en nutriments, une intensification de l'activité magmatiques (indiquée par une augmentation de l'influence hydrothermal et volcanique dans l'enregistrement sédimentaire), ainsi que le développement d'un environment de dépôt généralement appauvri en oxygéne durant la sédimentation des horizons Kellwasser. Parmis les changements environmentaux à l'origine des variations géochimiques observées dans les Horizons Kellwasser, les fluctuations rapides du niveau marin semblent être le paramètre le plus important. En ce sens les processus à long terme, comme la configuration semi-close de l 'océan Paléotéthys, et les processus à cours terme doivent être différenciés.

Les résultats obtenus montrent également que les marqueurs communément utilisés pour la reconnaissance des Horizons Kellwasser, tel que la teneur en matière organique, ne présentent pas toujours des valeurs caractéristiques. De plus, les variations de certains indicateurs, comme les rapports V/Cr et Ni/Co, se sont avérés ne pas être représentatifs des facteurs environmentaux leur étant généralement associés dans les Horizons Kellwasser. Ceci souligne l'intérêt de l'utilisation pour un même facteur environmental de plusieurs indicateurs dans le but d'éviter les erreurs d'interprétation. Finalement l'enrichissement observé en métaux, en nutriments ainsi que la diminution du niveau d'oxygène dans l'eau de mer durant la déposition des Horizons Kellwasser, couplé à une augmentation de l'activité bactérienne, doit avoir joué un rôle décisif dans la crise biologique de la limite Franien-Famennien.

En parallèle à cette approche classique, les teneurs en éléments traces ont été mesurées dans des pyrites authigènes le long du profil de Büdesheimer Bach dans le but de tester la capacité de cette méthode comme source d'informations supplémentaires sur les conditions de dépôt.

Cette méthode s'est avérée être rarement applicable pour la limite Frasnien/Famennien des profils étudiés.

Cependant les résultats obtenus ont mis en évidence la nécessité pour les scientifiques travaillant sur les pyrites, comme pour la détermination des isotopes du soufre, de déterminer leurs sites et mécanismes de formation dans le but d'obtenir des informations paléo-environmentales. Les teneurs en Ni, Co et Cu de la pyrite peuvent être utile pour identifier les mécanismes de formation des pyrites ainsi que leurs précurseurs.

Aprés discriminition des pyrites épigénétiques ainsi que des pyrites formées par la pyritisation de restes organiques, la corrélation positive observée entre As_{pyrite}, Cd_{pyrite} et DOP concorde avec les travaux précédents (Huerta-Diaz et Morse, 1992; Sternbeck et al., 2000). De plus, du fait du nombre relativement restreint des publications traitant de ce sujet, les résultats obtenus seront également utiles aux scientifiques travaillant sur l'utilisation de la teneur en éléments traces dans les pyrites comme indicateur de modification des conditions redox.

Acknowledgements

I am grateful to my supervisor Prof. Dr.Stüben, for giving me the opportunity to do this Ph.D study at Institut für Mineralogie und Geochemie, Universität Karlsruhe. Her experience of the subject, valuable guidance and suggestions were the key in improving the quality of this research. I am thankful to her for providing me all the necessary facilities for geochemical and mineralogical investigations. I'm also particularly grateful to the other member of the project the Dr. Berner, who was completely involved in my Ph.D project, starting from the field works (together with Dr. T. Neumann) to finally its completion. I am thankful to Prof. Dr. Grzegorz Racki of the Department of Earth Sciences, Silesian University, Poland, for accepting to be my 2nd examiner and providing some of his valuable time to review my work. This work was funded by the Deutsche Forschungsgemeinschaft (Project Stu 169/24) within a priority research program on the evolution of the Earth during the late Paleozoic (SPP 1054), coordinated by W. Buggisch. The authors benefited from the multi-faceted and magnanimous help of several colleagues, including extensive discussions with T. Algeo, R. Feist, Ch. Hartkopf-Fröder, M. Joachimski, U. Kramar, T. Neumann, E. Schindler and N. Tribovillard. I would like also to thank Rolf Simon and Suzanna Staub from the ANKA (Karlsruhe) for their help and the beam time they granted us. Technical and analytical assistance was accorded by the staff of the Institute of Mineralogy and Geochemistry, Universität Karlsruhe, Germany, including U. Kramar, C. Nikoloski, C. Mössner, G. Preuss and P. Zrinjscak. I express my gratitude to all of them. I am also thankful to Volker Zibat from the Laboratory of Electron Microscopy at the University of Karlsruhe for his help during the microprobe and SEM analysis. Mrs Bender and Nitz are warmly acknowledged for their administrative support all along my Phd. The moral and scientific support from my colleagues and friends (Bibhash, Frank, Habtamu, Nabil, Priyadarsi, Steffi) was also very helpful. Finally, I would like to thank my family and my fiancée, whose prayers and blessings always strengthened my confidence and make me capable to complete the work smoothly.

Table of contents

List of tables

List of figures

Lists of abbreviations

Ba*: Barium in excess

CDT: Canion Diablo Triolite

C_{org}: Organic carbon

CSA: Carbon Sulphur Analyser

CWA: Carbon Water Analyser

DOP: Degree of pyritization

DTMP: Degree of trace metal pyritization

ED-XRF: Energy Dispersive X-Ray fluorescence

EDAX: Energy Dispersive X-ray analysis

e.g.: For example (exempli gratia)

Fig.: Figure

F/F: Frasnian/Famennian boundary

GSSP: Global Stratotype Section and Point

ICP-MS: Inductively Coupled Plasma Mass Spectrometer

ICS: International Commission on Stratigraphy

i.e.: That is to say

IUGS: International Union of Geological Sciences

Ky: Kilo year

LKWH: Lower Kellwasser Horizon

My: Million years

P_2O_5*: Phosphate in excess

r: Correlation coefficient

tab.: Table

UKWH: Upper Kellwasser Horizon

XRD: X-Ray diffraction

XRF: X-Ray fluorescence

WD-XRF: Wavelength dispersive X-Ray fluorescence

wt.%: Percentage of weight

°C: Degree Celsius

I. Introduction

The Kellwasser (KW) bio-event occurring at the Frasnian/Famennian transition in the late Devonian (≈ 370 My) is one of the so-called "big five" mass extinctions in the earth history. In spite of the abundance of works related to this period, the ultimate cause or causes of this mass extinction is still a matter of debate.

To determine the paleoenvironmental changes, which took place during the Frasnian-Famennian transition, different strategies were applied, among which figures the use of geochemical proxies. This method provided some interesting clues concerning the processes at the origin of particularities recorded in the Kellwasser Horizons (Racki et al., 2002; Yudina et al., 2002; Riquier et al., in press). On the other hand, the recent depositional model of the late Devonian Appalachian basin (Sageman et al., 2003; Sageman and Lyons, 2004), based on a geochemical multiproxy approach, was never applied to European F/F boundary sections, especially at a regional scale. This method could, among other things, help to understand e.g., the cause of the two transgression pulses associated with the deposition of the Kellwasser Horizons (Buggisch, 1991), given that there is no general consensus to explain these rapid sea-level changes. Moreover the use of several proxies associated to the same paleoenvironmental factor, like anoxia, could allow by comparison either to strengthen or to question some interpretations. Finally by its ability to discern among different processes, a multiparametric geochemical approach, could allow to draw more reliable paleoenvironmental conclusions.

Therefore, in order to put constraints on possible causes responsible for the demise of the biota during the Frasnian-Famennian (F/F) transition, a geochemical multiproxy approach was chosen in this study to characterize the environmental changes with respect to detrital input, biogenic input, productivity, redox conditions, as well as hydrothermal and volcanic inputs.

For this study, several European Frasnian-Famennian key sections deposited in different paleogeographic settings were selected, including – in addition to the stratotype and parastratotype sections of Coumiac (Montagne Noire, France) and Steinbruch Schmidt/Branau (Germany), respectively, also some other sections thoroughly characterized by other authors (the drilling Büdesheimer Bach/Prümer Mulde, Germany; Kowala Section, Holy Cross Mountains, Poland; La Serre, France). Changes in the detrital flux along the

sections were evaluated on basis of both variations in mineral composition and in some diagnostic element ratios like Ti/Al. The biogenic flux was assessed as a function of the C_{org} content. The input of nutrients or the paleoproductivity was determined by the P_2O_5 and Ba in excess. The degree of anoxia during deposition was constrained by determining the concentration of redox sensitive metals (e.g., Fe, Mn) in the bulk sediment, specific element ratios (e.g., V/Cr), as well as the size of pyrite grains together with the degree of pyritization (DOP) in the Büdesheimer Bach core. The hydrothermal and volcanic influence in the sedimentary record was detected using e.g., the Al/(Al+Fe+Mn) and Zr/Al_2O_3 ratios.

In parallel to this classical approach, the trace element contents in authigenic pyrites along the Büdesheimer Bach section were recorded in order to test the capability of this method for paleoenvironment reconstruction.

Indeed in a recent study, the trace element contents of pyrite was used successfully as proxy for modifications of the redox conditions in Holocene sediments (Sternbeck et al., 2000). Moreover, as the elements with high degree of trace metal pyritization (like As, Mo) are built in pyrite completely, i.e. only as a function of their availability in the depositional environment (Huerta-Diaz and Morse, 1992; Stüben et al., 2002), relative changes in concentration of such elements in pyrite could provide some supplementary information on depositional conditions.

To achieve this goal, the degree of pyritization (DOP), the degree of trace metal pyritization (DTMP), trace elements contents in pyrites, sulphur isotopic composition (δ^{34}pyrite) as well as the pyrite morphology will be determined. Finally, the results of the paleoenvironmental study will be compared to the different pyrite parameters using Statistical tools.

II. The geochemistry of the Frasnian-Famennian transition for paleoenvironmental reconstruction

In the first place, we will present the state of the art concerning the investigated geological period, i.e. the Frasnian-Famennian transition in the Late Devonian. Then the sampling strategy will be explained and each sampled section will be presented. The different methods used for this multiproxy approach will be described shortly. Lastly, the results will be presented in terms of paleoenvironmental factors and their significance as indicator of the primary trigger of this extinction will be discussed.

1. The Frasnian/Famennian (F/F) boundary – a state of the art

In this chapter, we present the state of the art concerning the Frasnian-Famennian boundary in terms of stratigraphy, dating, paleogeographic reconstruction and hypotheses advanced to explain this major mass extinction in the earth history.

1.1. Stratigraphy

The Kellwasser (KW) bio-event is one of the so-called “big five” mass extinctions in the earth history, the other being the late Ordovician, the Permo-Trias boundary, the late Trias and the Cretaceous-Tertiary boundary.

The F/F stage boundary was defined by the Global Stratotype Section and Point (GSSP) in a section exposed near the Upper Coumiac quarry in the south-eastern Montagne Noire, France (Klapper et al., 1993), which was investigated in this study (see 2.4).

The numerical age of the F/F boundary vary in function of the authors between 364 My and 376.5 My (Tucker et al., 1998). According to Schindler (1990), the Kellwasser crisis covers one time interval from 1 to 2 My and the Upper Kellwasser Event 100 ky.

In most of the sections, the KW Horizons (Lower and Upper) are lithologically recognizable by their dark color due to enrichment in organic matter. The boundary between Lower and Upper gigas conodont zone correspond to the top of the Lower KW Horizon (LKWH) and the limit between the linguiformis and triangularis conodont zone, defined as the F/F boundary, correspond to the top of the Upper KW Horizon (UKWH) (Ziegler and Sandberg, 1990).

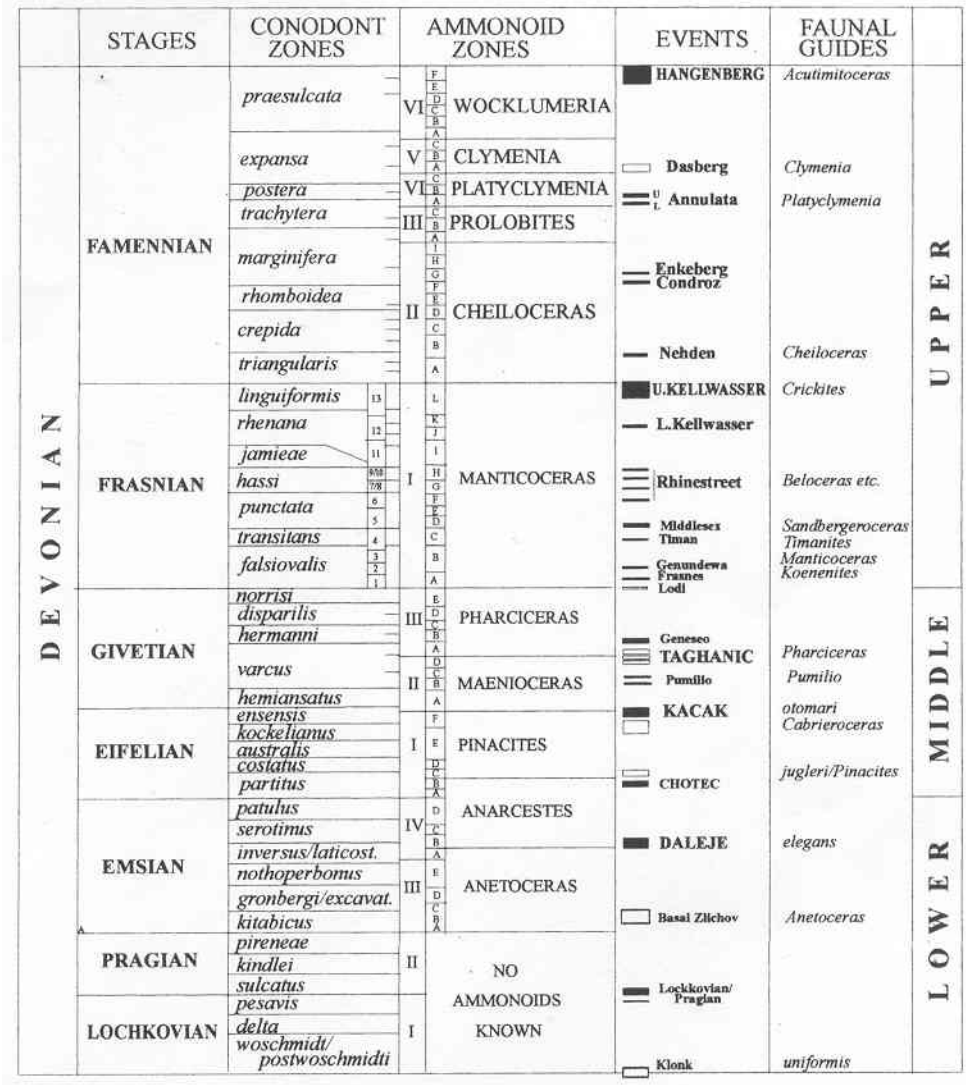

Figure 1. Diagram showing the main 'events' along the late Devonian. Black rectangles represent dysoxic or anoxic facies (House, 2002).

1.2. The Frasnian-Famennian bio-event

Several intermediary extinctions mark out the Devonian period (Hangenberg, Annulata, Enkeberg, Frasnes, Thaganic events: Fig. 1). These events have been detected by the

ammonoid evolution (House, 2002). The term of Kellwasser comes from the name of a Harz moutain valley in Germany where the interesting Horizons are well represented. During the Kellwasser Event a marine fauna change took place leading to the extinction of about 21% of the families, 50% of the genera and 75% of the species (Sepkoski, 1986). Based on this estimation, the Kellwasser event was defined as a major biotic crisis in 70s (McLaren, 1970).

The benthic fauna was hardly affected during the Frasnian-Famennian crisis and the changes are reported by Lethiers (1998). According to the author, in the reef communities about 80% of the coral genera extincted. 86% of the Brachiopods disappeared at the boundary. 80% of the benthic ostracods species vanished. The bryozoans were less affected and about 33% of the genera vanished with variations depending on the locations. The foraminifera were close to a total extinction. 18 out of 28 genera of the trilobites gradually extincted during the Frasnian (Buggisch, 1991) and out of 8 families still present at the end of the Frasnian only 3 survive in the Famennian (Lethiers, 1998).

The pelagic fauna was variously affected at the F/F boundary. Thus whereas the tentaculids, well represented in the Devonian, vanished at the boundary, the ammonoids e.g. showed important changes, but were more affected in the "Hangenberg" event at the Devonian-Carboniferous boundary (Fig. 1). The Conodonts diversity decreased strongly just before the F/F transition and about 90% of the Frasnian species vanished. The chitinozoans were at the end of their phylum. In the Montagne Noire, whereas absent in the upper Kellwasser Horizon, an exceptional abundance of a single chitinozoan species at the base of the Famennian was recognized (Paris et al., 1996). The entomozoids were not significantly affected and by contrary reach their acme in the Late Devonian.

Among the vertebrate, the agnathes vanished almost totally at the F/F boundary. The fishes like the placoderm or acanthodian, well represented in the Devonian, suffered high losses during the Kellwasser event, except those adapted to fresh water environment (McGhee, 1982). The first amphibian's tetrapods appearing at the end of the Devonian (Caroll, 1995) were not disturbed by the F/F crisis.

In the plant records, there is no indicator of a rapid extinction at the F/F boundary (Chaloner and Sheering, 1979). The Frasnian is marked by the appearance of the 30 m high progymnosperm *Archaeopteris*, which decline in the middle of the Famennian with the arrival

of the first seed plants (Beck, 1981). Apparently nothing interrupted the vascular plant evolution in the Devonian.

Similarly terrestrial arthropods were not affected by the biotic crisis.

In regard of the previous description the F/F biotic crisis seems to be restricted to the Marin realm.

1.3. Paleogeographical reconstruction

The paleogeographic configuration must be recognised as an important area of concern. It has been assumed for a while that the Paleo-Tethys Ocean was very wide in agreement with the paleomagnetic reconstruction. It is increasingly being recognised that this ocean was more a semi-closed basin to the east by the connection between the Laurussia and Gondwana continents (young et al., 2000), to the west by the Asiatic crustal fragments separating the Paleo-Tethys from the Panthalassa (or Paleo-Pacific ocean) and to the north by the Siberian and Kazakstanian blocks (Fig. 2).

We must bear in mind this very particular paleogeographic configuration, especially the shallow water depth passage between Laurussia and Gondwana, in a context of frequent sea-level oscillations. The opening of the Drake passage e.g., (about 37 My) is considered as the reason of the profound transition in climate-productivity pattern, i.e., a productivity maximal occurring during a presumably warmer period (Diester-Haass and Zahn, 1996).

The main convergent tectonic event occurring during the late Frasnian-Famennian time is the Eovariscan orogeny. The Ellesmerian Fold Belt in Artic Canada, the Antler orogeny in NW America, a part of the Appalachian orogeny, theVariscan belt in Europe and the Uralian belt result from this large-scale mountain building (Piqué et al., 1993; Tait et al., 1997; Murphy and Keppie, 1998; Matte, 2001; Peterhänsel and Pratt, 2001; Echarfaoui et al., 2002; Fig. 2). Continental uplift occurs in South America (Vicente, 1975) and in Australia (George et al., 2002; Fig. 2).

The main extensional tectonic event is the development of major rift systems that took place throughout Baltica and Siberia. The Dniepr-Donetsk-Pripyat system in the East European Craton (Fig. 2) went through the main phase of rifting on Baltica (Nikishin et al., 1996). Racki (1998) reviewed the tectonic, volcanic and hydrothermal activity at the F/F boundary.

There is growing evidence for important tectonic and volcanic activity during the F/F transition not only as mentioned before in the East European Craton (Nikishin et al., 1996; Wilson and Lyashkevitch, 1996, Fig. 1) but also in various domains of Eurasia (Veimarn et al., 1997). Other arguments can be brought like e.g., initiation of tectonic rifting (Bai et al., 1994; Wilson and Lyashkevitch, 1996), intensification of metallogenic processes (Chen and Gao, 1988; Turner, 1992; Veimarn et al., 1997; Racki, 1998), opening of major back arc basins (Sengör et al., 1998), intensive silicic exhalative volcanism and island arc volcanism (Racki and Cordey, 2000; Algeo, 1996) as well as massive generation of continental flood basalts (Pripyat-Dniepr-Donets, Wilson and Lyashkevitch, 1996; Fig. 2) and plume-influenced cratonic kimberlite and carbonatite emplacement (Kola Peninsula in the East European Craton, Kramm et al., 1993).

1.4. Possible causes and consequences

The ultimate cause or causes of this mass extinction is still a matter of debate. Some authors favored an impact or multiple impact hypothesis (McGhee, 2001), though no evidences were found in some of the sections (e.g., Steinbruch Schmidt, La Serre; McGhee et al., 1986; Girard et al., 1997).

Others postulated a general climatic cooling (Joachimski and Buggisch, 2002), though locally warm and humid conditions must have prevailed during the deposition of the KWH, as it was proposed for Steinbruch Schmidt (Devleeschouwer et al., 2002).

The onset of global anoxia is also often referred as the main trigger for the F/F mass extinction though no signs for anoxia was observed in many of the sections (Bratton et al., 1999; Copper, 2002; George and Chow, 2002).

Most of the authors emphasize the role of a general eutrophication of the oceans for which they give different explanations, like the evolution of vascular land plants (Algeo et al., 1995), installation of reducing conditions (Murphy et al., 2000), increased terrigenous supply (Girard et Lécuyer, 2002; Tribovillard et al., 2004), upwelling (Caplan et al., 1996; Giles et al., 2002) or a more intensive volcano-tectonic activity (Becker and House, 1994; Wilson and Lyashkevitch, 1996; Racki et al., 1998, 2000, 2002; Streel et al., 2000; Yudina et al., 2002; Ma and Bai, 2002; Tribovillard et al., 2004).

Sea-level fluctuations were also considered to have played a significant role in environmental changes (Johnson et al., 1985; Buggisch, 1991; Racki et al., 2002; Stephens and Sumner, 2003; Becker, 1993; Muchez, 1996; Streel et al., 2000; Devleeschouwer et al., 2002; Copper, 2002; Joachimski and Buggisch, 1993; George and Chow, 2002; Poty, 1999; Piecha, 2002).

Finally, some authors preferred a multi-causal scenario to explain the Kellwasser bio-event (Schindler, 1990; Lethiers et al., 1998, Lethiers and Casier, 1999; Racki, 1999b; House, 2002).

This aspect will be developed in the discussion part of the paleoenvironmental study. Two synthetic tables (tab. 1-2) were added in order to introduce the different hypotheses, their arguments in the literature as well as some contrary evidences.

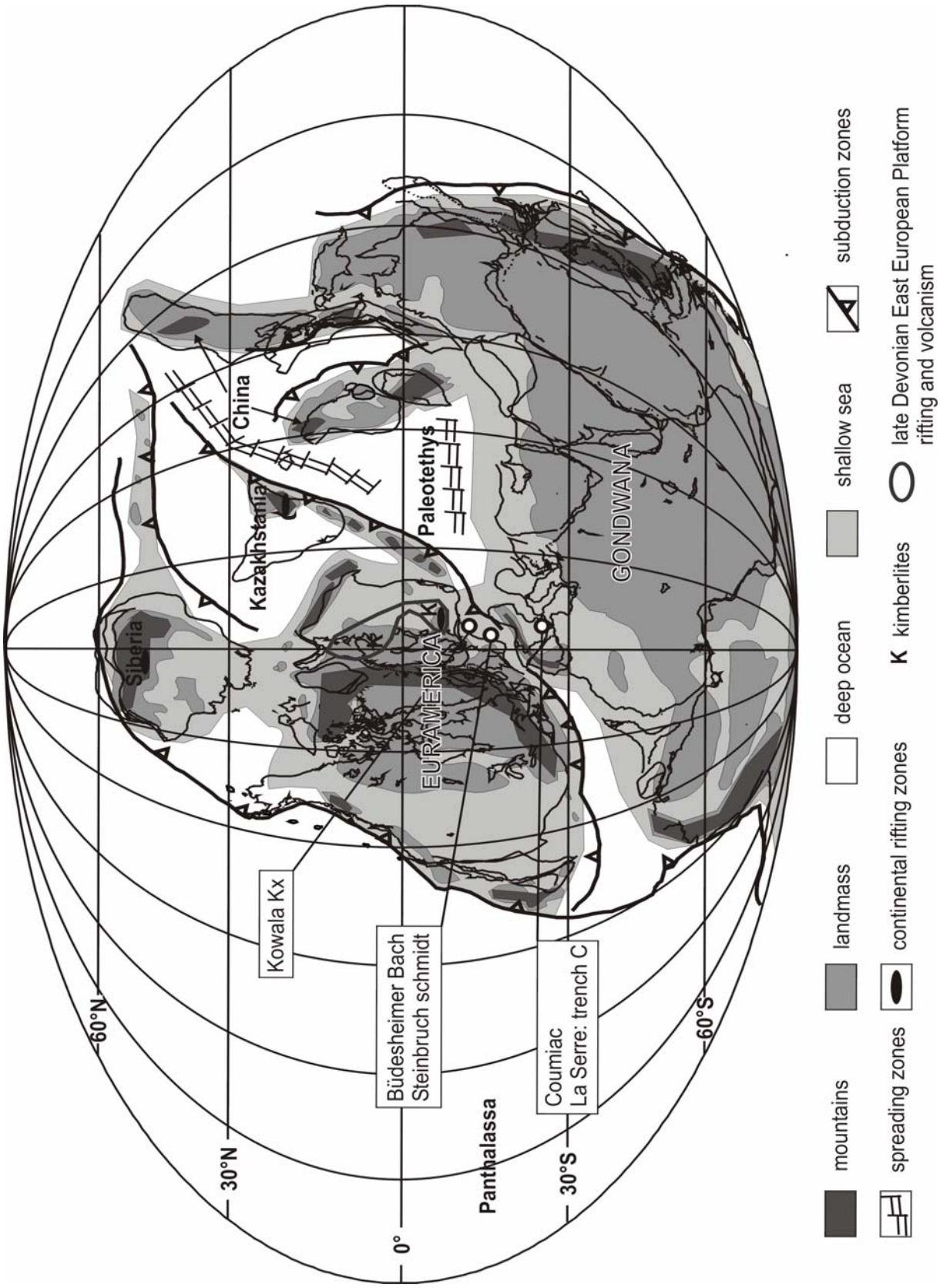

Figure 2. Paleogeographic reconstruction of the Upper Devonian (modified after Scotese and McKerrow, 1990 and Golonka et al., 1994) with the location of the investigated Frasnian/Famennian boundary sections, the location of spreading zones and continental rifting zones (Racki, 1998) as well as the location of the main areas of late Devonian rifting and associated volcanism of the East European Platform (Wilson and Lyashkevitch, 1996).

Causes	Arguments	Contrary evidences
Impact or extraterrestrial causes	**Wang et al., 1991**: Ir anomaly and breccia deposits South China sea. **Claeys and Casier, 1994:** Hony and Senzeille glass spherules (Belgium). **Over et al., 1997**: Ru:Ir and platinum enrichment (western New York State); no microtektites and shocked quartz. **Abbas et al., 1998**: carcinogenic and volcanogenic dark matter scenario. **Leitch and Vasisht, 1998**: sun´s encounters with spiral arms. **McGhee, 2001**: "multiple impact hypothesis". Potentials craters: Siljan (Sweden), Charlevoix (Quebec, Canada), Flynn Creek (**McGhee, 2001)**	**McGhee et al., 1986**: no evidence for a large-body impact (*Steinbruch Schmidt*), time gap: post dated F/F. **Girard et al., 1997**: no evidence (*La Serre, Coumiac*). **Morgan et al., 2004**: craters too small.
Climating cooling	**Caputo, 1985**: South America glaciation (Brazil) during the early Famennian **Stearn, 1987**: effect on Stromatoporoids. **Copper, 1986, 2002**: elimination of easterly tropical current. **Paris et al., 1996**: early Famennian +chitinozoan > lowering of ocean temperature (*La Serre*). **Streel et al., 2000**: early Famennian glaciation based on palynomorph analyses. **Joachimski and Buggisch, 2002**: positive O^{18} excursion in conodont apatite.	**Devleeschouwer et al., 2002:** Warm and humid condition during KWH, *Steinbruch Schmidt*.
Paleogeography	**Becker and House, 1994**: narrow seaways between the continents. **Young et al., 2000**: connexion Gondwana and Euramerica. **Copper, 2002**: compared to the closure of the Isthmus of Panama.	Paleomagnetic reconstruction
Anoxia	**Geldsetzer et al., 1987**: incursion of anoxic water (Medicine lake, Alberta, Canada). **Joachimski and Buggisch, 1993**: co-occurrences with sea-level fluctuations and global climatic changes. **Casier and Lethiers, 1998**: *Steinbruch Schmidt*, last 5cm of the UKWH under anoxic condition. **Joachimski et al., 2001**: *HCM* (Holy Cross Mountain, Poland) > anoxic from late Frasnian to early Famennian. **Ma and Bai, 2002**: probably anoxic event + hydrothermal activity responsible for the F/F biomass loss in South China. **Racki et al., 2002. Bond et al. , 2004.**	**Bratton et al., 1999**: Great basin, USA, anoxia predates the F/F boundary. **Copper, 2002**: do not explain terrestrial changes and the lack of anoxia in some sections. **George and Chow, 2002**: Canning basin, no anoxia at F/F.

Table 1. Synthetic table presenting the arguments advanced in the literature favouring an extraterrestrial cause, a climatic cooling, the paleogeopraphic configuration or the anoxia as the main trigger of the F/F crisis.

Causes		Arguments		Contrary evidences
Eutrophication	Land plant and continental input	**Algeo et al., 1995**: evolution of vascular land plants. **Girard and Lécuyer, 2002**: Ce of conodonts *HCM* > + terrigenous input. **Goddéris and Joachimski, 2004**. **Tribovillard et al., 2004**: enhanced influx of nutrients into the ocean due to the Eovariscan episode of uplift and the associated intense denudation of continental crust. **Chen et al., 2005.**	**Murphy, 2000**: late Devonian climatic cooling > increase seasonality > stratification and mixing water column. **Filipiak, 2002**: palynofacies in *HCM* > eutrophication of epeiric seas (probably diverse source of nutrients). **Whalen et al., 2002**: Alberta basin, Canada, microbial carbonates > environmental change > associated with maximum flooding and possibly maximum nutrification.	Lack of terrestrial large fossil forest Cannot explain short-term variations
	Upwelling	**Jewell, 1995**. **Caplan et al., 1996:** +phosphate+glauconite (Alberta, USA). **Giles et al., 2002:** Great basin USA, phosphatic microspherules > upwelling of P-rich oxygene depleted bottom water at the latest Frasnian.		
	volcanism and tectonic	**Becker and House, 1994**: volcanic degassing. **Wilson and Lyashkevitch, 1996**: Pripyat-Dnieper-Donets rift (Est European Platform) as potential causal factor. **Racki et al., 1998, 2000, 2002**: *HCM*, radiolarian and volcano-hydrothermal activity. **Racki, 1999a. Streel et al., 2000**: volcanism for warming UKWH. **Peterhänsel and Pratt, 2001**: bioerosion due to enhanced tectonically induced nutrient input. **Over, 2002**: central and eastern USA, regional basin tectonics. **Yudina et al., 2002**: tectono-volcanic phenomena in the incipiently closing Ural Ocean. **Geldsetzer et al., 1993. Hladil, 2002**: sliding or subsidence in Moravia, Czech republic. **Ma and Bai, 2002**: cf anoxia. **George and Chow, 2002**: Canning basin, tectonic active phase in the basin > stressful environment. **Mahmudy Gharaie et al., 2004 :** volcanism in Iran. **Morgan et al., 2004**: "Verneshot" event. **Tribovillard et al., 2004**: enhanced influx of nutrients into the ocean due to the Eovariscan episode of uplift and the associated intense denudation of continental crust. **Averbuch et al., 2005. Chen et al., 2005. Riquier et al (in press).**		**House, 2002:** no consistent evidence of volcanism or tectonism as a general cause of the late Devonian events.
Sea-level		**Buggisch, 1991**: autocyclic model. **Becker, 1993**: Anoxia and eustatic changes. **Joachimski and Buggisch, 1993. Muchez, 1996**: comparison of South China and Southern Belgium > KWH HST (highstand systems tract) and F/F LST (lowstand systems tract). **Poty, 1999**: extinction of upper Frasnian rugose corals due to rise of sea-level and cooling of the seawater. **Streel et al., 2000**: early Famennian regression. **Chen et al., 2002. Copper, 2002. Devleeschouwer et al., 2002:** *Steinbruch Schmidt*, KWH correspond to HST, sequence boundary located just above and are underlined by hardgrounds suggesting time gaps. **George and Chow., 2002. Piecha, 2002. Racki et al., 2002**: Poland, early Famennian eustatic fall. **Stephens and Sumner, 2003**: transgressive Canning basin (sea-level drop at early Famennian).		

Table 2. Synthetic table presenting the arguments advanced in the literature favouring the eutrophication or the sea-level changes as the main trigger of the F/F crisis.

2. Investigated sections

This chapter introduced the five Frasnian-Famennian boundary sections, which were selected in Germany, Poland and France for this study. In addition to the drilling core Büdesheimer Bach (Prümer Mulde, Germany), thoroughly investigated recently by an interdisciplinary research group of the priority program "Evolution of the earth system during the early Paleozoic by means of sedimentary geochemistry", the other sections included in the study were selected to have precisely documented macrofaunal stratigraphic record (the parastratotype of Steinbruch Schmidt, Germany and the stratotype of Coumiac, Montagne Noire, France), to be deposited in different paleogeographic settings (e.g., La Serre deposited in a deeper facies as compared to Coumiac) as well as to allow a comparison with the results of other geochemical investigations (the well studied section of Kowala, Poland).

2.1. Kowala (Kx section, Holy Cross Mountains, Poland)

F/F deposits are well exposed in the Kowala quarry in the southern Kielce region (Fig. 3-4). The well-known continuous sequence of the Checiny-Zbrza basin (Racki et al., 2002) was frequently sampled for various F/F studies (Joachimski et al., 2001). The Kowala section consists of black carbonaceous shales with intercalated carbonate beds (Fig. 3) deposited in a deep shelf facies. Four lithologic units were described (Vishnevkaya et al., 2002). The F/F boundary was localised by means of conodonts between the Palmatolepis linguiformis and triangularis zone, as well as based on the presence of a distinctive cherty bed (Racki et al., 2002)(Fig. 5).

The depletion of oxygen in seawater just after the F/F boundary is indicated in Kowala by Ce anomalies (Girard and Lécuyer, 2002). In their geochemical study on the basinal Kowala section, Joachimski et al. (2001) concluded that anoxic conditions must have prevailed during the late Frasnian and early Famennian. However, this is in contradiction with conclusions based on proxies like the V/Cr ratio (Racki et al., 2002). Additional geochemical investigations indicate a higher Zr/Al_2O_3 ratio near the F/F boundary not only at Kowala, but also in others sections of the south Polish-Morovian shelf basins, suggesting a higher eolian input of fine grained pyroclastic material (Racki et al., 2002).

Figure 3. Lithologs and samples position of the investigated sections. The conodont zones are according to Ziegler (1971) and Ziegler and Sandberg (1990). The Kowala log is modified after Racki et al. (2002), Büdesheimer Bach log modified after Joachimski et al. (2001), Steinbruch Schmidt log modified from Schindler (1990), Coumiac log modified after Becker and House (1994), La Serre log modified after Lethiers et al. (1998) (Bank numbers from Feist, 1990). The sample location is represented in the form of bank numbers or black dots. The question marks correspond to the uncertainties of the KWH equivalent position or the biostratigraphic limits. E: early; M: middle; L: late.

The same study documented also an increase in the biological productivity and in hydrothermal input during the Kellwasser event. Late Devonian volcanic activity was also pointed out in the Kowala 1 bore hole (Zakowa and Radlicz, 1990) and in some Moravian sections (Hladil, 2002). Magnetic susceptibility values indicate a transgressive trend at the end of the Frasnian followed by a regressive phase during the earliest Famennian (Racki et al., 2002). An early Famennian eustatic fall as well as an eutrophication and/or disturbance in the marine photic web close to the F/F boundary was postulated in a recent palynofacies study (Filipiak et al., 2002).

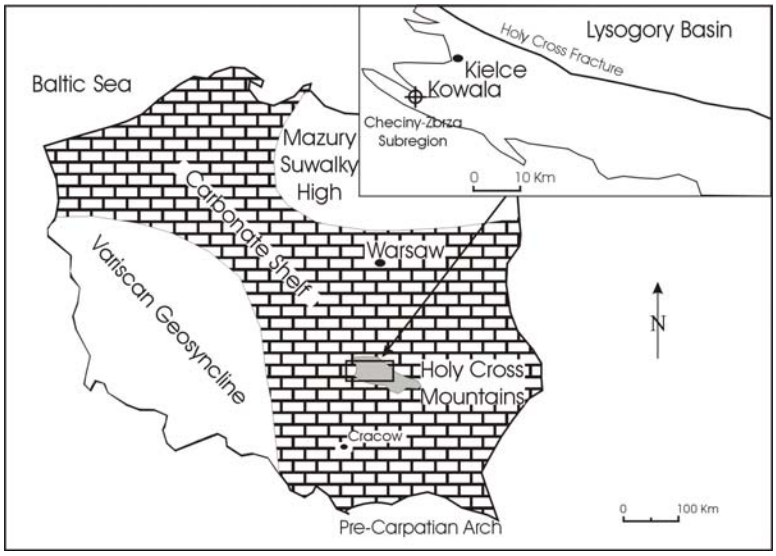

Figure 4. Location map of the Kowala section in Poland (modified after Racki et al., 2002).

Figure 5. Location of the Frasnian/Famennian boundary in the Kowala Kx section marked by the presence of a chert layer.

2.2. Büdesheimer Bach (Eifel Mountains, Germany)

The Büdesheimer Bach core (final depth 165 m, Fig. 6-7) was drilled at the northeastern edge of the Prüm syncline (Eifel Mountains, Fig. 6). The main stratigraphic units intercepted by the drilling are the Büdesheimer Goniatite Shales and the Ooser Plattenkalk Formation (Middle Adorfian to Nehdenian; Frasnian/Famennian) (Piecha, 1994). The section consists of gray to black coloured calcareous shales including turbiditic limestone beds (Fig. 3). Biostratigraphic dating is difficult because of the scarcity of conodonts in the limestone beds (Piecha, 1994). The twofold occurrence of the base of the late Rhenana zone (LKWH) is considered to be due to tectonic repetition as suggested by lithology and conodont association (Piecha, 1994). The presence of nektic and planktonic fauna and the lack of benthos suggest that the pyrite rich black shale parts were deposited in a euxinic bottom water environment. Bivalve fauna points to a shallow water depth (Piecha, 1994). The positive $\delta^{13}C_{carb}$ excursion during the "Kellwasser Horizons" is interpreted in terms of increased burial of organic matter (Joachimski et al., 2002). Based on the conodont color alteration index the sequence shows a thermal overprint at temperature below 100°C (Joachimski et al., 2002).

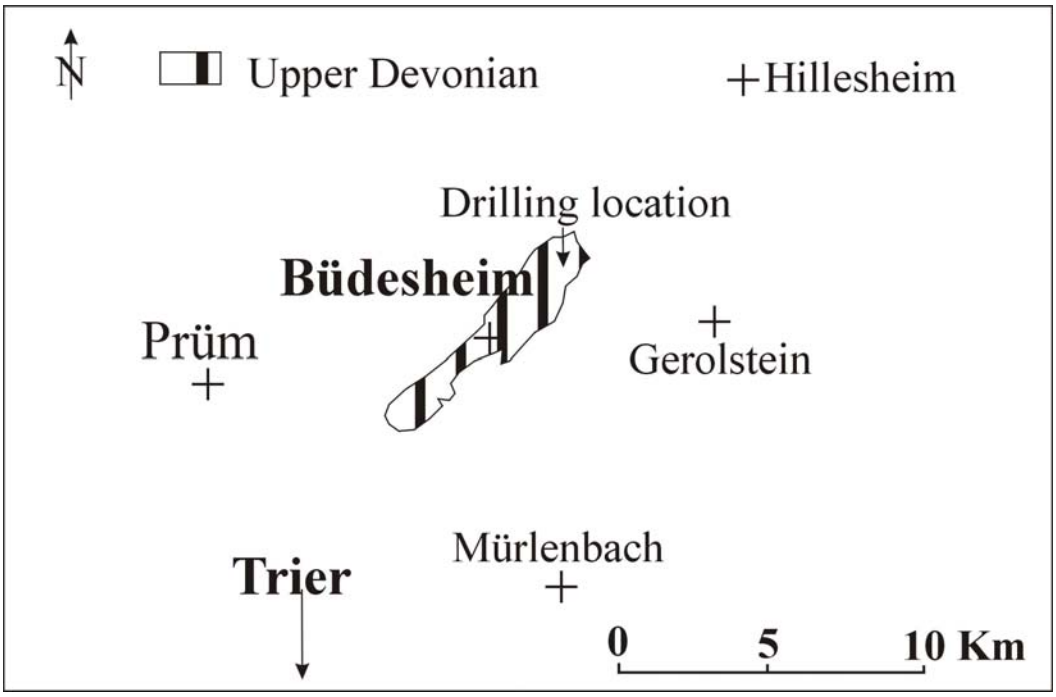

Figure 6. Location map of the Büdesheimer Bach core (modified after Piecha, 1994)

Figure 7. 4 meters core box of Büdesheimer Bach stored in the Senckenberg museum of Frankfurt.

2.3. Steinbruch Schmidt (Branau, Germany)

The quarry Schmidt is one of the best-examined sections, characterised by completeness and by exemplary development of the Kellwasser Horizons. The sequence in Steinbruch Schmidt was deposited on a submarine rise (Fig. 8), below the wave base level and consists of dark grey to black limestones (KWH, Fig. 3, 9, 10) intercalated within grey cephalopod limestones (Buggisch, 1991). The paleogeographic environment of the Rhenish Slate Mountains during the upper Devonian corresponds to a siliciclastic carbonate shelf, bordering the old red continent to the south. McGhee et al. (1986) carried out geochemical investigations aiming the identification of abnormal Ir concentrations, however, without success. Devleeschouwer et al. (2002) defined three main facies in this section, with the Kellwasser Horizons representing the basinal environment deposited at an inferred depth of up to 200 m and with the only presence of radiolarians. Magnetic susceptibility values (Devleeschouwer, 1999) clearly suggest variation in the detrital input into the ocean during the early Famennian. The authors interpreted the high kaolinite content at the F/F boundary as an indicator for hot and wet climatic conditions. Schindler (1990) interpreted the deposition of the black shales as a consequence of episodic rises of the anoxic layer. In contrast to a more generally accepted view (Buggisch, 1991; Schindler, 1990) according to which the whole UKWH was deposited under anoxic conditions, Casier and Lethiers (1998) considered only the last 5 cm of the UKWH as anoxic. The two positive carbon isotope excursions reported, also in other F/F boundary sections of central Europe (Joachimski and Buggisch, 1993) are interpreted to indicate an enhanced burial of organic carbon.

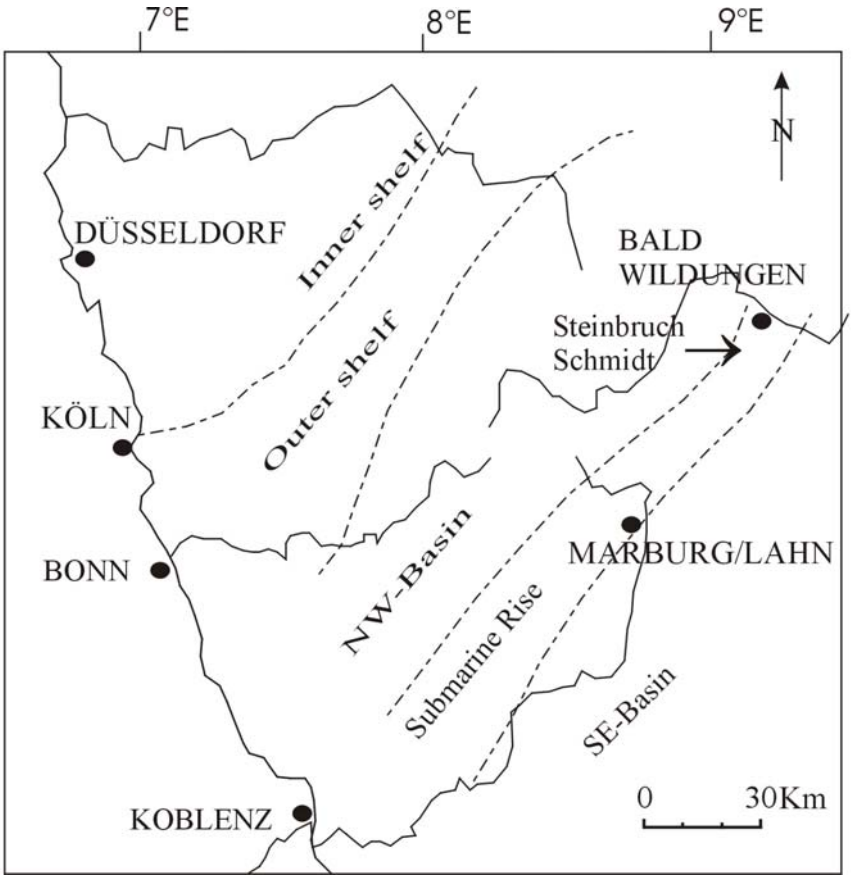

Figure 8. Location map of the Steinbruch Schmidt section (modified after Devleeschouwer et al., 2002).

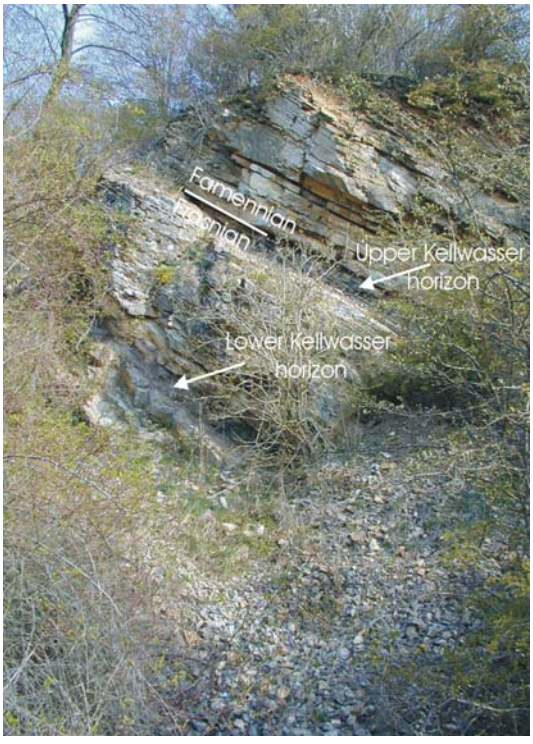

Figure 9. Location of the Frasnian/Famennian boundary and the two Kellwasser Horizons in the Steinbruch Schmidt section.

Figure 10. The lower Kellwasser Horizon with the position of the bank 20 (left) and the bank 26 (right).

2.4. **Coumiac and La Serre (Montagne Noire, southern France)**

The section above the Upper Coumiac quarry (Fig. 11, 12) was chosen in 1993 by the International Commission on Stratigraphy (ICS) and the International Union of Geological Sciences (IUGS) as the Global Stratotype Section and Point (GSSP). The decision was taken because of the exemplary documentation of the transition by means of macrofossil groups (Klapper et al., 1993). The section Coumiac consists of cephalopod and nodular limestones in which are intercalated the KWH, represented by mudstones and wackestones (Fig. 3, 13, 14). Dysaerobic conditions were assigned to the KWH due to faunal and colour changes (Schindler, 1990). Two positive carbon isotope excursions were reported in the vicinity of the KWH (Joachimski and Buggisch, 1993). The section is strongly affected by diagenetic alteration (Préat et al., 1999) so that much care was taken after sampling to extract appropriate material for geochemical investigations. The section La Serre Trench C is located in the stratotype area of the southeastern Montagne Noire (Fig. 11, 15). The Uppermost Frasnian in the La Serre trench C section consists of alternating dark, carbon-rich marlstones and argilites (Fig. 3, 16). Only the carbonate banks were sampled due to the strong superficial alteration of the argilite. La Serre is considered as a distal basinal time equivalent of the sections deposited on a submarine rise (e.g., Coumiac) (House et al., 1988). Because in the literature for this section the earlier standard zones (Ziegler, 1971) were used, whereas for the other sections we applied the revised standard correlation (Ziegler and Sandberg, 1990), we adopted the scheme of Klapper and Becker (1999) in order to allow a correlation with the LKWH. Because in this

comparison the top of the Upper *rhenana* zone is corresponding approximately to the top of the Lower *gigas* zone, the LKWH equivalent was placed hypothetically in the bank no. 9, reaching up to the beginning of bank 10 (bank numbers according to Feist, 1990; Schindler, 1990). The magnetosusceptibility event and cyclostratigraphy (MSEC) study by Crik et al. (2002) on the F/F boundary in different localities allowed reasonable correlations in using the La Serre trench C as reference sequence. No evidence for extraterrestrial impact remainders was found in the La Serre trench C section such as high Ir values, Ni-rich spinels or microtektites (Girard et al., 1997). Anoxic conditions prevailing at the F/F boundary and during the early Famennian were postulated based on the ostracod assemblage (Lethiers et al., 1998). Rapid paleoenvironmental changes were identified based on the variation in the concentration of different palynomorph groups (Paris et al., 1996), with the most remarkable being an exceptional abundance of a single chitinozoan species at the base of the Famennian. This anomaly was ascribed to a conjunction of several factors like higher productivity coupled with a presumed lowering of the ocean water temperature, restricted terrestrial input as well as the disappearance of predators or competitors (Paris et al., 1996).

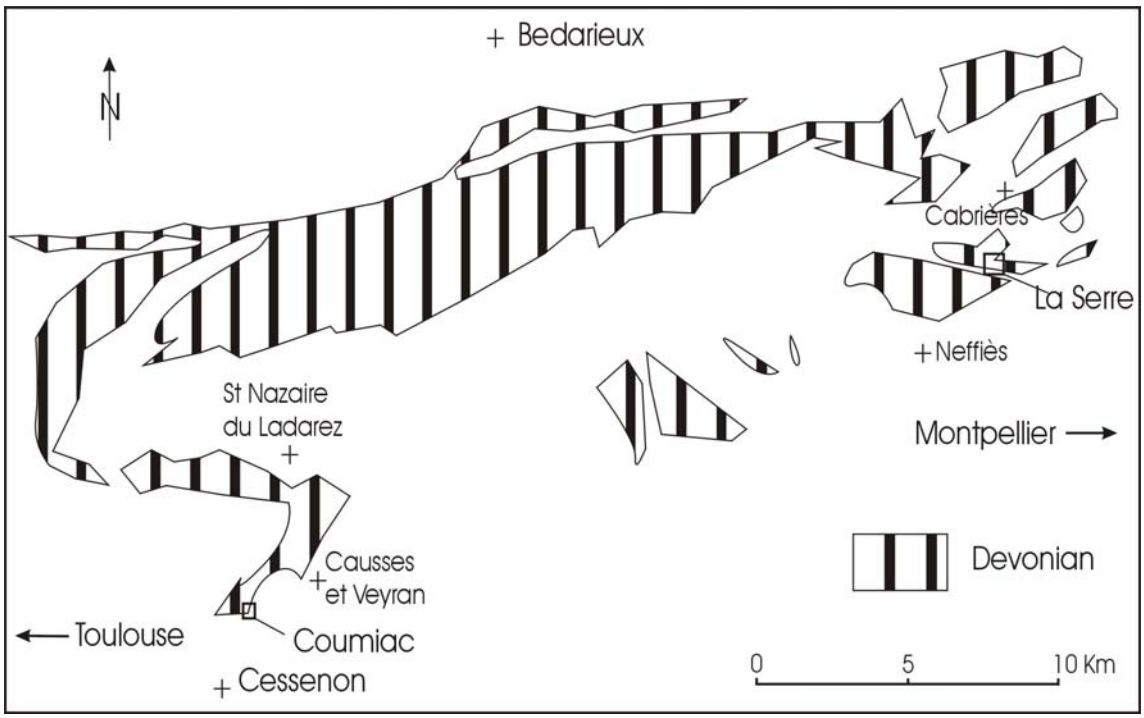

Figure 11. Location map of the Devonian of the Montagne Noire as well as Coumiac and La Serre (modified after House et al., 1985).

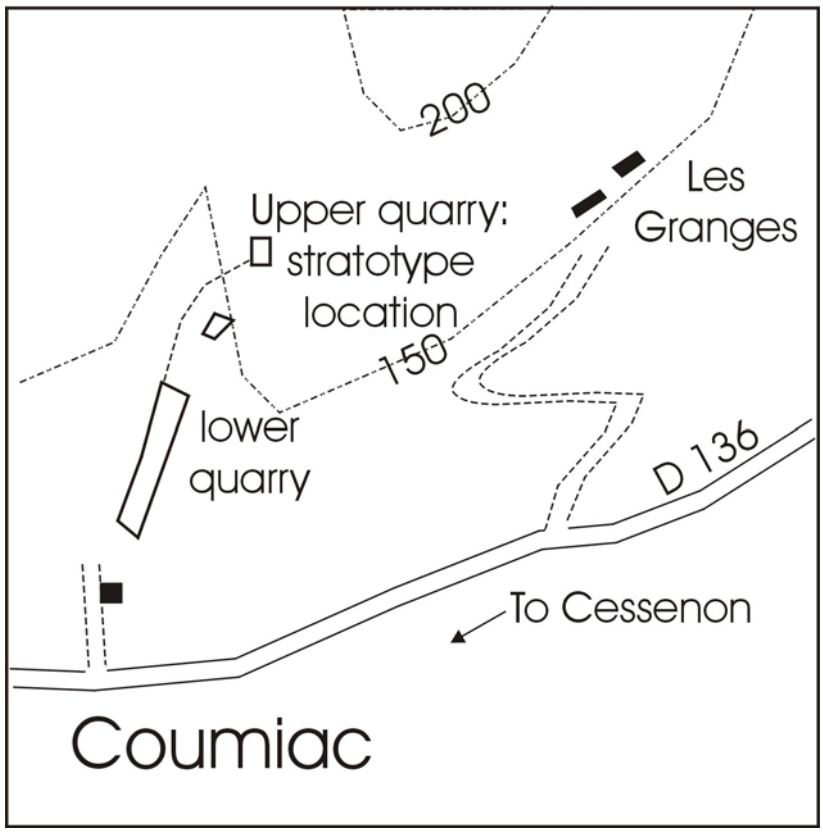

Figure 12. Location map of Coumiac (modified after House et al., 1985).

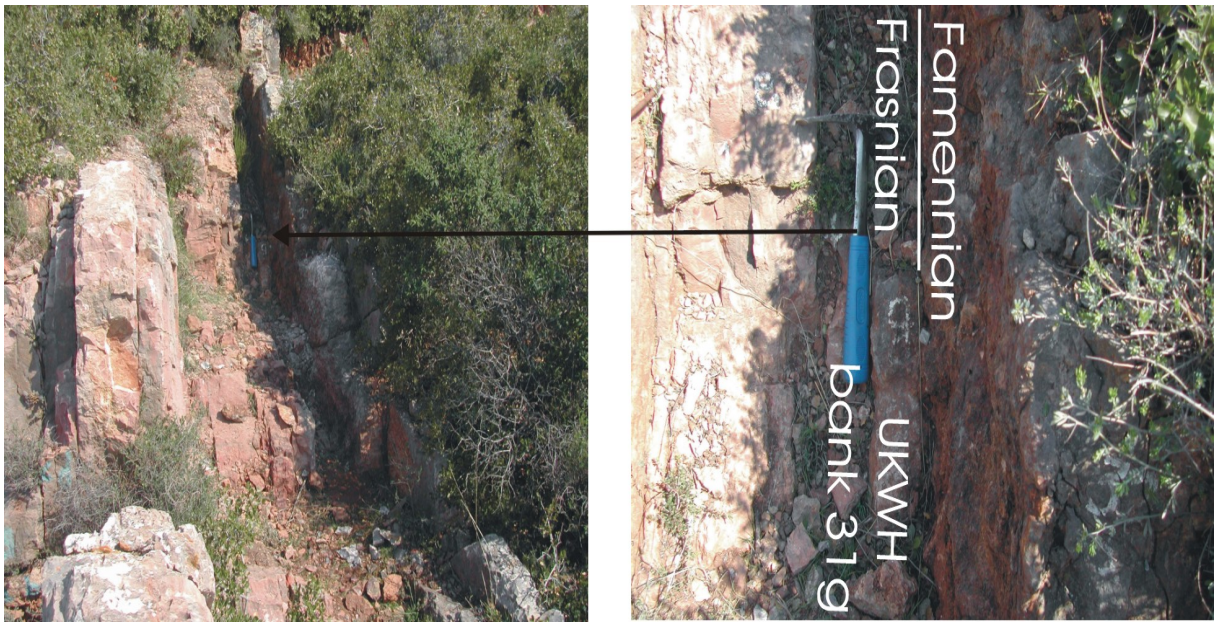

Figure 13. Location of the Frasnian/Famennian boundary and the Upper Kellwasser Horizon (Bank 31 g) in the Coumiac section (Stratotype).

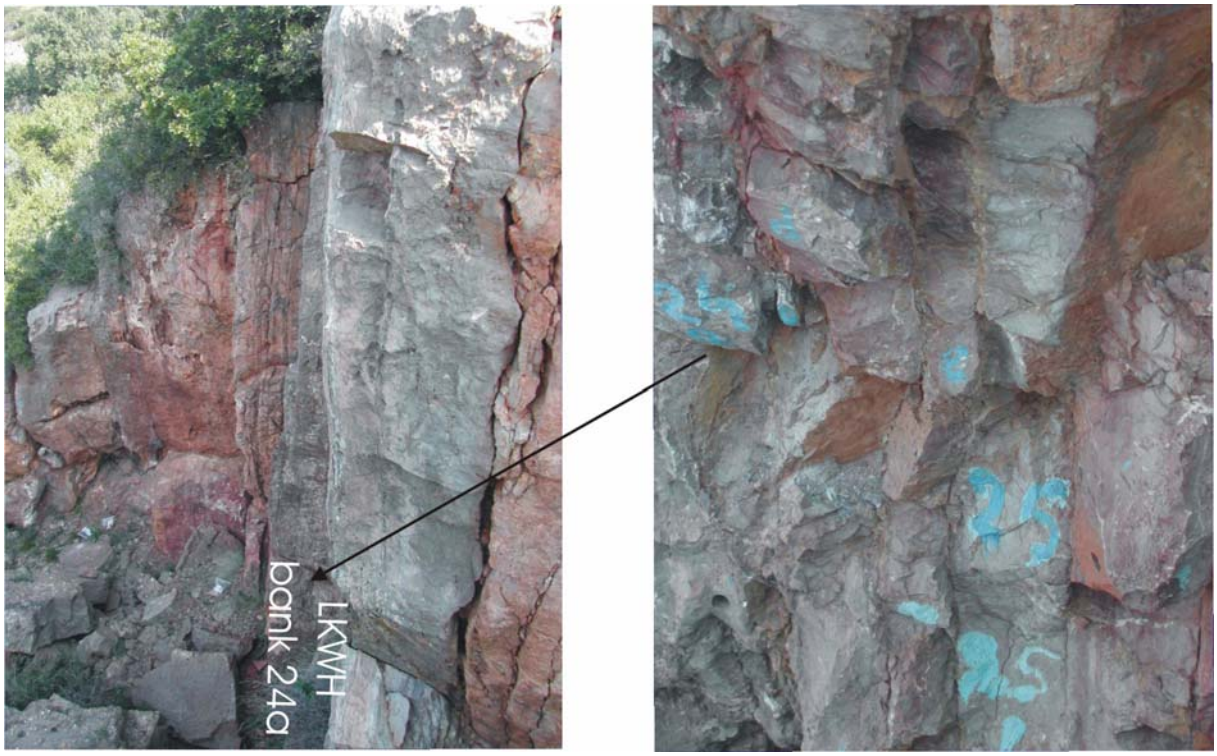

Figure 14. Location of the Lower Kellwasser Horizon (Bank 24 a) in the Coumiac section (Stratotype).

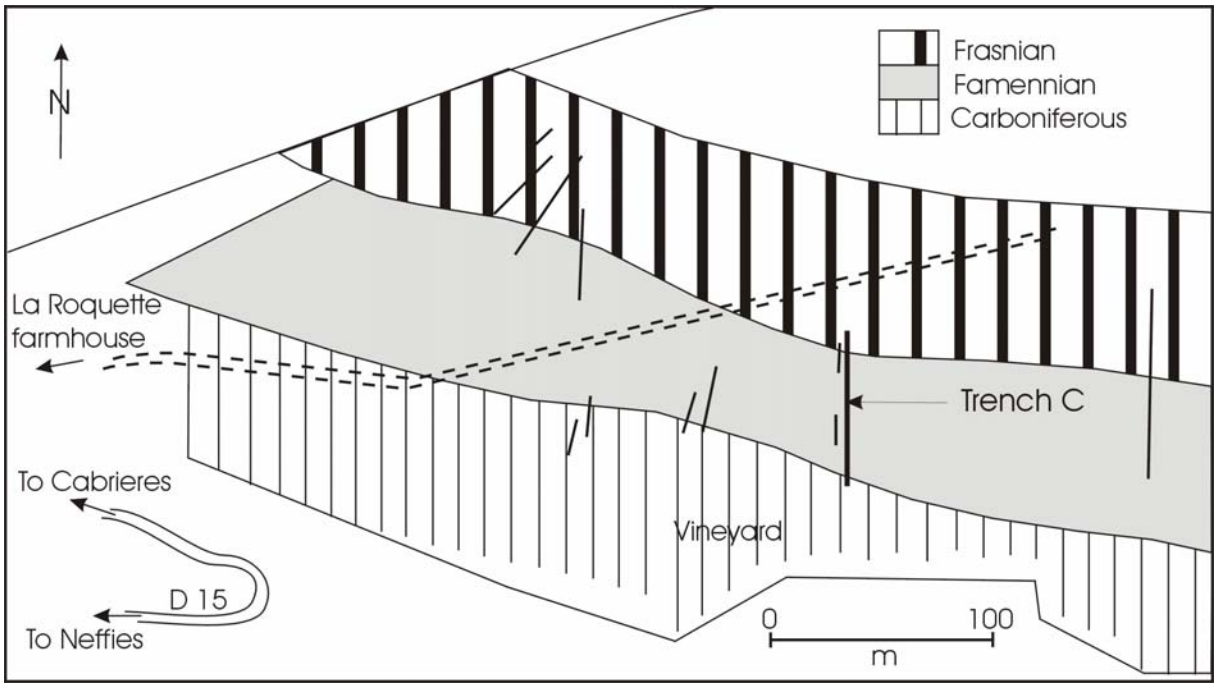

Figure 15. Location map of La Serre trench C (modified after House et al., 1985).

Figure 16. Location of the Frasnian/Famennian boundary in the La Serre trench C section.

3. Methods

The different methods applied for this study are succinctly presented in this chapter.

3.1. X-ray diffraction (XRD)

Sample was crushed manually with caution to fine particle size. With the help of a glass slide it was smeared into a plastic sample holder, so that most of the crystals would have a preferred orientation.

Bulk samples were run on a Siemens (D500) diffractometer, using a Cu target (wavelength for the $K_{\alpha 1}$ radiation: 1.5418 Å) and were measured from 3º to 63º at a speed of 0.5º / minute, with a step width of 0.01º. The minerals were identified from their 'd' spacings, using Bragg's law ($n\lambda = 2d \sin\theta$, where 'd' is the distance between successive atomic plane of a certain crystal, 'λ' is the monochromatic wavelength of the incident beam and 'θ' is the incident angle).

3.2. Microprobe analysis and scanning electron microscope

Composition of individual grains were analysed with electron microprobe analyser (SX50 cameca) and photos of mineral phases were taken with a Digital Scanning Microscope (DSM 960 Zeiss) in the Laboratory of Electron Microscopy at the University of Karlsruhe.

3.3. X-ray fluorescence analysis (XRF)

Major elements were measured by wavelength dispersive X-ray fluorescence (WD-XRF), which use crystals to disperse the component wavelength of the X-ray spectrum emitted from the sample. Trace elements were measured by energy dispersive X-ray fluorescence (ED-XRF), which achieves the same purpose by electronic sorting of pulses of different amplitude produced by X-ray photons of different energies (Williams, 1987).

Powder specimens were prepared for ED-XRF analysis. Bulk samples were ground to fine powders in an agate mortar, and precautions were taken to avoid any contamination of the specimen. The specimens were kept at constant particle size to avoid the risk of variation

in fluorescence intensities. Powder samples were put in plastic sample cups and were covered by thin plastic sheets very tightly with the help of plastic bands. The covered surface was kept very smooth to avoid scattering of X-rays. The samples were measured against the soil standard GXR-2 (Govindaraju, 1994) using Cu and Pd filters in Spectrace 5000 instrument. Details on the analytical procedure and detection limits for the bulk rock samples are referred in Kramar (1997).

Conventional fused glass disks are favoured for the measurement of major element, as the decomposition of a portion of sample and flux produces a homogeneous glass and it eliminates the particle size and the mineralogical effects (Tertian and Claisse, 1982). Fused glass disks were prepared for WD-XRF analysis by mixing one part of desalted dry sample with 4 or 10 parts of lithium tetraborate flux (SPECTROMELT). After properly mixing, they were heated using gas burners for a period of 30 minutes. Heating was done in platinum crucibles. During fusion the melt was agitated for the production of homogeneous glass. The ideal specimen shape for XRF measurement is a flat polished disc and this was obtained by casting the molten glass in a circular mould of required size. The samples were measured against the BE-N standard in the SRS 303 AS instrument.

	Cu (ppm)	Zn (ppm)	As (ppm)	Rb (ppm)	Sr (ppm)	Y (ppm)	Zr (ppm)	Ag (ppm)	Sb (ppm)	Ba (ppm)	La (ppm)	Ce (ppm)	Pb (ppm)
Detection limit (ppm)	<7	<5	<5	<2	<2	<3	<5	<0.7	<2	<10	<10	<10	<5
GXR-2 standard (ppm)	76	530	25	78	160	17	269	17	49	2240	25.6	51.4	690
Standard deviation (ppm)	4.8	7.6	3.5	0.5	3.7	0.5	6.3	0.7	0.6	26.3	5.0	3.0	23.0
Accuracy (±%)	4.5	1.5	26.7	5.7	9.3	17.6	9.9	3.4	0.5	10.1	6.1	11.4	1.4
Precision (±%)	6.6	1.4	11.2	0.7	2.6	2.3	2.6	4.5	1.3	1.3	20.7	5.2	3.3

Table 3. Characteristics of the ED-XRF trace elements results.

	Na_2O (%)	MgO (%)	Al_2O_3 (%)	SiO_2 (%)	P_2O_5 (%)	CaO (%)	K_2O (%)	TiO_2 (%)	MnO (%)	Fe_2O_3 (%)	V (ppm)	Cr (ppm)	Co (ppm)	Ni (ppm)
BE-N standard (ppm)	3.18	13.15	10.07	38.2	1.05	13.87	1.37	2.61	0.2	12.84	235	360	60	267
Standard deviation (% or ppm)	0.02	0.07	0.16	0.26	0.01	0.01	0.01	0.02	0.002	0.02	0.30	2.99	4.75	1.87
Accuracy (±%)	2.0	1.8	1.2	2.1	15.6	3.7	5.2	1.8	2.4	2.0	0.6	5.2	7.9	9.3
Precision (±%)	0.5	0.5	1.6	0.7	0.8	0.1	0.4	0.8	0.9	0.1	0.1	0.9	7.3	0.6

Table 4. Characteristics of the WD-XRF major and trace elements results.

3.4. Carbon water analysis (CWA)

Organic carbon in the sediments was estimated through measurement of inorganic carbon content by Leybold 5003 carbon water analyser (CWA) and then subtracting it from total carbon value. For inorganic carbon analysis, the instrument was calibrated with respect to $CaCO_3$. Approximately 250 ml of dry sample was used for the measurements. The sample was burnt with a steady flow of N_2 and the carbonates were converted into CO_2. The output was obtained in terms of percentage of CO_2.

3.5. Carbon sulphur analysis (CSA)

Leybold 5003 carbon sulphur analyser (CSA) was used to measure total carbon and sulphur in percentage. It was calibrated with respect to the 0.42 % C containing free cutting steels. Other constituents of the standard are S (0.147 %), Si (0.46 %), P (0.031 %), and Mn (1.15 %). For the analysis, approximately 100 mg of dry sample was added to approximately 500 mg of iron cheap accelerator. To this mixture tungsten was added such that the ratio between tungsten accelerator and iron cheap accelerator was 3:1. The instrument oxidises the carbon and sulphur present in the sample with a constant flow of O_2.

4. Results and interpretation

This chapter present the results of the paleoenvironmental study based principally on a multiproxy approach.

4.1. Paleoenvironmental factors

In order to put constraints on possible causes responsible for the demise of the biota during the Kellwasser Event, we aimed at characterizing the environmental changes with respect to detrital input, biogenic input, productivity, redox conditions, as well as the hydrothermal and volcanic inputs during the deposition of the Kellwasser Horizons.

4.1.1. Detrital input

To assess the detrital input the Al-normalized Ti and Si contents and the Na/K and K/Fe+Mg ratios were used in addition to the results of the X-ray diffraction (see quartz). In hemipelagic sediments Al is generally regarded as the main conservative element being used as a proxy for clay minerals. High Ti/Al ratio reflects enhanced delivery of riverine detritus (Murphy et al., 2000; Meyers et al., 2001), because Ti is generally associated with the heavy mineral grains. Thus, increased Ti concentrations relative to Al would reflect relative sea-level fall and coast line progradation and vice versa (Sageman et al., 2003), though it can also represent a higher eolian input (Bertrand et al., 1996) or of volcanic ash (Sageman et al., 2003). The Si to Al ratio reflects the amount of Si in excess to Si bound in aluminosilicates. As such the Si/Al ratio may indicate an enhanced quartz delivery due to eolian input (Pye and Krinsley, 1986; Werne et al., 2002) or mirror increased input of biogenic silicon and thus act as a productivity signal (Davis et al., 1999). Ratios involving alkaline and/or ferromagnesian elements like K/(Fe+Mg) or Na/K ratios are generally interpreted to reflect an increase or decrease in riverine siliciclastic flux as compared to a relatively constant volcaniclastic background (Sageman and Lyons, 2004). However any geochemical ratio involving K is difficult to interpret without closely associated mineralogical data. Indeed the amount of K can change merely as a function of changes in the clay-mineral assemblage, e.g., between more illitic versus more smectitic. The significance of such changes are difficult to interpret because more smectite can be due to increased subaerial weathering intensity, to increased

hydrothermal weathering of basalts, or to changes in sea-level and/ or riverine discharge. Thus the result of these ratios must be interpreted in relation with the other detrital input indicators. Moreover the multiple processes involved in the Fe deposition like the detrital input, the hydrothermal input (see 4.1.5), the Fe remobilisation or Fe precipitation as authigenic pyrite under anoxic conditions (see 4.1.4), coupled to the complexity of the K deposition speak against the use of proxy like K/(Fe+Mg) for paleoenvironmental study in a context where the mentioned processes are recorded.

In the Kowala section there is a decrease in detrital input in the *linguiformis* conodont zone as reflected e.g., by the Al_2O_3 (Fig.17) content, but also by the absence of clay minerals. The high Si/Al ratio or quartz content (Fig. 18 and 20) at the same level indicates an increase in biogenic quartz as already observed at Kowala and in other sections of the Morovian shelf by other authors (Racki et al., 2002; Vishnevskaya et al., 2002). These high excess Si contents in the *linguiformis* zone are assigned to siliceous sponge associations and radiolarians (Vishnevskaya et al., 2002). Detrital and biogenic quartz can be easily discriminated e.g., in a Zr vs. SiO_2 diagram. In addition, a decrease of the detrital input relative to a volcaniclastic component as indicated by the increase of the Na/K ratio may be interpreted in terms of a relative sea-level rise (Fig. 21). In this context the high Ti/Al ratio (Fig. 19) is considered to indicate an increased volcanic input, as it was already suggested for the Kowala section based on the Zr/Al_2O_3 ratio and on the amount of the insoluble residue (Racki et al., 2002).

By using the same mineralogical and geochemical approach a decrease of the detrital input was observed in the Büdesheimer Bach core at the level of the KWH. The more proximal facies of this section shows more pronounced variations in the content of muscovite or chlorite. It is interesting to notice the sharp breaks in the upward increasing trend of the detrital input (as indicated e.g., by the Al_2O_3 content; Fig. 17) at the level of the two KWH. However because of the scarcity of conodonts in the limestone beds (Piecha, 1994), the biostratigraphic dating of the upper Kellwasser Horizon is uncertain. The general lowering of the detrital input not observed in the upper Kellwasser Horizon (Fig. 17) would suggest also to consider cautiously the biostratigraphic dating at this level. An increase of the biogenic quartz is preferred to explain the increase of Si/Al ratio in the LKWH (Fig. 20) because radiolarians were found at a depth corresponding to these Horizons (Piecha, 1994). The simultaneous decrease of the Ti/Al ratios and increase of Na/K ratios (Fig. 19 and 21) are interpreted to reflect a relative sea-level rise during this time interval. The same interpretation holds also for the Steinbruch Schmidt section. The sporadic increase of the Si/Al ratio can be

attributed to the presence of radiolarians in the Kellwasser Horizons as already observed by Devleeschouwer et al. (2002).

In the two sections of the Montagne Noire, Coumiac and La Serre, the low amount of quartz and Al_2O_3 in the KWH also indicate a decrease in the detrital input during this time (Fig. 17 and 18). Similar to the Kowala section a simultaneous increase of the Ti/Al and Na/K ratios reflects a higher input of volcanic material, but could be also due to the weathering of basaltic rocks. The significant increase of Si/Al ratio in the LKW equivalent of the La Serre section occurs in the vicinity of the silicificated banks (terminal parts of banks 8 and 9, Fig. 3). Coupled with higher Ti/Al and Na/K ratios, the high Si/Al ratios could be ascribed to higher volcanic or eolian input, given that the Zr vs. SiO_2 diagram does not indicate a substantial contribution of biogenic quartz.

An increase of the Si/Al ratio can also reflect a relative sea-level rise and coastline progradation (Sageman et al., 2003).

The decrease in the detrital input in the Kellwasser Horizons is a common feature in all of the investigated sections and is interpreted in terms of a relative sea-level rise during this time. The enhanced of the detrital input in the Famennian *triangularis* zone (Fig. 17) of the German and French sections, already observed in many sections, is interpreted as reflecting a relative sea-level fall following a climatic cooling.

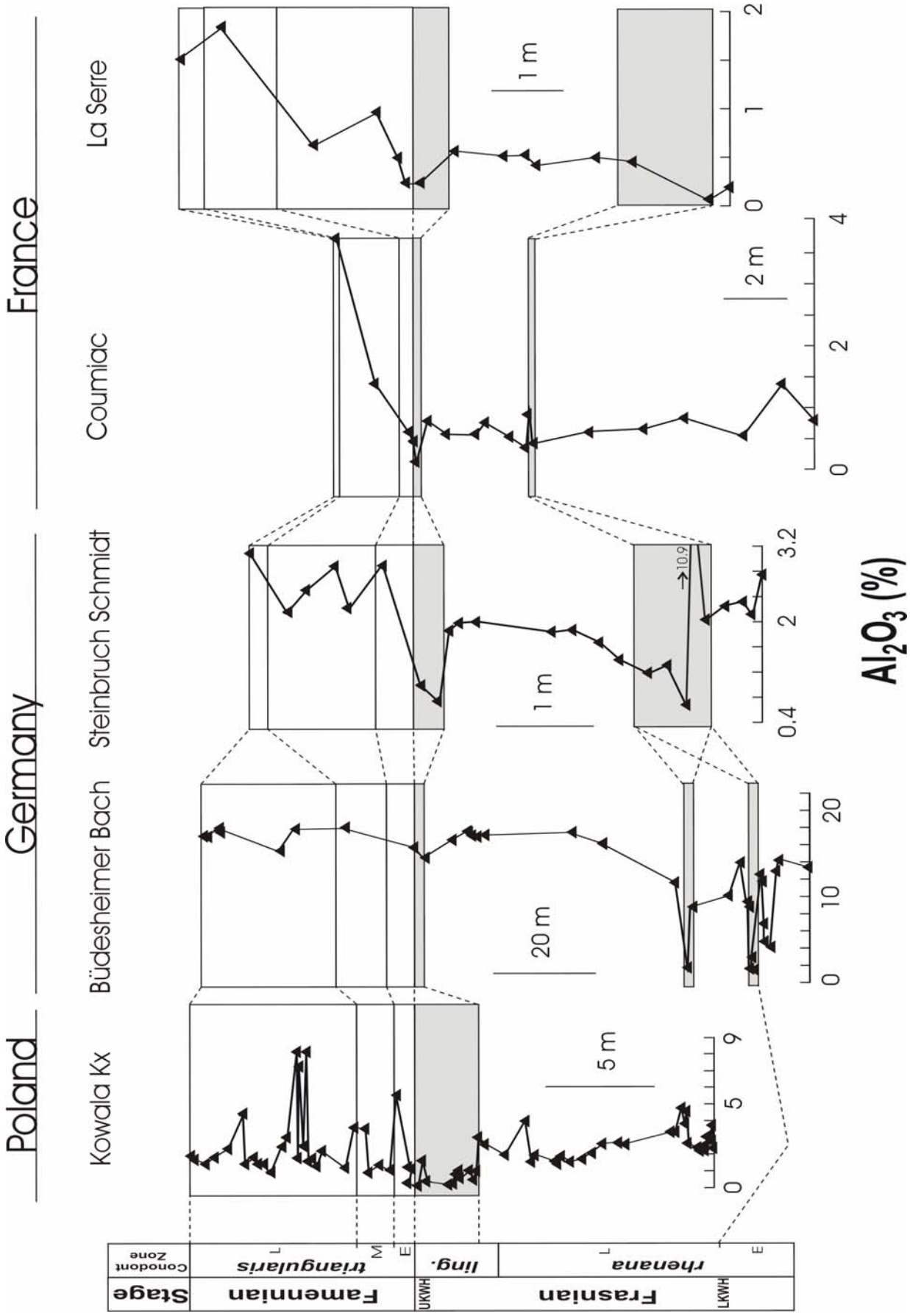

Figure 17. Distribution of the Al_2O_3 (%) contents along the sections.

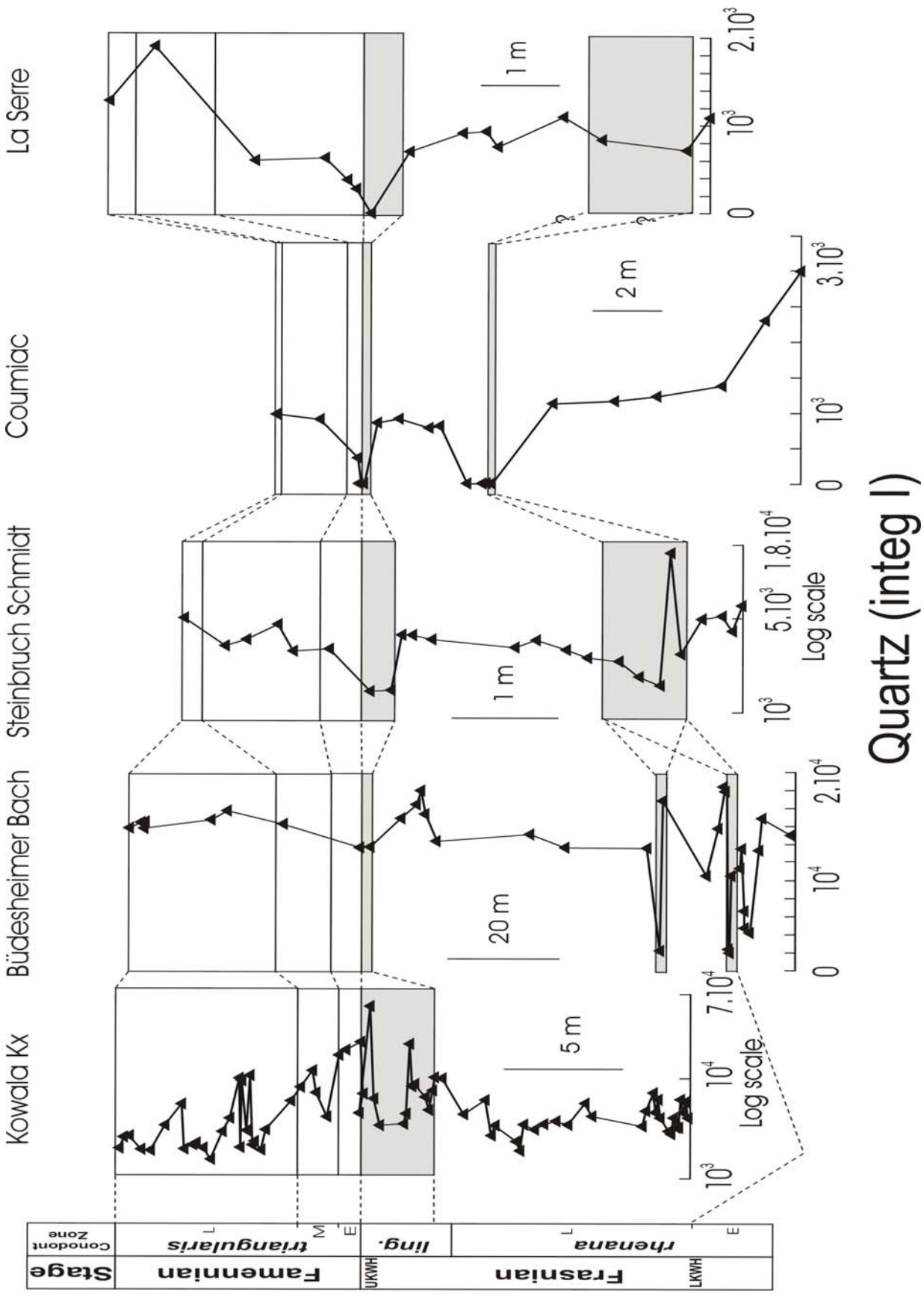

Figure 18. Distribution of the quartz contents (Integrated intensity of the X-ray diffraction results) along the sections.

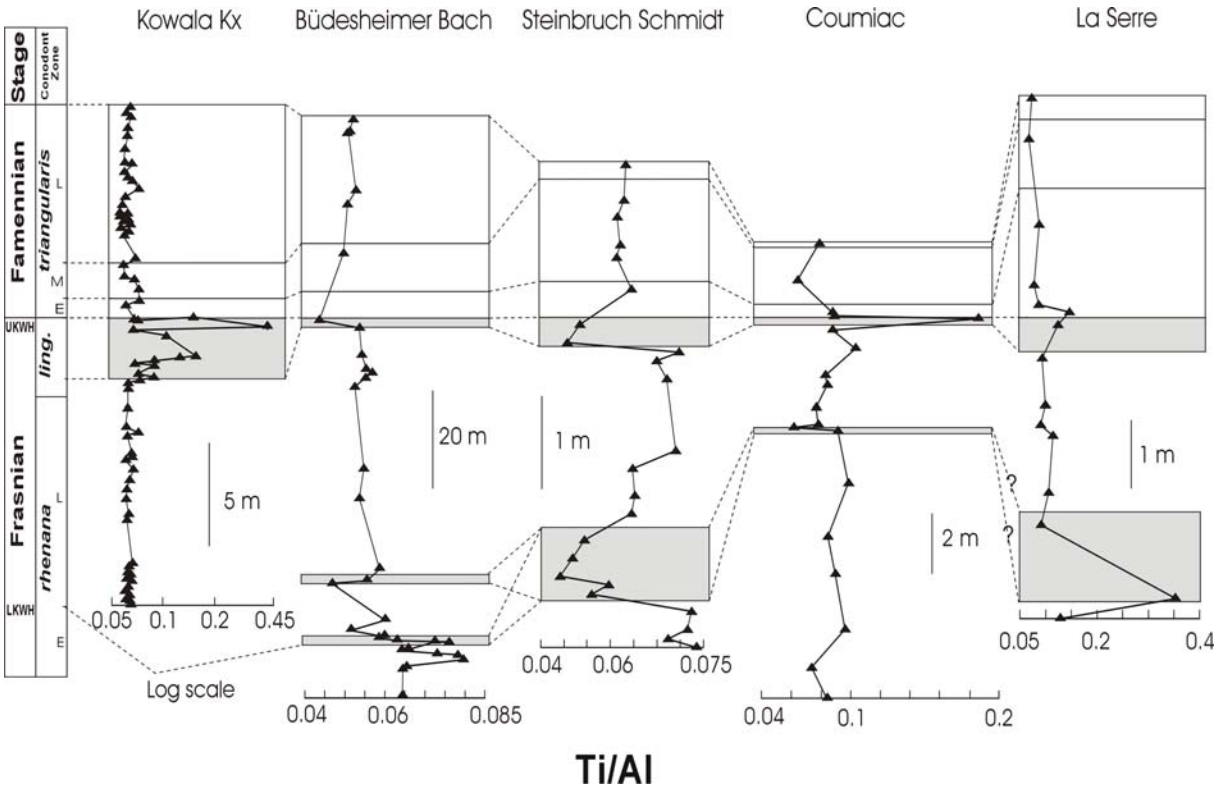

Figure 19. Distribution of the Ti/Al ratios along the sections.

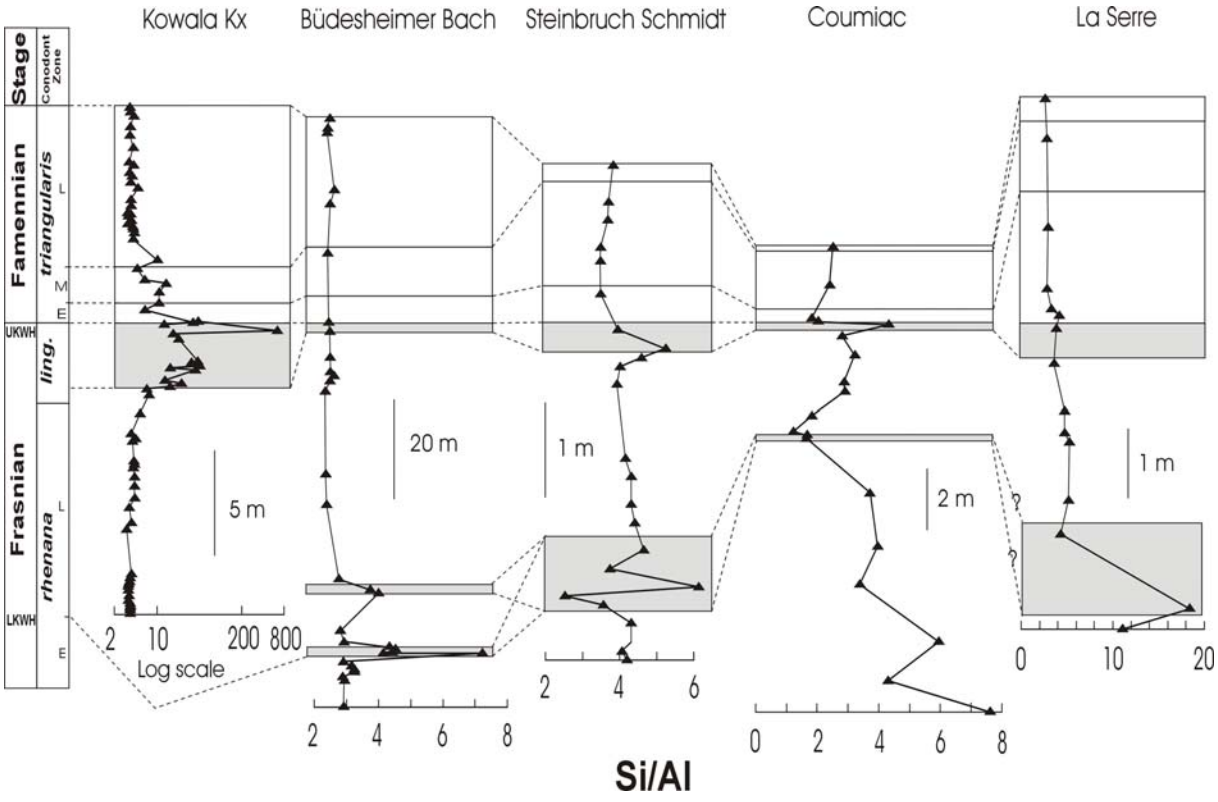

Figure 20. Distribution of the Si/Al ratios along the sections.

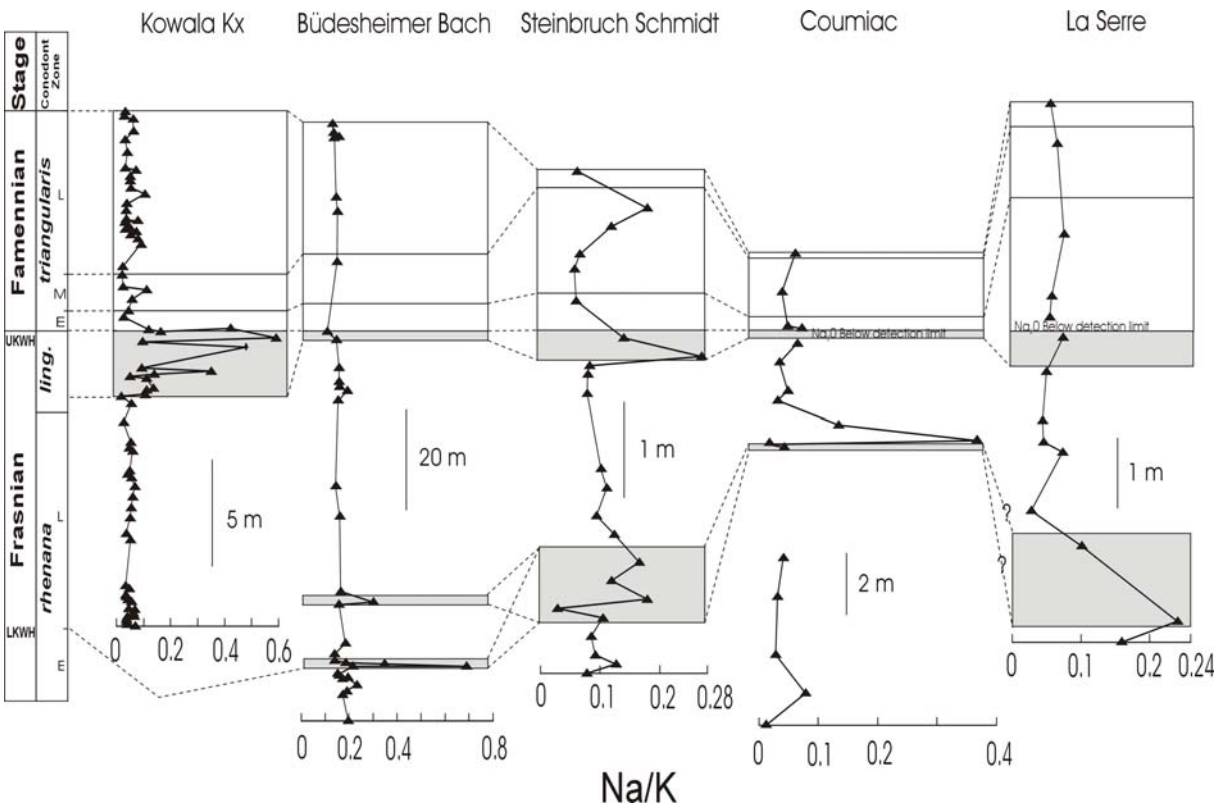

Figure 21. Distribution of the Na/K ratios along the sections.

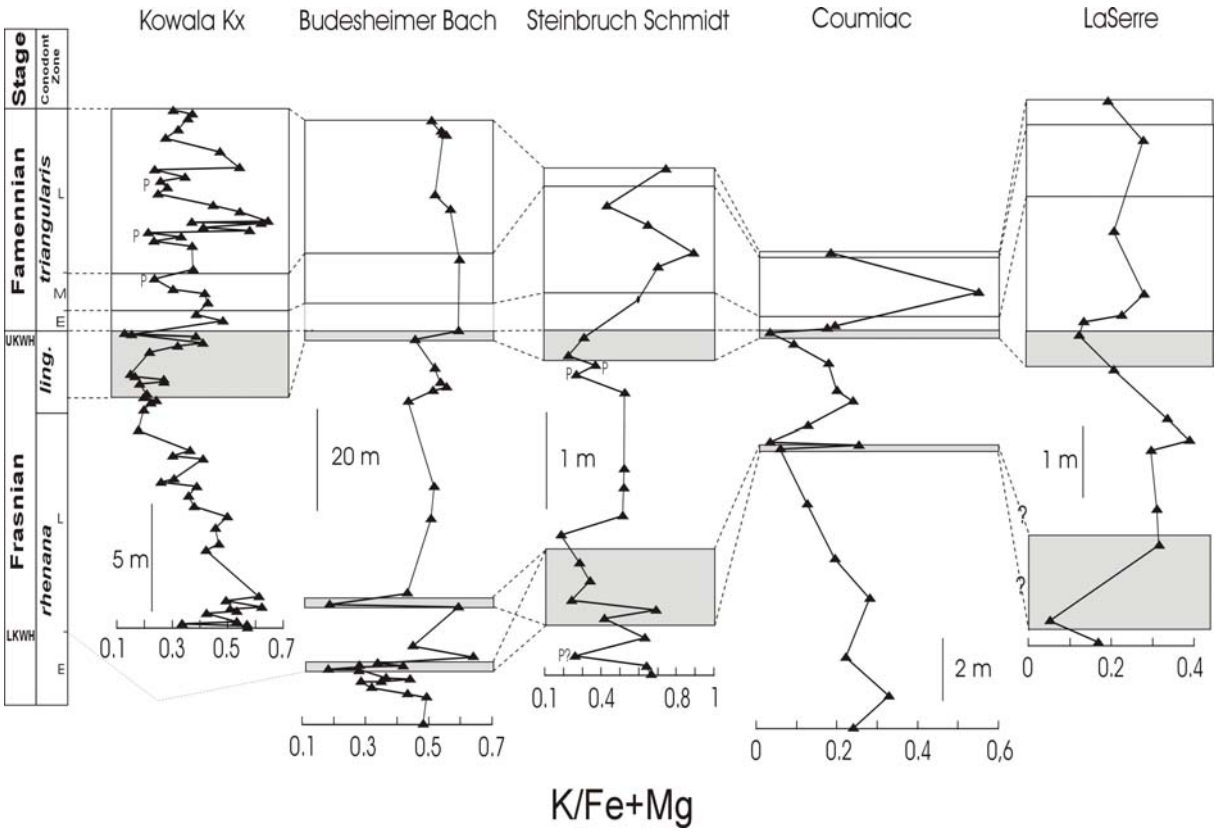

Figure 22. Distribution of the K/Fe+Mg ratios along the sections.

4.1.2. Input of organic carbon

An increase of the organic carbon burial at the time of the KWH deposition is easily recognizable in the European sections, particularly in those from Germany and France, by the characteristic presence of dark bituminous limestones (Buggisch, 1991).

The Büdesheimer Bach core is a typical example for this (Fig. 23). Nevertheless, as our results show, increased C_{org} contents seems not to be always restricted to the KWH, like e.g., in Steinbruch Schmidt, where higher concentrations were found also in between the two KWH, notably in bank 37. In this section the variation of C_{org} contents is not very pronounced, with values ranging between 1% to maximum 4%. A relative increase of C_{org} may be due to a decrease in detrital input, i.e. lower sedimentation rates eventually will countersteer the "dilution effect" (Sageman et al., 2003; Sageman and Lyons, 2004).

Similarly, in the Coumiac section, the increase of organic carbon content up to 1 wt.% in the *linguiformis* zone (compared to a mean value of 0.5 wt.%), absent in the LKWH, is coupled with the lowest amount of detrital component.

In contrast, in the La Serre section though there is an evident increase of the organic carbon content in the UKWH, the maximum is reached in the *triangularis* zone.

Moreover, the frequently mentioned enrichment in organic carbon in the *linguiformis* zone is sometimes even absent. This is especially evident in the Kowala section, in which the *linguiformis* zone has the lowest content of organic carbon.

Resuming, the enrichment of organic carbon in the KW Horizons is not a common feature to all of the sections investigated.

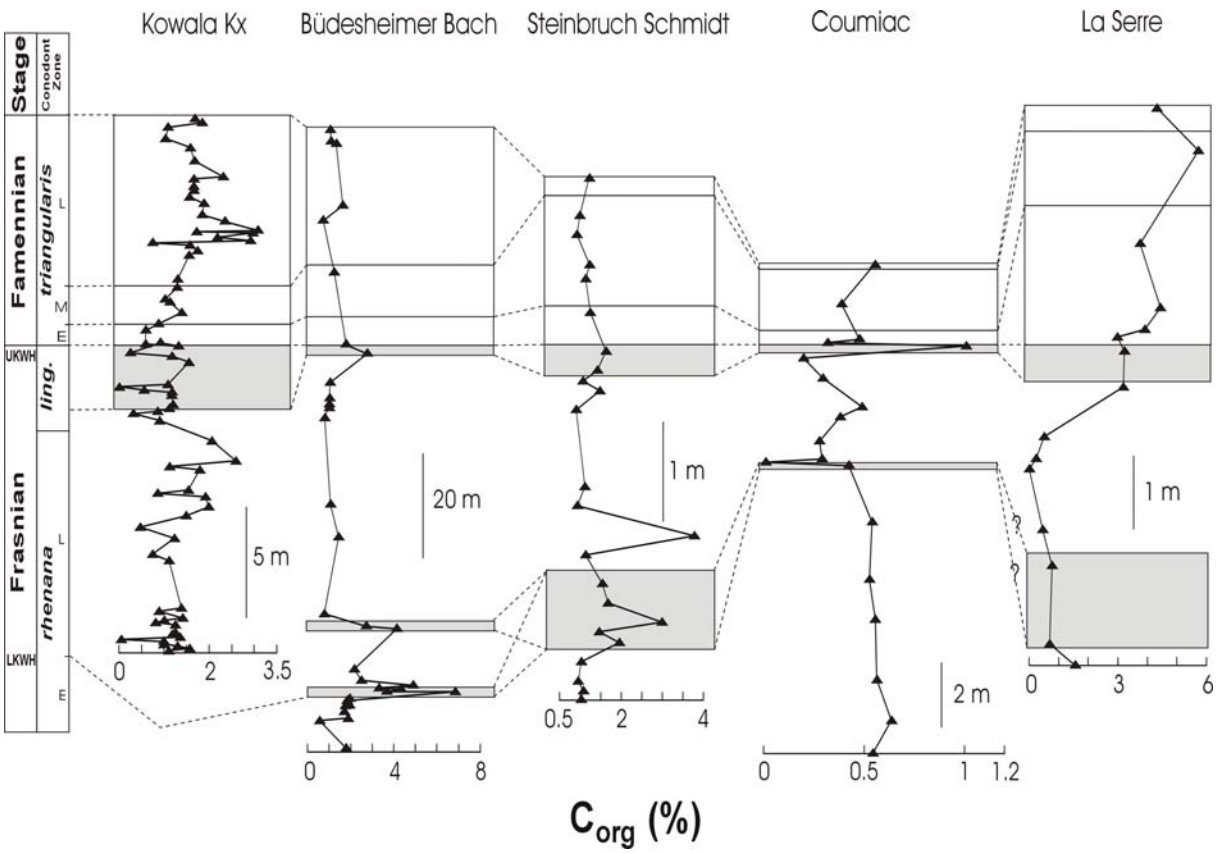

Figure 23. Distribution of the C_{org} (%) contents along the sections.

4.1.3. Nutrient input and productivity

The non-detrital part of P in the sediment was proposed as an indicator for biological productivity (Schmitz et al., 1997). The "P_2O_5 in excess" (P_2O_5*) can be calculated by dividing the P_2O_5 content by the Al_2O_3 content of the sample normalized with the average Al_2O_3 content of the continental crust (e.g., P_2O_5*= P_2O_5/ (Al_2O_3 x 15%), Schmitz et al., 1997). With some restrictions, Ba and SiO_2 in excess can be also used as productivity proxies (Schmitz et al., 1997). Nevertheless, the remobilisation of Ba and P under anoxic conditions may alter this signal (Ingall and Jahnke, 1997; McManus et al., 1998), while an increase in the Si/Al ratio (see 4.1) may reflect enhanced eolian input instead of higher productivity (Pye and Krinsley, 1986; Werne et al., 2002). Most of the sections are enriched in P_2O_5* (Fig. 24) in both the *linguiformis* zone (UKWH) and at the base of the late *rhenana* zone (LKWH). Investigations with the electron microprobe allowed a closer characterization of the P bearing minerals. In samples from the chert layer representing the F/F boundary in the Kowala section (Fig. 3 and 5), additionally to different P-bearing minerals, like tiny grains (1-2 µm) of

xenotime, monazite, and fluoroapatite (Fig. 26), more frequently, 10 µm large crystals of barite (Fig. 26) were identified. In the Steinbruch Schmidt section, in samples from the UKWH (Bank 62 and 64), fluoroapatite and other P bearing phases, enriched in REE (La, Ce) were detected. A similar association of P with lanthanides was observed in the UKWH of the Büdesheimer Bach core. Phosphorous may be associated also with Fe-oxyhydroxides (McManus et al., 1997). The relatively high P content of the conodonts (Girard and Albarede, 1996) may lead to a correlation between P_2O_5* and the abundance of the organisms buried in the sediment. It is noteworthy that in the more typical basinal facies of the Kowala and La Serre sections, the enrichment in P persists until the base of the early *triangularis* zone. The very high P_2O_5* value in bank 14 (F1 biozone; early Famennian, Fig. 3) correlates not only with a high fluoroapatite content (as evidenced by the microprobe analyses), but also fits well with the high abundance of a chitinozoan species in this bank (Paris et al., 1996). Except for Coumiac, where Ba is below the detection limit in the KWH, the general enrichment of Ba in excess in the KWH (as documented by the presence of barite) could be also due to enhanced productivity (Fig. 25). Nevertheless in the case where anoxic conditions or intense sulfate-reduction can be certified (see next paragraph), remobilisation of Ba and P could have occurred and resulted in the concentration of these elements not necessarily precisely in the level where the highest productivity had prevailed. A comparison between nutrient input and organic carbon accumulation (Fig. 23) generally shows a decoupling between productivity and organic matter burial.

Resuming, the enrichment in nutrients or/and the increase of productivity in the KW Horizons is common features to all of the sections investigated. These results are in agreement with C-isotope investigations of Joachimski and Buggisch, 1993 and Joachimski et al. (2001, 2002).

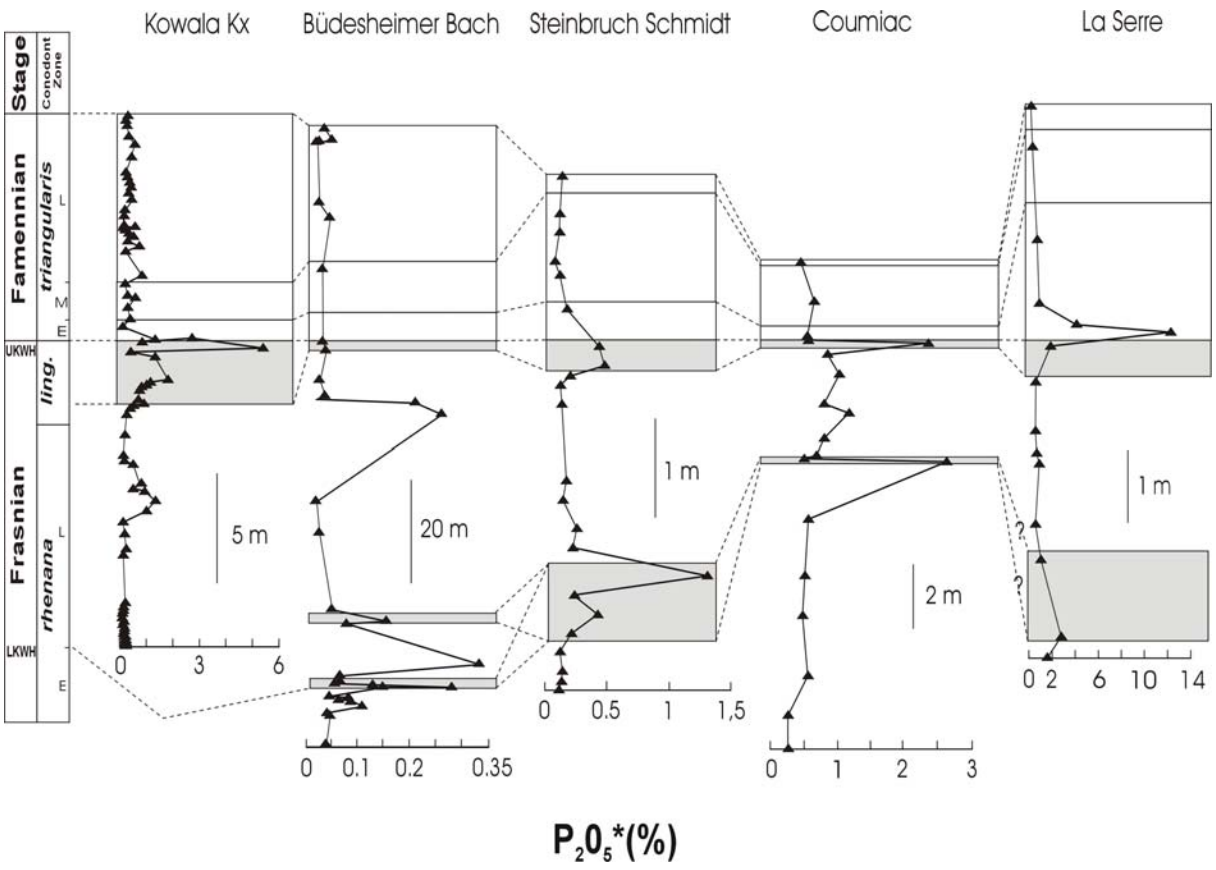

Figure 24. Distribution of the P_2O_5 content in excess ($P_2O_5^*$) along the sections.

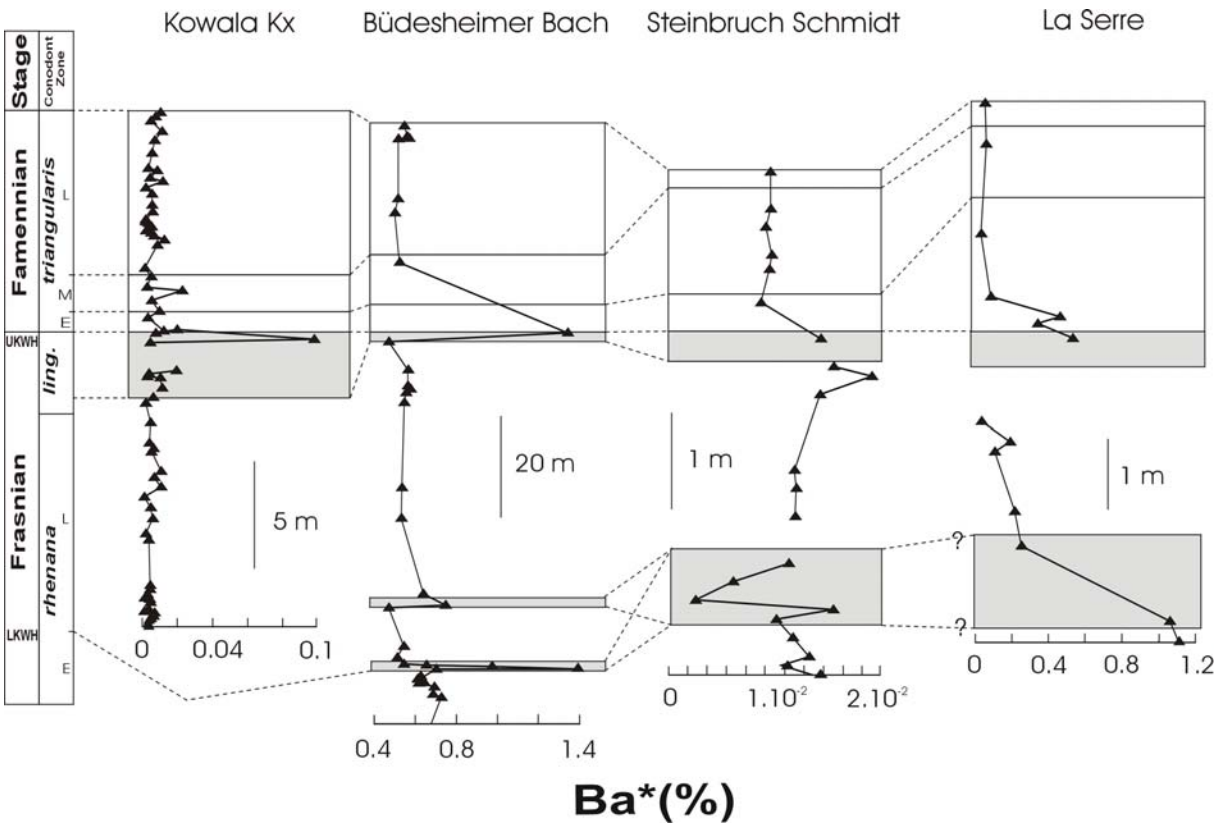

Figure 25. Distribution of the Ba content in excess (Ba*) along the sections.

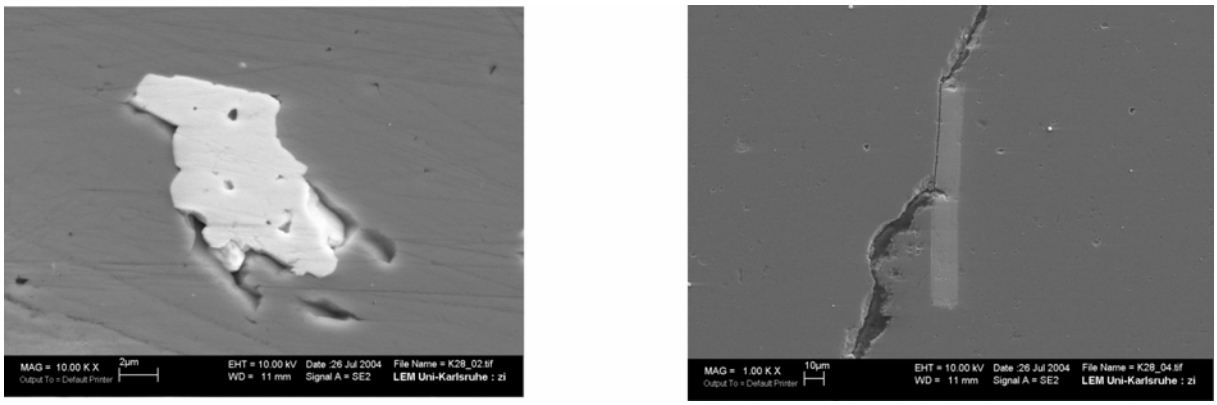

Figure 26. Barite (left) and FluoroApatite at the F/F boundary of the Kowala section (right).

4.1.4. Degree of oxygenation

Different element ratios (e.g., V/Cr, Ni/Co, U/Th, etc.) and the Al-normalized content of redox sensitive or chalcophile elements (e.g., Fe, Mn, U, V, Zn, Pb, Cu, Ni) are used in geochemistry to estimate the degree of bottom water oxygenation during sedimentation (Jones and Manning, 1994; Bratton et al., 1999; Joachimski et al., 2001; Racki et al., 2002; Yudina et al., 2002; Algeo and Maynard, 2004; Cruse and Lyons, 2004). However, because many of these elements (e.g., Pb, Zn, Cu, Co, Ag, Mo) are typically associated with hydrothermal activity (e.g., Eckhardt et al., 1997; Von Damm, 1995; Kuhn et al., 2000; 2003; Pierret et al., 2000; Sander and Koschinsky, 2000; Wheat et al., 2003; Hübner et al., 2004) the cause of their enrichment is often ambiguous (Cruse and Lyons, 2004). In this study the use of V/Cr and Ni/Co were preferred (Fig. 27 and 28), because the concentration of commonly used elements, like Mo, were sometimes below the detection limit and therefore couldn't permit a systematic comparison. Similarly elements like Pb, Zn, Cu, As or Ag were also often below the detection limit which didn't allowed to make for all sections multivariate analysis to tease out the relative importance of the redox controls versus hydrothermal enrichment.

In addition to element contents or ratios, the presence of authigenic minerals formed in a well-constrained redox range is also often used as proxy parameters to assess the degree of bottom water oxygenation. The degree of pyritization of Fe (DOP) is one of the most commonly used geochemical parameters (Berner, 1970, 1984; Leventhal and Taylor, 1990; Middelburg, 1991; Sageman et al., 2003) and could be successfully applied for the Büdesheimer Bach core (Fig. 27). Studies in modern anoxic environments, like in the Cariaco basin or in the Black Sea,

showed that the presence and size of framboidal pyrite is an even more reliable anoxia proxy (Wilkin et al., 1996, 1997, Wilkin and Arthur, 2000). Framboidal grains less than 5 μm in size typically indicate anoxic to anoxic-sulfidic conditions. The distribution of pyrite framboids in the KWH was investigated by means of SEM and microprobe.

According to Hoffman et al. (1998) a V to Cr ratio of 5 corresponds to the limit between dysoxic and anoxic conditions (shown as a dashed line in Fig. 27). In the basinal sections of Kowala and La Serre (Fig. 27), the V/Cr values reach the anoxic domain in the lower and middle *triangularis* zone as well as in the middle to upper *Rhenana* zone. In the KWH the low V/Cr ratios generally indicate oxic/dysoxic conditions. The most significant increase in the V/Cr ratio occurs in the KWH of the stratotype section of Coumiac, though the values still correspond to dysoxic conditions. In Steinbruch Schmidt, there are no noteworthy variations in the ratio of these elements, except for Bank 23 (LKWH) in which however, the increase of V/Cr could be explained by a higher content of clay minerals that adsorbed V. In this section, in addition to the V/Cr ratios, the presence of iron oxides (sometimes in association with pyrite grains), also suggests dysoxic rather than anoxic conditions. The V/Cr ratios in the Büdesheimer Bach core (Fig. 27) apparently contradict the conclusions suggested by the DOP values, because while the V/Cr ratios are low in both KWH, the DOP reach values of up to 0.7 in the LKWH and about 0.6 in the UKWH, suggesting anoxic and dysoxic conditions, respectively. Moreover, most of the pyrite framboids identified with the microprobe are less than 5 μm in size, not only in both of the KWH of the Büdesheimer Bach section (Fig. 29 and 30), but also in the UKWH of the sections Coumiac (bank 31g, Fig. 35) and La Serre (bank 14 d, Fig. 30). A tentative explanation for this apparent inconsistency is given in the next paragraph. Similarly the Ni/Co ratios (Fig. 28), for which values higher than 7 are representative of anoxic conditions, are not correlated to the DOP in the Büdesheimer Bach core and to the pyrite framboids size criteria in Coumiac and La Serre. Based on this proxy only the samples belonging to the middle and late *triangularis* zone of La Serre were deposited under anoxic conditions whereas dysoxic conditions appears sporadically in the late *triangularis* zone of the kowala section.

In conclusion, based on the geochemical proxies used, it seems that the deposition of the KW Horizons under anoxic conditions is not a common feature to all of the sections investigated.

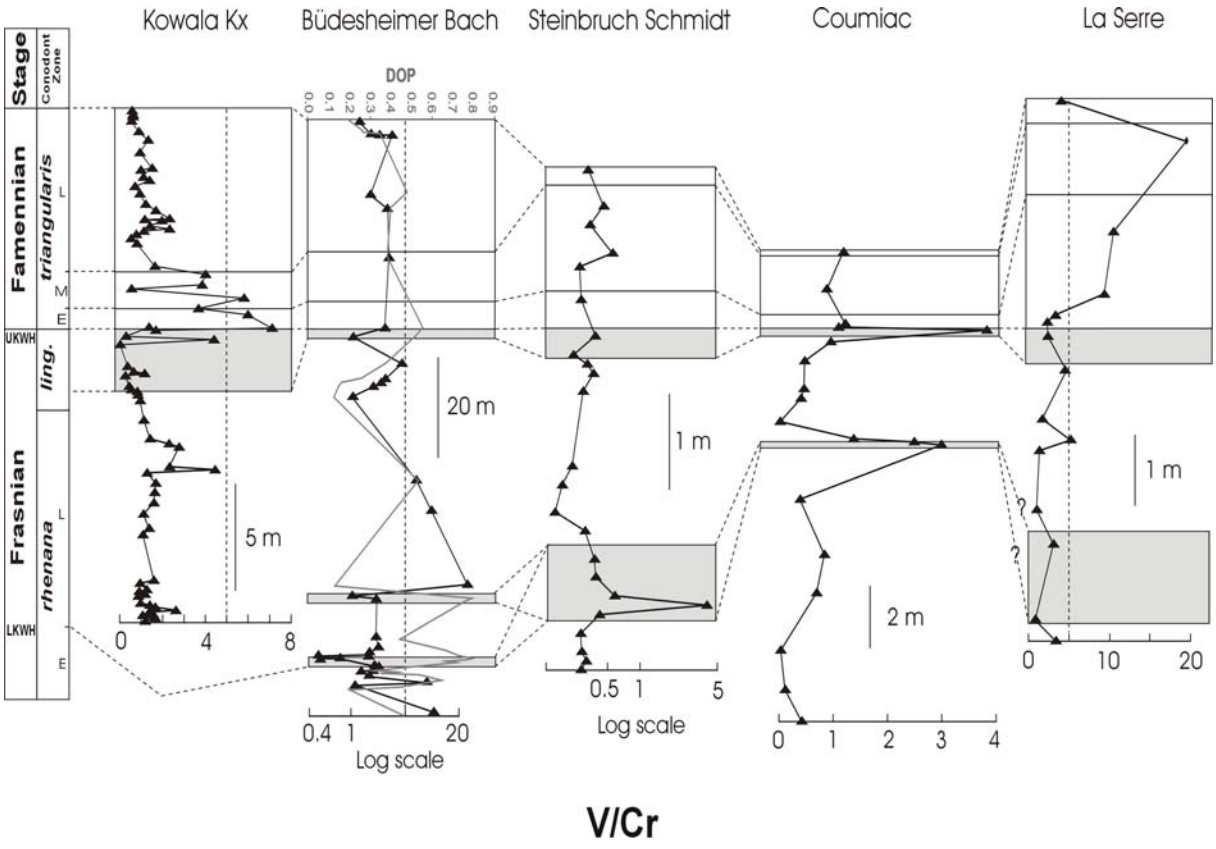

Figure 27. Distribution of the V/Cr ratios along the sections and of the degree of pyritization (DOP) along the Büdesheimer Bach core. The dashed lines mark the limit between dysoxic and anoxic conditions (Hoffman et al., 1998).

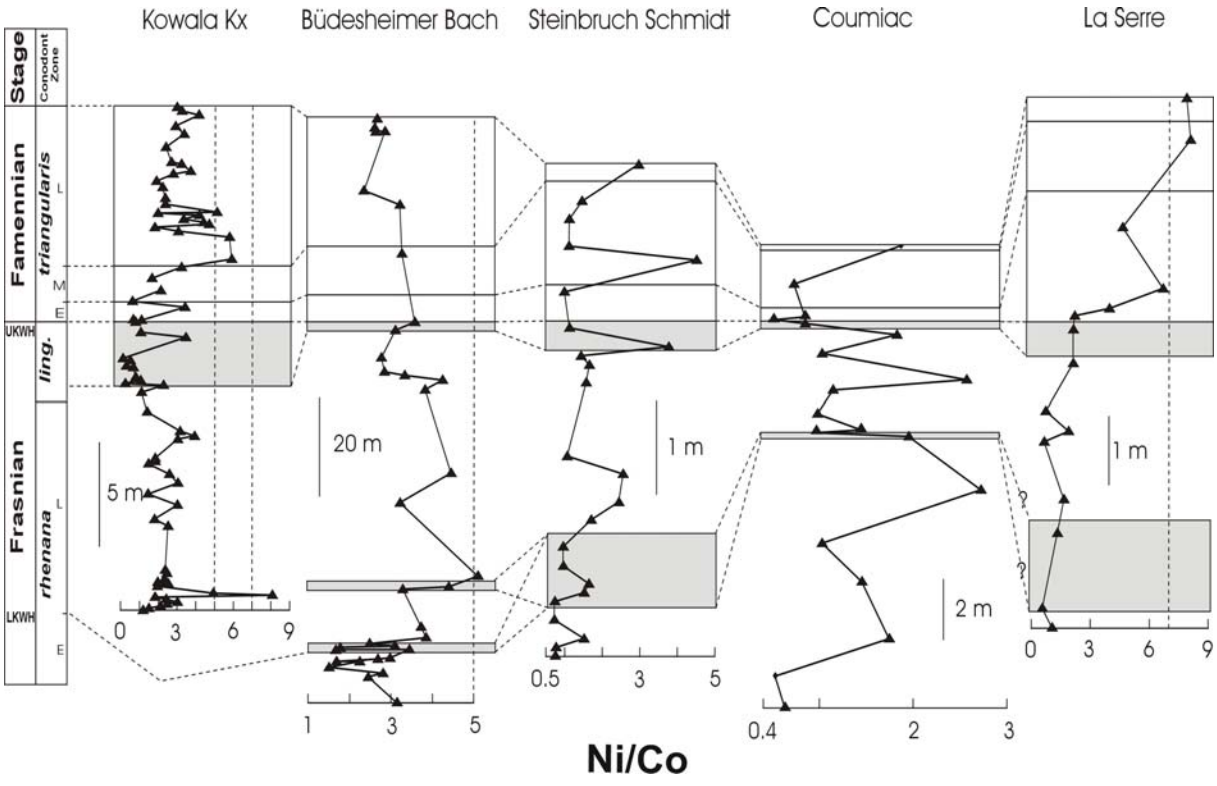

Figure 28. Distribution of the Ni/Co ratios along the sections.

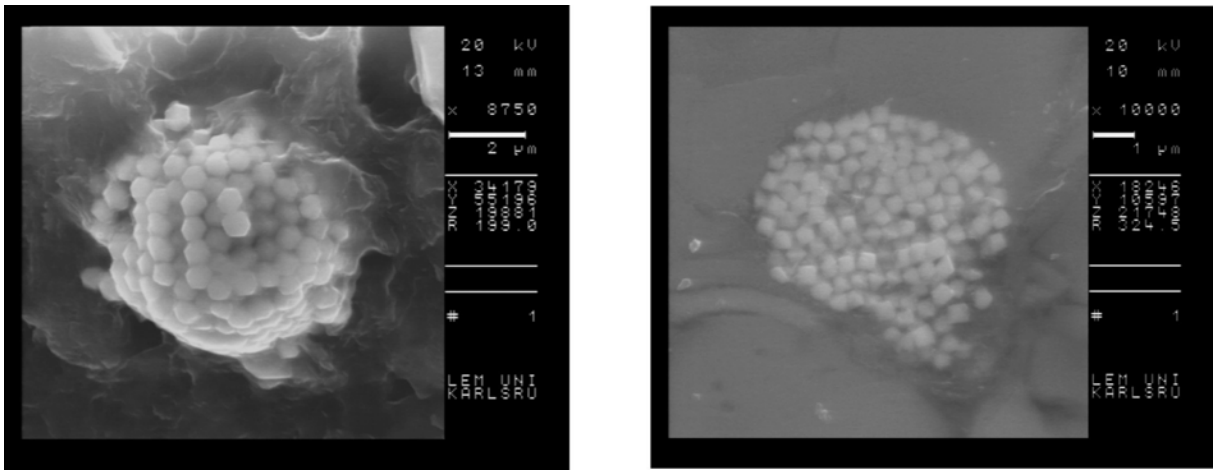

Figure 29. Framboidal pyrite in the UKWH of the Büdesheimer Bach core: depth 71.8 m (left) and in the LKWH of the Büdesheimer Bach core: depth 126.5 m (right).

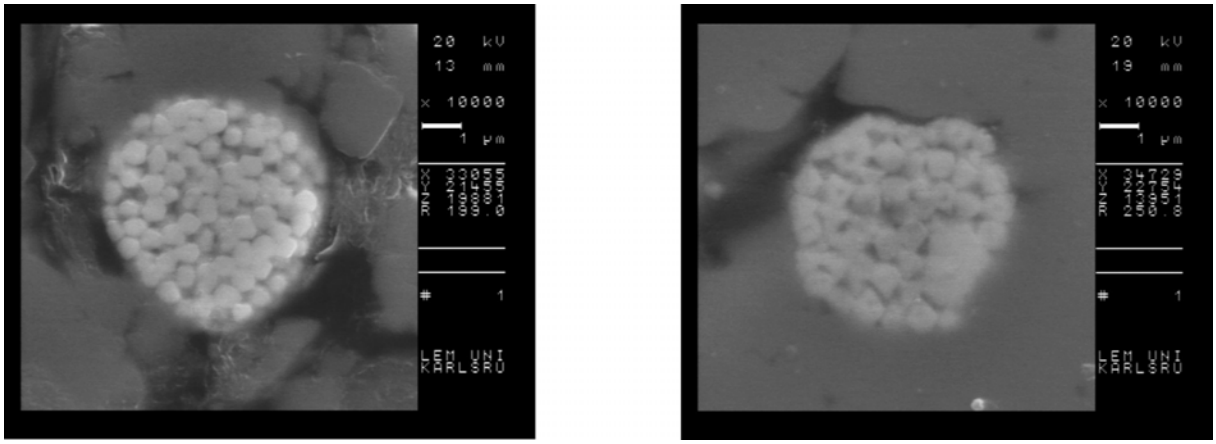

Figure 30. Framboidal pyrite in the LKWH of the Büdesheimer Bach core: depth 139.35 m (left) and in the UKWH of La Serre: bank 14d (right).

4.1.5. Hydrothermal input

The detection of hydrothermal input into a sedimentary record by means of geochemical methods is generally based on the above-average concentration of some diagnostic trace elements such as Cu, Zn, Co, Mo, As, Pb, Ag, Ba, but also on particularities in the distribution of some major elements like Fe, Mn, Si, Ca or Mg (e.g., Von Damm, 1995; Eckhardt et al., 1997; Kuhn et al., 2000; 2003; Hübner et al., 2004). Recent observations in the Juan de Fuca and the North Fidjian Basin (Sander and Koschinsky, 2000; Wheat et al.,

2003) showed that the concentration and speciation of Cr and Co in seawater is also widely controlled by hydrothermal activity, and Pierret et al. (2000) demonstrated the utility of the Cr to Zr ratio to detect hydrothermal influence. The occurrence of a possible hydrothermal input at the F/F boundary was already studied by several authors, using the Al/(Al+Fe+Mn) ratio. A value <0.35 is generally considered to be characteristic for metalliferous sediments (Racki et al., 2002; Yudina et al., 2002). At the level of the KWH there is a significant decrease in the Al/(Al+Fe+Mn) ratio to values that are in most cases below 0.35 in all of the investigated sections (Fig. 31). X-ray diffraction results indicate that the occasionally low Al/(Al+Fe+Mn) ratios outside the KWH are due to the presence of pyrite. In both of the basinal sections Kowala and La Serre, the low ratios still persist at the base of the early *triangularis* zone. It is particularly noteworthy the constant increase in Fe and Mn relative to Al in the stratotype section (Coumiac) up to the base of the upper *rhenana* zone. The less pronounced decrease in the UKWH of the Büdesheimer Bach core is probably due to a stronger continental influence at the transition from Frasnian to the Famennian (Fig. 17). However, the pyrite content (from XRD) does not correlate with the Al/(Al+Fe+Mn) ratio in this section and consequently cannot explain its low values. A statistical evaluation of the data by factor analysis, but even simple cross plots reveal a significant negative correlation between the Al/(Al+Fe+Mn) ratio and the Al-normalized contents in typically hydrothermal elements like Pb, Zn, Cu, Ag, Ni and As. Investigations with the microprobe allowed a closer insight into the nature of these metal enrichments in some of the KWH samples. In the UKWH of the Steinbruch Schmidt section (Banks 62 to 64) Cu and Pb sulfides (chalcocite, galena) as well as tiny grains (1-2 µm) of As-Sb sulfosalts (possibly getchellite?) could be identified. Additionally, Fe-oxides in association with silica were frequently encountered. In the UKWH of Coumiac (Bank 31g), the enrichment of Fe relative to Al is due to the presence of pyrite framboids less than 5 µm in size (Fig. 35). In the cherty bank of the Kowala section, in addition to sulfides (e.g., sphalerite and an Fe bearing NiAs-sulfide, possibly gersdorffite), V-rich Fe-oxide grains as well as dolomite crystals with low contents of Fe and Mn were found. The mineral speciation of Mn, i.e. the origin of high Mn/Al ratios (Fig. 33) is more difficult to constrain by microprobe analyses. Nevertheless, the strong correlation between the Mn/Al and Fe/Al ratios and the association of slightly elevated Mn concentrations with Fe-oxi/hydroxides (e.g., in Bank 62, Steinbruch Schmidt) indicate that Fe-oxi/hydroxides, Fe-sulfides (mainly pyrite) and possibly dolomite are the main Mn carrier minerals in the KWH. The Cr/Al ratio in the KWH is high in all of the sections (Fig. 32). In context of the former annotated inconsistency between the high DOP values and low V/Cr ratios (suggesting contradictory oxygenation conditions; see

4.4), it is especially relevant to notice the parallel increase of the Mn/Al and Cr/Al ratios in the KWH (Fig. 32 and 33). Because of the mobility of Mn under reducing conditions, the Mn/Al ratio is also used as a paleo-oxygenation proxy (Bratton et al., 1999). However, in cases in which the relative amounts of both Cr and Mn are controlled only by the redox state of the depositional environment, their Al-normalized concentrations should be inversely correlated (Calvert and Petersen, 1993). Consequently, the parallel increase of the Cr/Al and Mn/Al ratios in the KWH indicates an external (i.e., hydrothermal) input of Cr and Mn to the sediment. The apparently contradictory results indicated by the DOP and V/Cr (see also Ni/Co) ratios emphasize the necessity of a careful analysis of the geochemical data in order to avoid possible misinterpretations. In addition to a common hydrothermal source, the correlation of the Al-normalized Cr, Fe and Mn contents may be due to the adsorption of Cr on Fe- and/or Mn-oxi/hydroxides (Achterberg et al., 1997).

The results presented before (sections 4.1.4 and 4.1.5) indicate that the input into the sediment of Fe of hydrothermal origin may have led - in function of the prevailing redox state - to enhanced formation of either authigenic sulfides (primarily framboidal pyrite: Fig. 20, 30 and 35) or of Fe-oxides/hydroxides (Fig. 35 and 36). The temporal proximity of enhanced hydrothermal influence (Coumiac: 31e1; La Serre: 13a) and the onset of anoxic conditions (Coumiac: 31g; La Serre 14d) in the sections Coumiac and La Serre is interesting and relevant in terms of understanding the mechanisms which eventually lead to the development of anoxia. So, the steady decrease of the Al/(Al+Fe+Mn) ratios up to a minimum in the LKWH at Coumiac, put constraints on the chronology of the events, suggesting a continuously increasing hydrothermal input as the primary cause for the development of anoxia. Moreover, the *Triangularis* zone considered to be deposited under anoxic conditions at La Serre (Lethiers et al., 1998; see also 4.1.4) does not present any significant enrichment in Fe or Cr relative to Al (see also the early and middle *Triangularis* zone of Kowala, section 4.5), so that the formation of pyrite was possibly Fe-limited at La Serre during this time. These results indicate that the observed (hydrothermal) signals during the deposition of the KWH can not be explained by anoxia alone, or in other words, complexation by organic matter (Fig. 23) or the formation of authigenic sulfides (Fig. 34) can not be the primary cause for the observed metal enrichments. Moreover the stratotype of Coumiac illustrate that the increase of volcanogenic background relative to the detrital input (as Na/K) due to the sea-level rise can also not explain alone the enrichment in metal relative to Al given that the aluminiun content

(Fig. 17) or Na/K ratio (Fig. 31) do not fit the observed constant decrease of the Al/(Al+Fe+Mn) ratio (Fig. 31). This observation is also valid for the La Serre section.

Concluding this section, it could be shown that during the deposition of the Kellwasser Horizons there was an increased hydrothermal influence in all of the investigated sections.

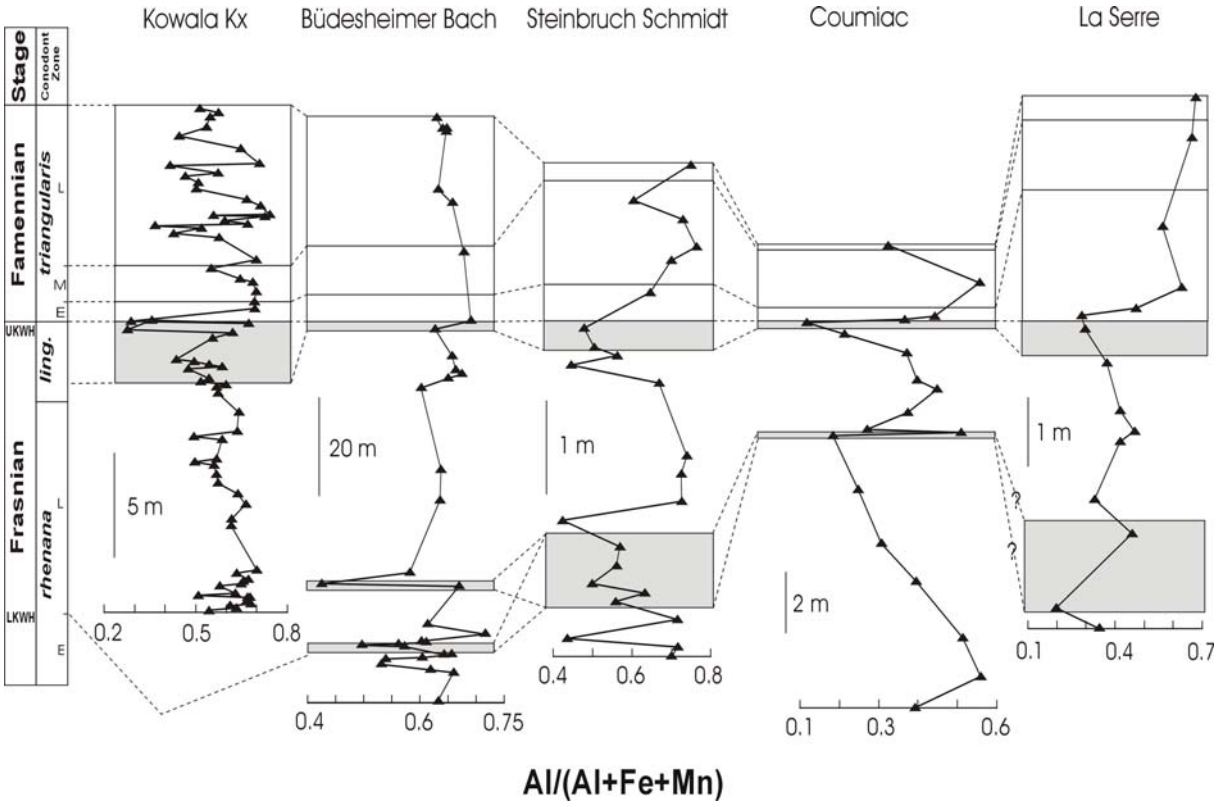

Figure 31. Distribution of the Al/(Al+Fe+Mn) ratios along the sections.

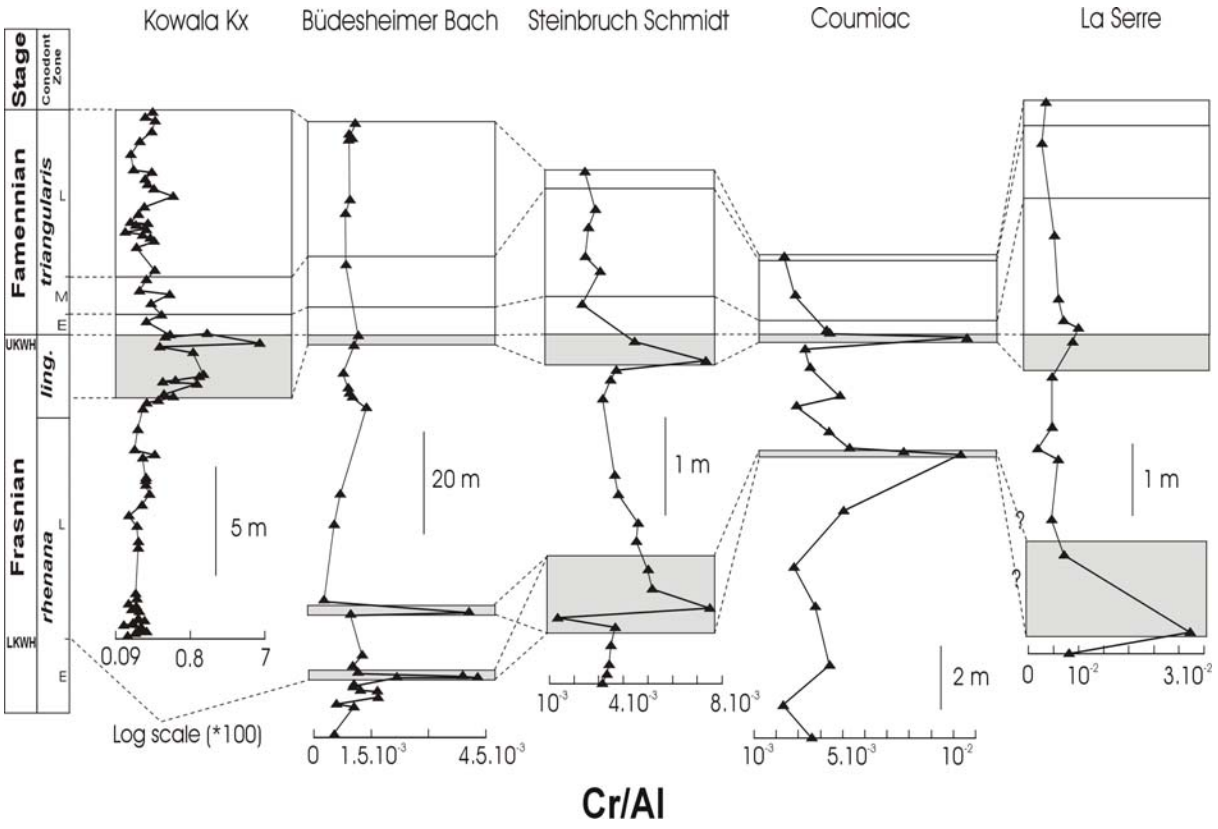

Figure 32. Distribution of the Cr/Al ratios along the sections.

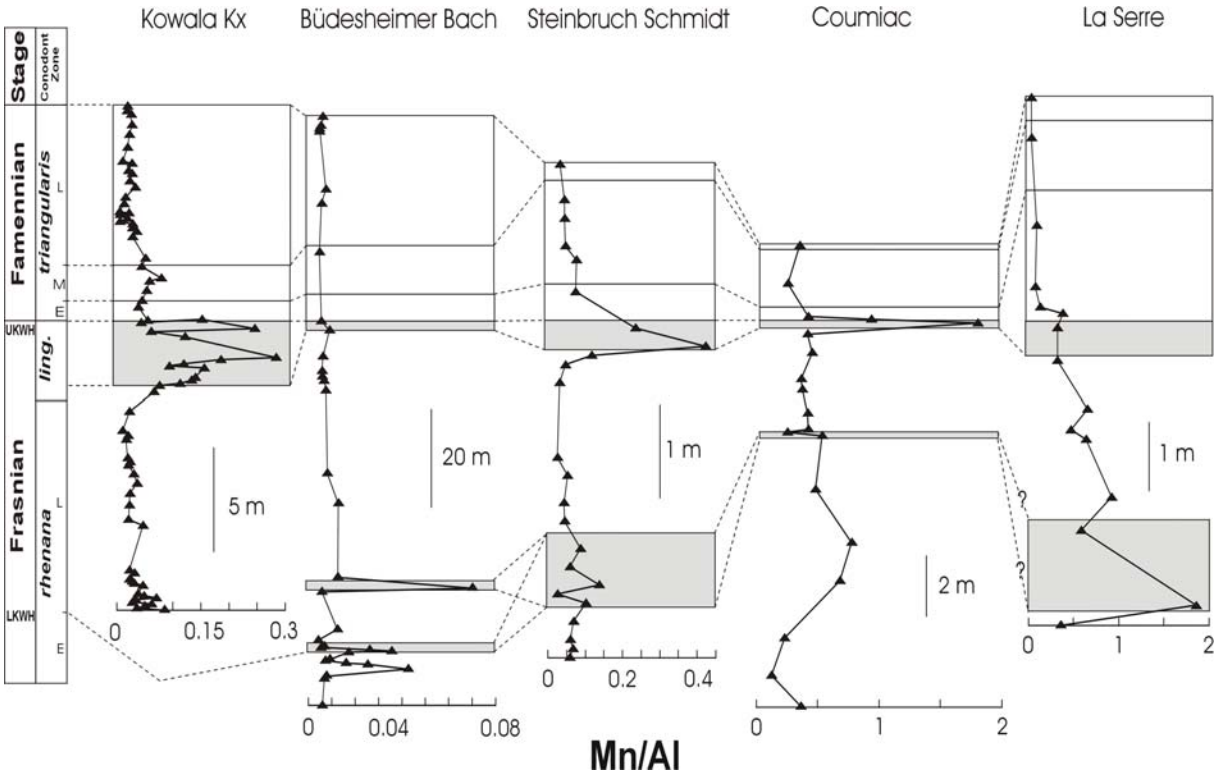

Figure 33. Distribution of the Mn/Al ratios along the sections.

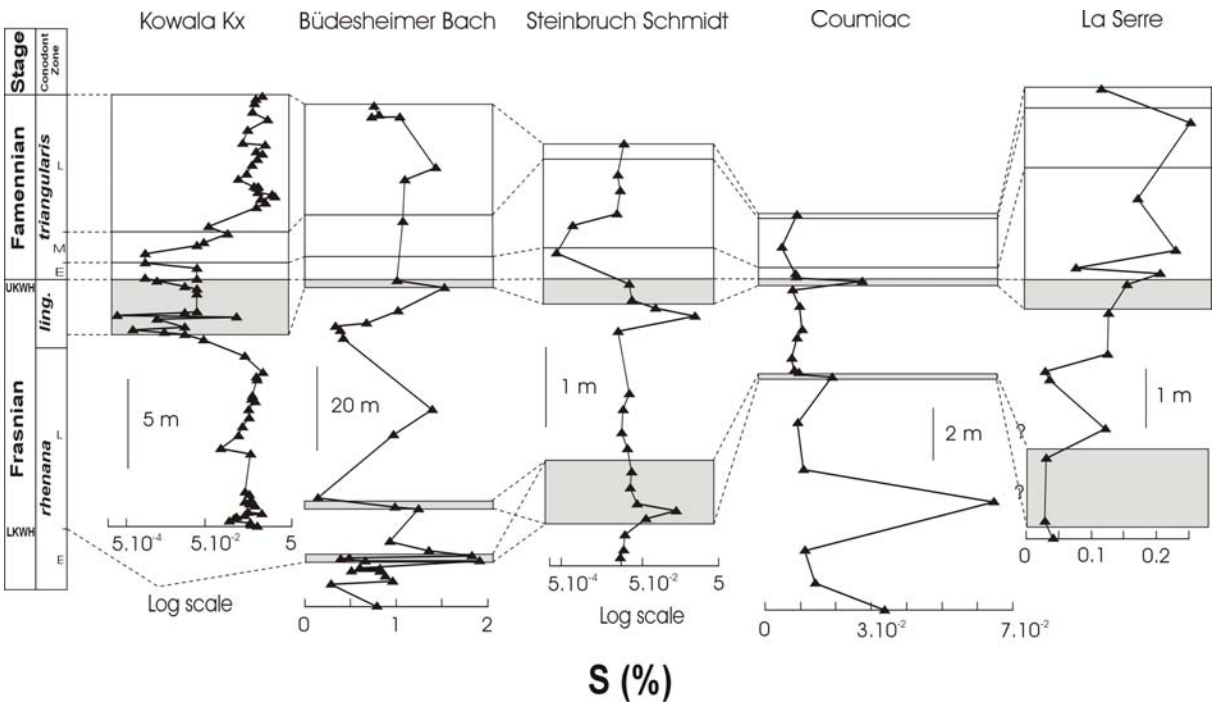

Figure 34. Distribution of the S contents (wt.%) along the sections.

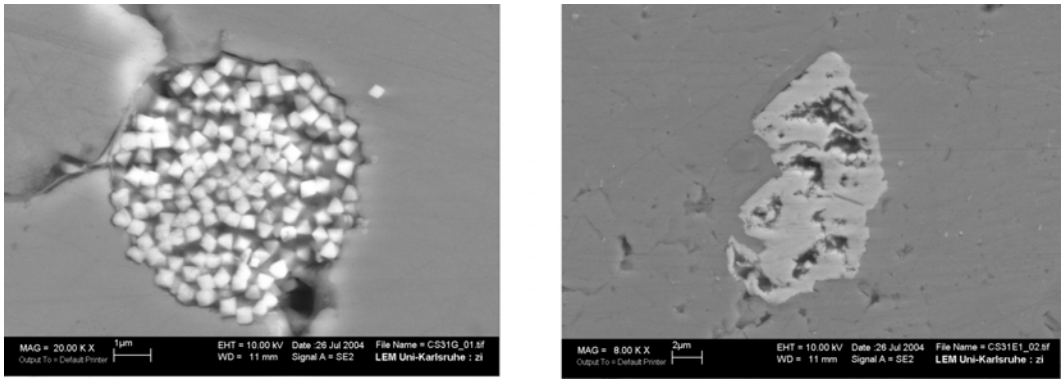

Figure 35. Framboidal pyrite at the F/F boundary in the bank 31g and iron oxide (with Si) in the bank 31 e1of the Coumiac section (left).

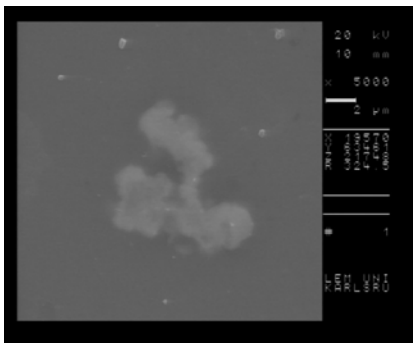

Figure 36. Iron oxide (with Si) in the bank 13a of the La Serre.

4.1.6. Volcanic input

The Zr/Al_2O_3 ratio (Fig. 37) is considered to reflect the input of fine-grained volcaniclastic particles (Suzuki et al., 1998) and as such was already used as a proxy to assess the amount of volcanic contribution in different F/F boundary studies (e.g., Racki et al., 2002; Yudina et al., 2002). As mentioned above, the Ti/Al ratio (Fig. 19) possibly can be interpreted in a similar way. Both proxies show a parallel tendency in all of the sections studied. While in the basinal sections of Kowala and La Serre the ratios indicate an enhanced volcanic signal, in the UKWH of the Büdesheimer Bach core this seems to be overlapped by the terrestrial detrital input due to a stronger continental influence (Fig. 17). Studying the volcanic and hydrothermal history of modern ridge segments, Kuhn et al. (2000) observed that the volcanic detritus was stronger concentrated along the central rift valley. Consequently, variations in bottom current may be the reason for the differing distribution pattern observed in the Steinbruch Schmidt section, which has sediments deposited on a submarine rise (Buggisch, 1991). However other local conditions specific to the German sections could have been involved. Similar to the nutrient (Fig. 24 and 25) and the hydrothermal inputs (Fig. 31), the share of volcaniclastic components is also higher at the base of the early *triangularis* zone in the Kowala and La Serre sections. Correlated to the Cr/Al ratio and enriched in all the KWH, the Mg/Al ratio could point out the mafic source of Mg. Moreover similarly to the decoupling between metal enrichment and anoxic condition (see 5.1.5), the Mg/Al ratio increase could be hardly explained only by the formation of dolomite due to anoxic condition, this enhanced of Mg/Al being absent from the early and middle *Triangularis* zone of Kowala and la Serre. The increase of the Mg/Al ratio in the KWH could be also an indirect effect of the lowering of the continental detrital input and an increase of the volcaniclastic background fraction in such context. The difference between the Zr/Al_2O_3 (or Ti/Al) and the Mg/Al ratios in the UKWH of the Büdesheimer Bach core and the KWH of the Steinbruch Schmidt section could be due to different processes of deposition of these elements (e.g. in particle or dissolved form). These differences observed in the German sections could be due e.g., to the presence of mountain ranges having a barrier effect for the wind transport particles. As for the other interesting observations made, the comparison with other sections in Germany and in Morocco would be helpful.

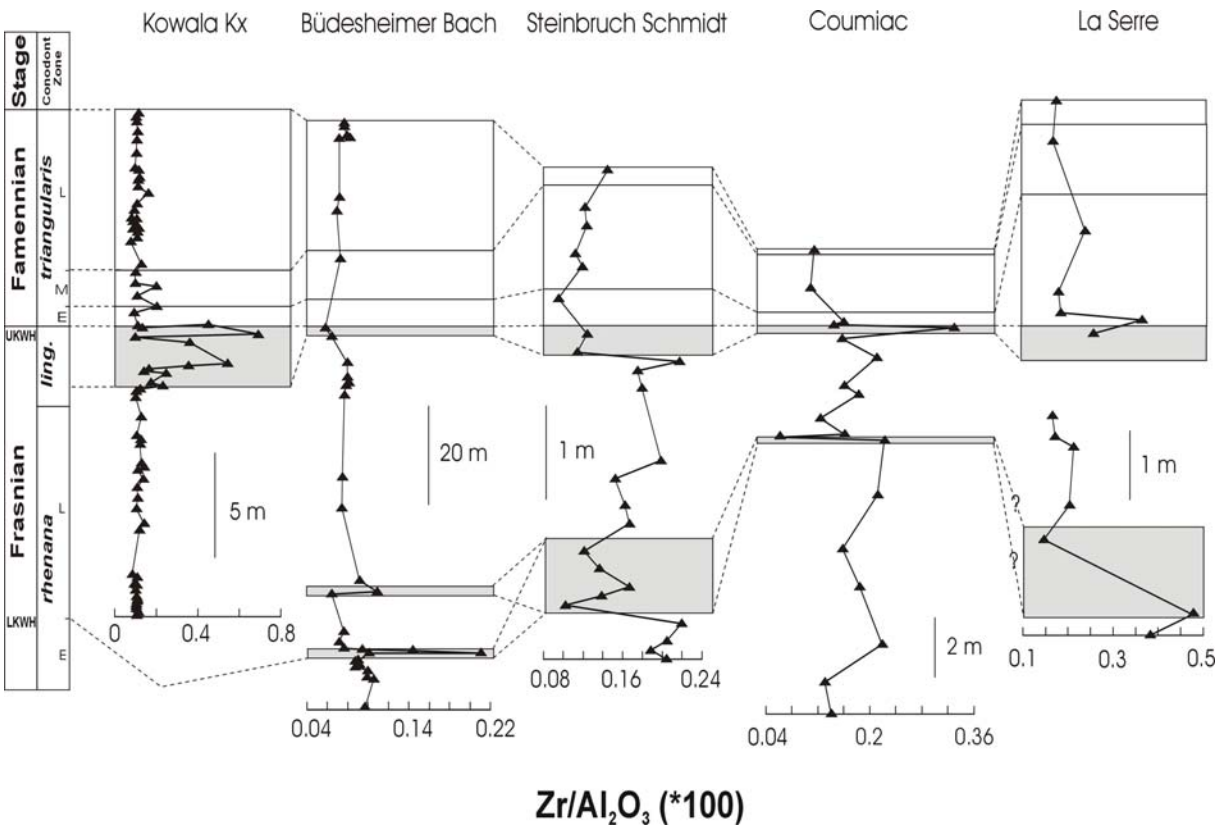

Figure 37. Distribution of the Zr/Al_2O_3 (*100) ratios along the sections.

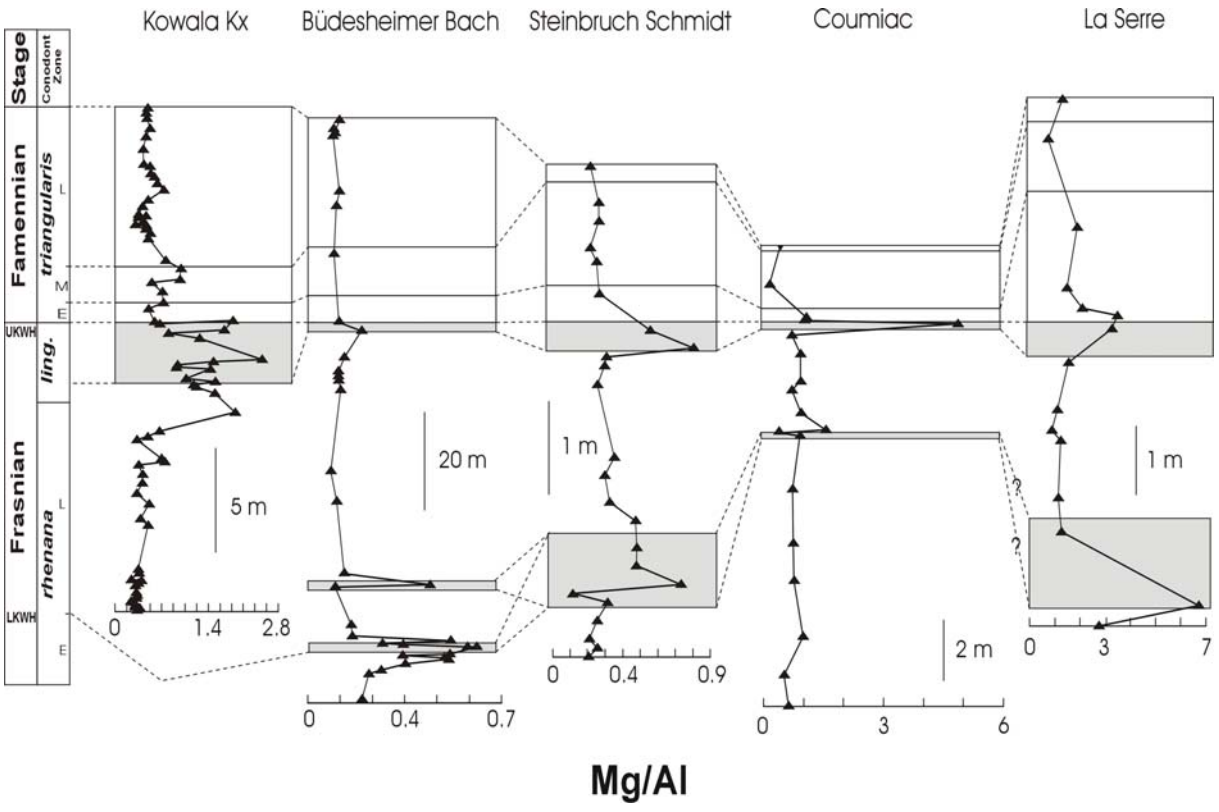

Figure 38. Distribution of the Mg/Al ratios along the sections.

4.1.7. Multivariate statistic

The comparison of the results of different paleoenvironmental proxies or indicators for each section allows the discrimination between global/regional and local environmental features. Indeed, some of the element ratios used, like the indicators for detrital input (e.g., Ti/Al), reflect more typically local or regional conditions. On the other hand, the general decrease in the Al and/or quartz content in the Kellwasser Horizon could be assigned to a general sea-level rise, as already observed in the South Laurussia and the North Gondawana (e.g., Schindler, 1990; Buggisch, 1991). This signal, noticed in all of the sections, could have strongly influenced the other element ratios used, in terms of balance between volcaniclastic background and detrital input. A multivariate statistic study by means of factor analysis, on a cumulative data set from all sections, might yield some additional insights into the complex and intricate relationships between the different proxies. The statistical data analysis was performed using the software package Statistica (StatSoft Inc., USA). To allow a cumulative analysis, before processing, data were normalized for each section separately. The matrix of factor loadings was rotated by the normalized Varimax algorithm.

Ba* was not included because it could be not evaluated in all sections (i.e., Coumiac). As a hydrothermal indicator, instead of the Cr/Al ratio, the more common Cr/Zr (Pierret et al., 2000) and Fe/Ti ratios (Boström, 1983) were used.

A model with four factors, which explains 73% of the initial variance of the data set, was adopted to assess the relationship between the different parameters (Fig. 39).

Factor 1 consists primarily of indicators reflecting potentially volcaniclastic and/or eolian input, as well as sea-level changes (Ti/Al, Zr/Al_2O_3 and Si/Al), but also includes the productivity proxies P_20_5* and Si/Al. The Mn/Al and Cr/Zr ratios, initially used as clues for hydrothermal input and redox conditions, have relatively high loadings on both Factor 1 and 2, suggesting a more complex behavior.

Factor 2 includes parameters commonly used as hydrothermal proxies, with “high” negative loading for the Al/(Al+Fe+Mn) ratio and high positive loading for the Fe/Ti ratio. The opposite algebraic signs are due to the inverse correlation between them. The moderately high

negative value for Al_2O_3 indicates that periods of intensive hydrothermal activity generally are coupled with low detrital input.

Based on the loadings of C_{org} and S, Factor 3 can be interpreted to reflect redox conditions, with higher deposition of C_{org} and authigenic sulfides during anoxic periods, and vice versa during times of normal water oxygenation. The only slightly higher loading of the Mn/Al ratio indicates that in the context of the investigated sections this parameter cannot be used as a reliable proxy for anoxia. (see, 4.3 and 4.5).

Factor 4 includes the V/Cr ratio, which commonly is used as an indicator for anoxic conditions. However, in this case it is not associated with the anoxia factor, but instead appears to be closely correlated with the detrital input, as expressed by the Al_2O_3 content of the sediment.

The results of the factor analysis are generally in agreement with the conventional interpretation and use of the proxy parameters, but in addition reveal some useful details on the complex interconnections among the different environmental indicators.
The results suggest that times of low detrital input and sea-level rise were generally coincident with stronger hydrothermal influence, and sometimes also with a higher eolian and/or volcaniclastic input and productivity.
Because the V/Cr ratio is not related to Factor 3 (“anoxia”), but rather to the Al_2O_3 content (detrital input), this indicates that it cannot be used without restrictions as an indicator for redox conditions. Similarly, nor variations in Mn/Al ratio can be assigned unambiguously to changes in degree of water oxygenation.
As pointed out before (see the section on the detrital input) in the German sections the increase in P_20_5*, Mn/Al and Si/Al is not correlated with the Ti/Al and Zr/Al_2O_3 values, which makes necessary the presentation and discussion of the results on individual sections.

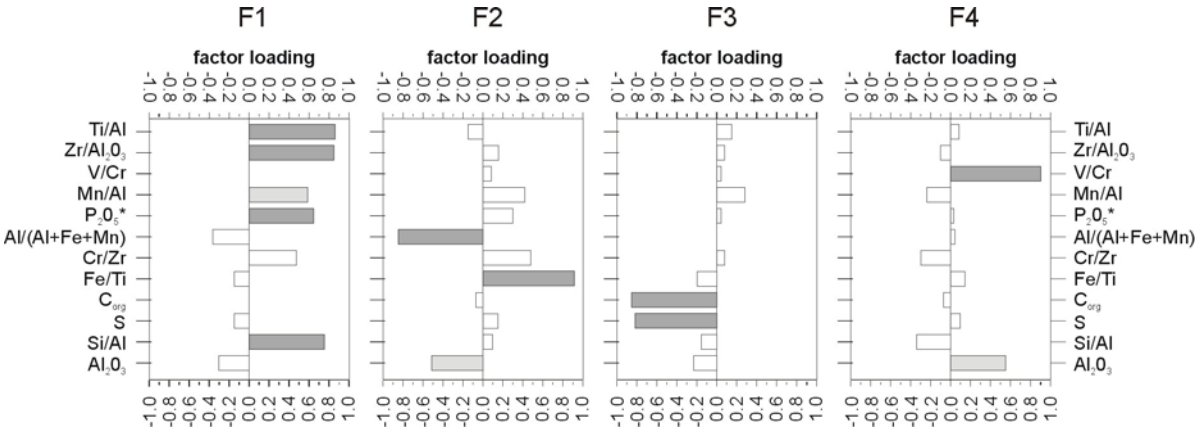

Figure 39. Factor loadings of the different standardized proxies/indicators used in the paleoenvironmental study.

A second factor analysis was applied (Fig. 40) in which we included also the major elements, the Mg/Al, K/Al and Ni/Co ratios. Again a model of four factors was adopted, which explains 70 % of the initial variance of the data set, was adopted to assess the relationship between the different parameters.

Factor 1 consists of major elements and represents the detrital input.

Factor 2 includes indicators previously interpreted as reflecting, in function of the context a volcaniclastic and/or eolian origin as well as sea-level changes (Ti/Al, Zr/Al_2O_3 and Si/Al), the productivity indicators (P_20_5* and Si/Al), the Mn/Al and Cr/Zr ratios to which are in addition the Mg/Al and K/Al ratios.

Factor 3 consists of proxies commonly used to detect a hydrothermal influence with a low value of the Al/Al+Fe+Mn ratio and a high value for the Fe/Ti. As previously, it is interesting to notice that this factor is positively correlated with most of the factor 2 indicators and inversely correlated with most of the detrital input indicators corresponding to the factor 1.

Factor 4 includes the C_{org} and S content. The inverse correlation between this two parameters and the MnO content give credence to the previous assumption that this factor could be linked to the deposition under anoxic conditions given that under anoxic conditions the manganese oxi/hydroxides are the first minerals dissolved.

This factor analysis gives the same relationship among the proxies or indicators than the first one and show once again that the V/Cr as well as the Ni/Co ratios cannot generally be used as anoxic condition indicators in the section studied. However, as mentioned for the first factor analysis, a log presentation is favoured to distinguish between the local and/or global aspect of the variations observed.

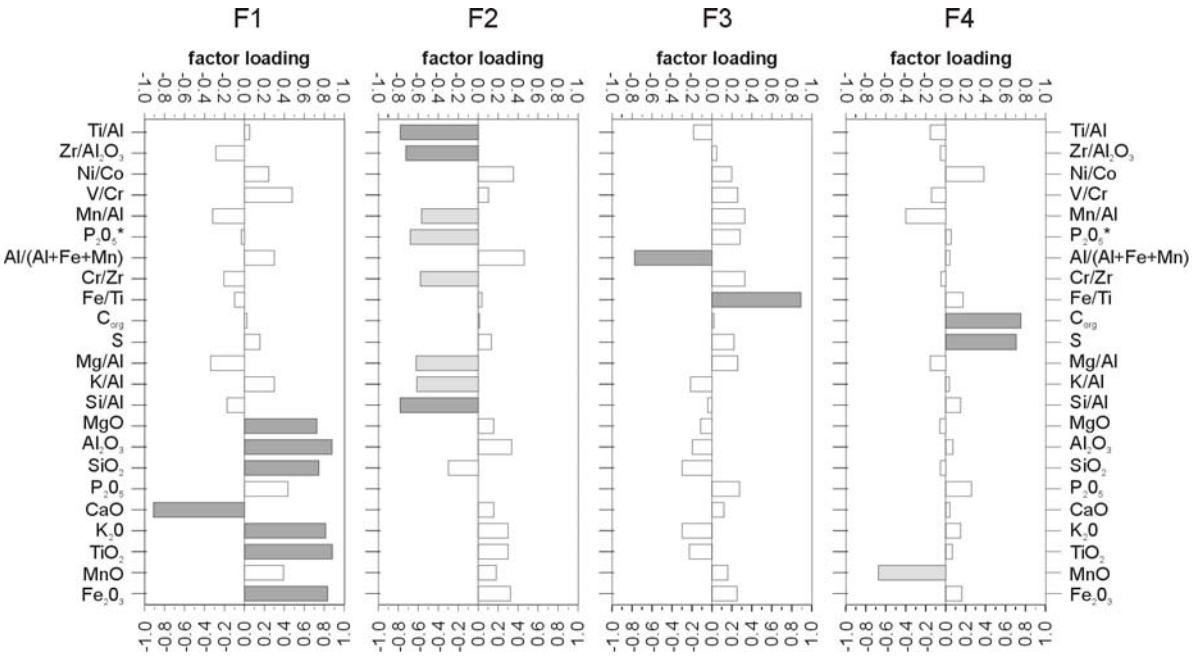

Figure 40. Factor loadings of the different standardized proxies/indicators used in the paleoenvironmental study and some others not presented before.

The results of the interpretation of the environmental indicators are summarized in table 5. Obviously, trends in C_{org} deposition are correlated with oxygenation level, as indicated by DOP values and observations with SEM. But it is interesting to note, that in the section of Steinbruch Schmidt, despite the relative increase in C_{org} content during the Kellwasser event, there is no change in parameters, which are indicative for the degree of oxygenation of the seawater. This could be due to the prevalence of dysoxic rather than anoxic conditions, which are difficult to distinguish unambiguously with the geochemical and mineralogical methods used in this study. The term “no change” used in the table refers to layers, which do not contain the last 5 cm of the UKWH, considered by Casier and Lethiers (1998) as anoxic. However, it is important to mention that according to our results the entire Upper Kellwasser Horizon was not deposited under anoxic conditions.

Factors \ Sections		Kowala: Kx section	Büdesheimer Bach		Steinbruch Schmidt		Coumiac: stratotype		La Serre: trench C	
		UKHH equivalent (eq)	UKWH	LKWH	UKWH	LKWH	UKWH	LKWH	UKWH	LKWH eq
Detrital input	Al_2O_3 (%)	-	-	-	-	-	-	-	-*	-
	Ti/Al	+	-	-	-	-	+	no change	+*	+
	Si/Al	+	no change	+	+	Variable (var)	+	-	(+)	+
Organic matter		-	+	+	+	+	+	no change	(+)	no change
					n.r				n.r	
Nutrients input or Paleo-productivity	P_2O_5*	+	no change	+	+	+	+	+	+*	+
			n.r							
	Ba*	+	+	+	+	(-) (var)	bdl	bdl	+*	+*
					n.r					
Hydrothermal signal	Al/(Al+Fe+Mn)	- 0.35	(-)	-	-	-	-0.35	-0.35	-0.35*	-0.35
	Cr/Zr	+	(+)	+	+	+	+	+	+*	+
Volcanic input (Zr/Al_2O_3)		+	-	+	-	-	+	no change	+*	+
Oxygen level (DOP; SEM; microprobe)		no change	-	-	no change	no change	-	-	-	?
Remark		Changes in paleoenvironmental factors common to all of the KWH include: (i) the decrease of the detrital input coupled with sea-level rise; (ii) increase of nutrient input and/or of productivity (iii) a stronger hydrothermal sig nal.								

Table 5. Summarized observations made in the Kellwasser Horizons from all the sections. bdl: below detection limit; n.r: not restricted to the Kellwasser Horizons; *: including La Serre 14 F1 early triangularis; (): no significant changes.

4.2. Discussion

The adopted geochemical multiproxy approach permits to postulate a relative sea-level rise coupled with higher nutrient input, the intensification of magmatic activity, as indicated by increased hydrothermal and volcanic influence as well as the development of a generally more oxygen deficient depositional environment during the deposition of the Kellwasser Horizons. We will confront in the following discussion our results to others geological and geochemical datas in order to finally draw a synthetic model of the F/F bio-crisis.

There are growing evidences that the Paleotethys was a semi-closed basin during the late Devonian (Fig. 1), bordered by the connection between Laurussia and Gondwana to the east (Young et al., 2000), by crustal fragments separating the Paleotethys from the Panthalassa (or Paleo-Pacific Ocean) to the west and by the Siberian and Kazakhstanian blocks to the north. In context of the frequent sea-level oscillations one must bear in mind this particular paleogeographic configuration, especially the shallow water depth at the passage between Laurussia and Gondwana to the east (Becker and House, 1994). In analogy to the opening of the Drake passage about 37 My ago, which is considered as the triggering factor for the profound changes in the climate-productivity pattern (Diester-Haass and Zahn, 1996), oscillation in water depth at this shallow passage between the two continental landmasses could have played a key role in the global paleoclimatic evolution of the late Paleozoic.

Changes in sea-level as postulated on basis of the detrital input can be hardly explained by changes in volume of the polar ice caps, because there are no evidences for glaciation until the middle of Famennian (Johnson et al., 1985; Becker and House, 1994). Nevertheless, the absence of evidence of glaciation during a considered geological epoch does not necessarily refute the occurrence of such glaciation, because glacial deposits are notoriously subject to reworking. Plate tectonic processes, like mid-plate uplift and submarine volcanism were associated in the Devonian with eustatic sea-level changes (Johnson et al., 1985). In a model of Cathles and Hallam (1991) short-term global sea-level fluctuations were attributed to stress-induced changes in plate density, associated with rapid rift formation. Racki (1998) reviewed the tectonic, volcanic and hydrothermal activity of this time slice and pointed out that tectonism received little attention to explain the puzzling features of the F/F boundary until now. But there is growing evidence for important tectonic and volcanic activity during the F/F transition in the East European Craton (Nikishin et al., 1996, Fig. 1) and in various

domains of Eurasia (Veimarn et al., 1997), and on a whole, some authors consider the related cataclysmic events as the primary cause for demise of the biota (Wilson and Lyashkevitch, 1996, Mahmudy Gharaie et al., 2004). A series of arguments can be brought which all support the possible occurrence of such events, like e.g., initiation of tectonic rifting (Bai et al., 1994; Wilson and Lyashkevitch, 1996), intensification of metallogenic processes (Chen and Gao, 1988; Turner, 1992; Veimarn et al., 1997; Racki, 1998), opening of major back arc basins (Sengör et al., 1998), intensive silicic exhalative volcanism and island arc volcanism (Racki, 1999a, Racki and Cordey, 2000; Algeo, 1996) as well as massive generation of continental flood basalts (Pripyat-Dniepr-Donets, Wilson and Lyashkevitch, 1996) and plume-influenced cratonic kimberlite and carbonatite emplacement (Kola Peninsula, Kramm et al., 1993). In agreement with these observations, our results also strongly support an enhanced hydrothermal and volcanic activity during the deposition of the KWH. These processes, in connection with a rearrangement of the lithospheric plates (Coffin and Eldholm, 1994; Sheridan, 1997; Kerr, 1998) and a reconfiguration of the subduction zones (Gurnis, 1990) characteristic for the late Devonian (Fig. 1), could be at the origin of the observed relative sea-level rise.

The change from a well-oxygenated environment to dysoxic / anoxic deposition conditions at the F/F boundary, as reported by several authors, cannot be always unambiguously ascertained by means of geochemical criteria. This uncertainty is due not only to the external input of hydrothermal elements, of which some are typically enriched also under anoxic conditions, but also to the positive feedback among hydrothermal processes and anoxia. Based on geochemical modelling, some authors (e.g. Carpenter and Lohmann, 1997) concluded that the flux of S, Fe, Mn, CH_4 and H_2 from submarine hydrothermal systems closely control the burial of organic carbon through the consumption of oxygen by inorganic and/or biologically mediated oxidation processes. Additionally, the relative solubility of oxygen in water is inversely proportional to temperature (with a relative decrease of about 2% for each 1°C; DeBoer, 1986), so that an increase in heat flow alone, due to hydrothermalism, could have lead to anoxia. Such a possibility was already proposed by some authors to explain the development of anoxic events in the Jurassic and Cretaceous oceans (Jones and Jenkyns, 2001).

Some authors have also pleaded for a possible connection between periods of intensive hydrothermal circulation and increased microbial activity (e.g., Burns et al., 2000). An

excessive bacterially controlled bioproductivity was noticed during the UKW crisis by Joachimski et al. (2001) and Whalen et al. (2002), while other authors proposed a model involving Fe-bacteria to explain the red pigmentation of the KWH observed at Coumiac and Pic du Visoux, France (Préat et al., 1999). Such kind of bacteria with a high biodiversity (Moyer et al., 1995) is reported from different modern environments. Iron bacteria are found today not only at active deep sea hydrothermal vents (Karl et al., 1988) and in association with ferromanganese concretions (Burnett and Nealson, 1981), but are common also at the water - sediment interface in deep, calm, dysaerobic waters (Ehrlich, 1990). EDAX analysis of bacteriogenic coatings on shells revealed a complex chemical composition with Fe, Mn, Mg, Ca, K, P, Si, S (Gillan and Cadée, 2000). Such kind of encrustations could have played a major role in the enrichment of some of the elements as described above. Metal toxicity, coupled with drop in water oxygenation had certainly disastrous consequences for living organisms. But also other negative vital effects due to an excessive bacterial activity, such as the decrease of swimming and burrowing ability of benthic organisms (Gillan et al., 2004), the promotion of shell dissolution by bacterial microborers (Knauth-Köhler et al., 1996) or promotion of diffusion of toxic S^{2-} ions into their bodies (Vismann, 1991) may have played an important role in the demise of the biota at the F/F boundary.

By lowering the water transparency or fostering bacterial activity and mucus production, the increase of nutrient availability / paleo-productivity may have had also contributed to a general biotic recession. As well known, water transparency is particularly important for reef building communities (Hallock, 1988). A connection between nutrient excess and microbial carbonate formation was documented in the Late Devonian of the Alberta Basin, Canada (Whalen et al., 2002), though an enhanced nutrient input can also lead to carbonate bioerosion and hiatus as suggested e.g., by Peterhänsel and Pratt (2001). Indications for an over-fertilization close to the F/F boundary are documented in the Morovian shelf, but also in other regions (Giles et al., 2002; Girard and Lécuyer, 2002; Ma and Bai, 2002; Racki et al., 1998, 2002; Racki and Cordey, 2000; Yudina et al., 2002). The role of Fe as an important micronutrient with a non-negligible control on productivity (de Baar et al., 1995) should be also taken into account when the causes for a possible over-fertilization of the late Devonian oceans are considered.

The source of an excessive input of nutrients however is still a matter of debate. The evolution of vascular land plants (Algeo et al., 1995), upwelling (Caplan et al., 1996; Giles et al., 2002), enhanced terrigenous supply (Girard and Lécuyer, 2002; Chen et al., 2005) or a

high volcano-tectonic activity (Becker and House, 1994; Wilson and Lyashkevitch, 1996; Racki et al., 1998, 2002, Racki and Cordey, 2000; Streel et al., 2000; Yudina et al., 2002; Ma and Bai, 2002; Mahmudy Gharaie et al., 2004) are the most frequently called reasons. According to Sageman et al. (2003) the fluvial nutrient input is mostly restricted to the near-estuarine environment, except for continental scaled watersheds like the actual Amazon River system. Therefore this hypothesis did not receive much attention as a possible source for an excessive nutrient increase at the F/F boundary. Additionally, the decrease in detrital input as observed in all of the sections, even including the more proximal facies of Büdesheimer Bach, speaks against a nutrient input coupled with increased terrigenous supply, though this argument could be refuted by assuming an enhanced influx of nutrients in dissolved form. In that sense Tribovillard et al. (2004) ascribed the enhanced influx of nutrients into the ocean to the Eovariscan episode of uplift and the associated intense denudation of continental crust. In this context a high flux of river born nutrients (particularly of P) to the ocean should be considered, which could have occurred due to the intensive chemical weathering that followed an excessive volcanic CO_2 exhalation and global warming (Filipelli, 1999; Jones and Jenkyns, 2001). But other causalistic chains, leading to high productivity can be also envisaged. A remobilisation of nutrients, like N or P from deep basins, under anoxic conditions (Ingall and Jahnke, 1997; McManus et al., 1998) followed by endo-upwelling seems plausible, especially if one keeps in mind the increase in the biomass of siliceous biota in some regions during this time (Racki, 1999a; Racki et al., 2002; Vishnevskaya et al., 2002). For Schieber (2000), the secular changes of the in situ quartz silt component should reflect variation in weathering and climate, as well as changes in the rate of sea floor spreading. The author mentioned that late Devonian carbonaceous mudstones of the North American continent present in several localities an anomalous quartz content showing an authigenic origin.

In their model Riquier et al. (in press) combined the effect of both tectonic activity (uplift of the Eovariscan belt) and anoxia to explain the increase of nutrient input at the F/F transition. Alternatively, eutrophication due to an excessive release of P, Fe or Si from volcanic ash can be considered (Frogner et al., 2001), as supported by the distinct volcanic / hydrothermal signal at the F/F boundary. To account for periods of high biological productivity and oceanic anoxic events which occurred frequently during Jurassic and Cretaceous times, Jones and Jenkys (2001) proposed a model according to which these critical episodes resulted as a combined effect of over-fertilization by an excessive input of Fe due to the enhanced production of oceanic crust and the associated hydrothermal activity, coupled with the

development of upwelling zones due to increased zonal wind velocities under global warming conditions.

As discussed before, some of the observed environmental changes at the F/F boundary, like e.g., the high metal contents, can represent the concurring effect of different factors, including specific redox conditions, high bio-productivity and intensive bacterial and/or hydrothermal/volcanic activities (Gillan and de Ridder, 2001). The interaction between these factors makes the environmental interpretation of single geochemical signals often ambiguous. Our results emphasize the necessity for using a multiproxy approach for a variety of different paleogeographic settings in order to avoid misinterpretations and to recognize paleoenvironmental trends of global relevance. Additionally, the use of a multiparametric geochemical approach permits to carry out more reliable stratigraphic correlations, like e.g., in the case of Bank 9 of the La Serre section, which turned out to correspond to the KWH not only in terms of detrital and nutrient input, but also in respect of the intensity of volcanic and hydrothermal influence. Such a correlation was not possible before using only discrete geochemical parameters, like the content in organic C.

Based on the results presented before, we favour a model in which we assign a key role to endogenous/ magmatic processes in order to explain the environmental changes which took place at the F/F boundary in the area between the south of Laurussia and north of Gondwana. The endogenous hypothesis was already proposed by several authors to explain the KW crisis (Whyte, 1977; Dvorak et al; 1988; Garzanti, 1993; Becker and House, 1994; Racki, 1998, 1999a). Others combined the endogenous model with ascribing an additional role to an increased nutrient input and/or a thermal stimulus produced by a massive submarine volcanism and associated phenomena (Vogt, 1989; Coffin and Eldholm, 1994; Vermeij, 1995, Racki, 1999a). There are also some analogies with the model of Kerr (1998), which relate the environmental changes at the Cenomanian-Turonian boundary to the physical and chemical processes connected to the formation of large igneous provinces. Studying the Devonian of the Montagne Noire, Becker et al. (1994) pointed out the possible role of intraplate volcanism in the development of dysoxia/anoxia and in the occurrence of rapid sea-level fluctuations during the Kellwasser crisis. They traced back the related environmental changes to a variety of mechanisms, like cratonic over-flooding, climatic overheating, upwelling and eutrophication in a quasi-Pangea like configuration of the Paleotethys. The model presented (Fig. 41) synthesizes the processes already advanced to explain the F/F biotic crisis. Long

term and short-term events have to be differentiated. Among the environmental changes at the origin of the geochemical variations recorded in the Kellwasser Horizons, the rapid sea-level fluctuations seem to be the most important parameter. According to current findings, pulses of continental rifting could explain the rapid eustatic oscillations recorded in the Kellwasser Horizons. However, House (2002) favoured a common explanation to all of the late Devonian events, relating the observed transgression-regression cycles to orbital forcing. Other hypotheses, like the development of land plants or tectonic processes are not adequate to explain short-term variations and irrefutable arguments for an impact or multiple impact hypotheses are still lacking. Based on the paleogeographic reconstruction (Fig. 2), the relative sea-level rise during the KW event as indicated in this study by the decreasing detrital input, could have led to the reconnection of bottom water circulation between the Paleotethys and the western part of Panthalassa, and to a flooding of the southern shores of Laurussia and the northern parts of Gondwana by water enriched in nutrients, metals and impoverished in oxygen (Fig. 41). The driving mechanism for the bottom water circulation could reside in difference in salinity gradient, similar to that between the modern Mediterranean and the Atlantic Ocean. The similarities observed in the development of the Kellwasser Horizons in France or Morocco (Riquier et al., in press), could be due to the particular paleogeographic configuration of the area, while distinct features of the individual sections can be attributed to differences in distance to the source of volcanism / hydrothermalism, in bottom water currents (basin morphology, presence of barriers, etc.), in geomorphology or tectonic (proximity of mountains ranges, etc.) and in signal preservation (Zimmerle, 1985).

Finally, the adaptation of the model presented to the others late Devonian events could prove to be interesting.

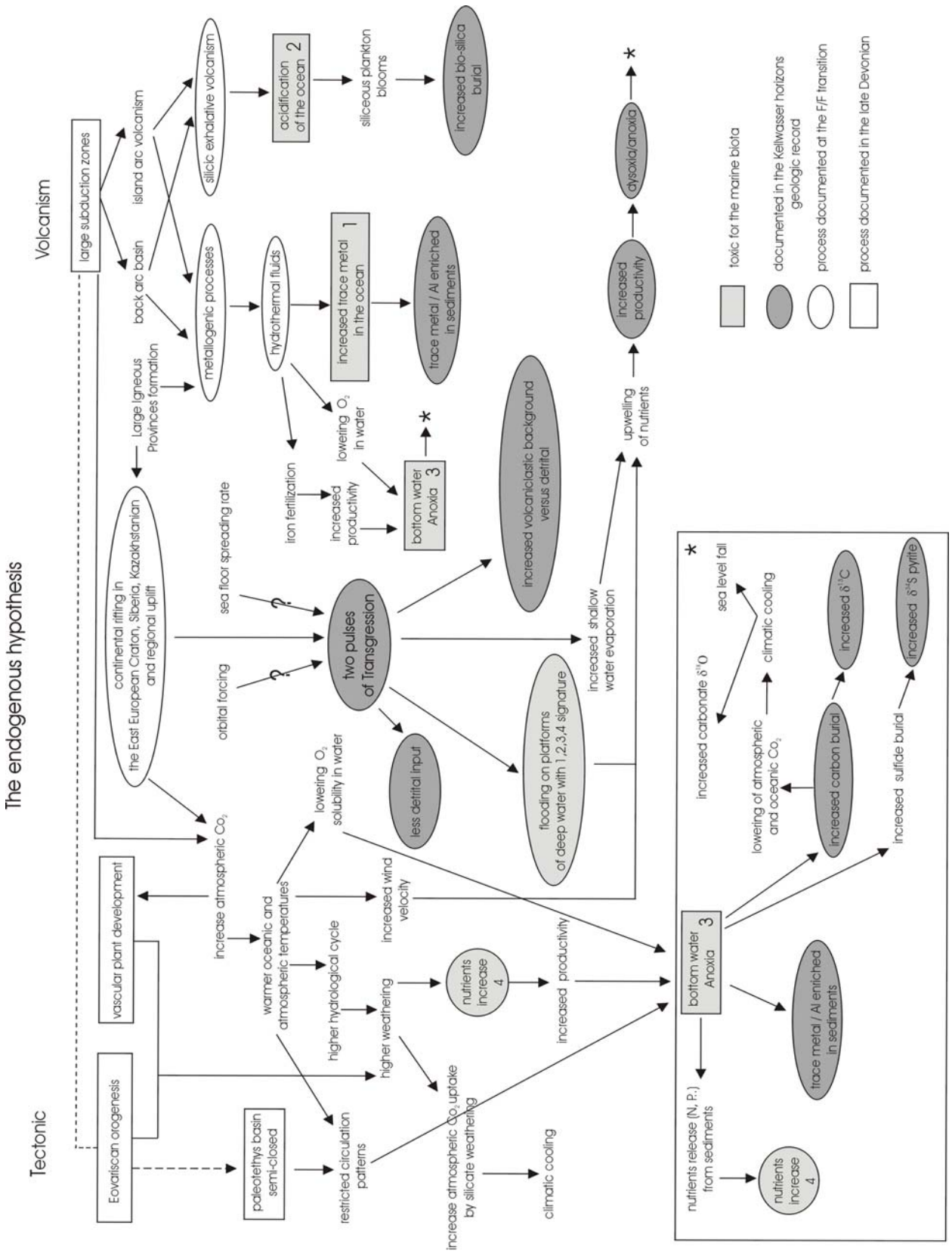

Figure 41. Flow-chart illustrating the possible links between different processes documented in the Late Devonian or at the F/F transition, the characteristics of the Kellwasser Horizons and the induced environmental stress for the marine biota.

III. Pyrite geochemistry at the Frasnian-Famennian boundary (the Büdesheimer Bach section)

The second part of the thesis presents the results of a study on the geochemistry of pyrite at the F/F boundary in the Büdesheimer Bach section. After presentation of the state of the art concerning the geochemistry of pyrite, the different methods used will be described. Finally the potential of the trace element spectrum of authigenic pyrite preserved in the sediments will be evaluated as a source for supplementary information on depositional conditions.

1. Geochemistry of authigenic pyrite – a state of the art

1.1. Conditions of pyrite formation

As reviewed in paragraph 4.1.4 different geochemical indicators or proxies can be used for the characterisation of the depositional conditions or for the reconstruction of redox conditions like certain element ratios in host rocks (e.g., Mo/Al, V/Cr, Ni/Co, U/Th, DOP, etc). Nevertheless, diagenetic and post diagenetic remobilisation of elements in the sediments can lead to substantial problems using data from bulk sediments (e.g. Alberdi Genolet and Tocco, 1999; Lüschen et al., 2001; see also 4.1.4 and 4.1.5). Pyrite represents a chemical homogeneous matrix and its trace element content is not changed substantially even if affected by metamorphic overprint (Berner, 1993). Consequently, the content of trace elements in pyrite for clarifying genetic questions has the advantage that samples of very complex composition and different nature can be compared directly, without having to take into consideration matrix effects or drastic late post-diagenetic changes. Only a stronger metamorphic remobilization can lead to substantial changes in the composition of certain trace elements, e.g., to a preferential uptake of Co by pyrite and of Ni by pyrrhotin (Loftus-Hills and Solomon, 1967; Bralia et al., 1979).

Pyrite can result from very different mechanisms and is stable or metastable over broad temperature and pressure ranges, and at well-defined pH and Eh conditions (e.g., Barton and Skinner, 1979; Barker and Parks, 1986). Pyrite is an almost ubiquitous mineral, which can be

found in magmatic, sedimentary and metamorphic rocks. The use of trace element pattern of pyrite as a genetic fingerprint in exploration was documented in many cases (e.g. Huston et al 1995; Ho et al 1995; Murao et al 1996; Barton and Hallbauer 1996; Mongenot et al., 1996). It is reasonable to assume, that sedimentary pyrite may yield information on the sedimentation environment. Pyrite in sedimentary rocks can be of authigenic (syn /diagenetic), detritic or epigenetic origin. The mechanisms of formation of sedimentary pyrite were already examined in detail (e.g. Berner 1970; Berner, 1984; Goldhaber and Kaplan, 1974; Raiswell and Berner, 1985; Morse et al., 1987; Schoonen and Barnes 1991, Fig. 42).

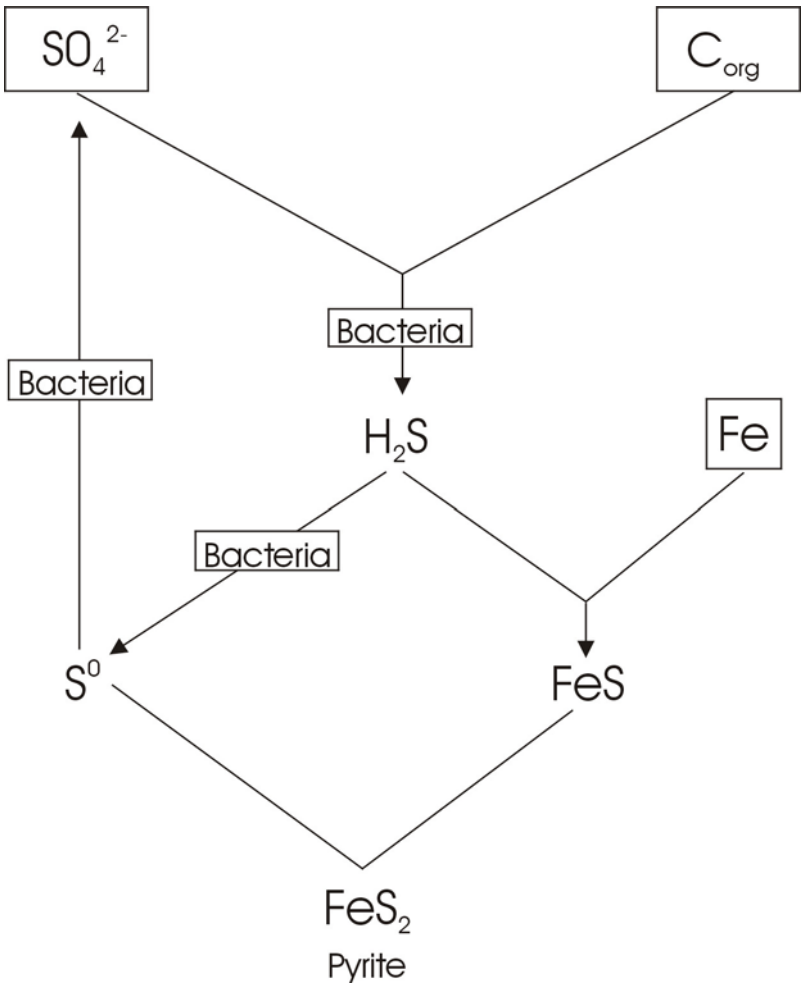

Figure 42. Representation of the overall process of sedimentary pyrite formation (modified after Berner, 1970).

Authigenic pyrite forms due to bacterial sulfate reduction in a strongly anoxic sulfidic environment. Syngenetic pyrite can form in anoxic bottom waters already above the water/sediment interface. But pyrite can develop in early stages of diagenesis also under normal marine conditions, within the sediment, when due to the bacterial mineralization of

organic matter a reducing microenvironment suitable for sulfate-reducing bacteria develops. The authigenic pyrite genesis runs over the intermediate stage of metastable Fe-sulfide-phases (Mackinawit, Greigit, Shoonen and Barnes, 1991) and leads finally to formation of framboidal to euhedral crystals or crystal aggregates (Sawlowicz, 1993; Wilkin and Barnes, 1997). Several publications (Wilkin et al., 1996; 1997; Wilkin and Barnes, 1997) deal with the conditions and mechanisms of formation of framboidal pyrites. Beside a direct precipitation of dissolved Fe^{2+} with the biogenically produced H_2S, a direct sulfidisation of iron oxides is also possible (Morse and Arakaki, 1993; Huston et al., 1995). The authigenic pyrite genesis is a redox sensitive, microbiologically controlled process and is in close quantitative relationship with the microbially metabolisable organic carbon, the sulfate and the reactive iron supply in the sedimentation environment. From the interaction of these factors in pelitic siliciclastic sediments, result a simple linear correlation between the proportion of metabolisable organic carbon and the reduced sulfate, bound as pyrite. In addition to the earlier investigations of Berner (1970) and Goldhaber and Kaplan (1974), there is a very extensive literature on this topic (e.g. Berner, 1982; 1984; Berner and Raiswell, 1984; Anderson et al., 1987; Raiswell et al., 1988; Morse and Emeis, 1990; Lyons and Berner, 1992). The pattern of the C_{org} vs S regression line (slope and intercept) depends on the given redox conditions, on the Corg, Fe and sulfate supply as well as on the sedimentation rate (Goldhaber and Kaplan 1974; Leventhal, 1983; Raiswell and Berner 1985; Middelburg, 1991; Morse and Berner, 1995). Therefore the C_{org}/S ratio in sedimentary rocks was extensively used as proxy for paleoenvironmental reconstructions (Berner and Raiswell, 1984; Raiswell and Al-Biatty, 1989; Raiswell and Berner, 1986; Donelly et al 1988; Goodfellow, 1987). Leventhal (1987), Anderson et al. (1987), Raiswell and al-Biatty (1989), Chowdhury and Noble (1996) and Alaasm et al (1996) applied the method to Paleozoic sequences.

The sulphur isotopic composition of pyrite can provide also additional information about the depositional conditions during their formation and was already applied to constrain the environmental changes associated with the Kellwasser Event (Geldsetzer et al., 1987; Wang et al., 1996, Joachimski et al., 2001).

1.2. Trace elements study in sedimentary pyrite

Contrary to the abundance of work on the formation of the sedimentary pyrites, a relatively small number of publications is dealing with the trace element incorporation in

pyrites (e.g. Dill and Kemper, 1990; Huerta Diaz, 1989; Harrison, 1991; Huerta Diaz and Morse, 1992; Morse 1992, 1994; Berner and Puchelt, 1995; Graham and Robertson, 1995; Rickard et al., 1995; Dill et al., 1996, Barton and Hallbauer, 1996; Sternbeck et al., 2000). Authigenic pyrite has proven to be an important sink/trap for many trace elements.

Trace elements in pyrite can occur in the following forms (Huston et al., 1995): (1) as micro inclusions of independent metal sulfides (e.g. Cu, Zn, Pb, Ag, Bi, Sb), (2) surface adsorption and (3) coprecipitation, and formation of "solid solutions". The lattice substitution can take place stoichiometrically (Co, Ni for Fe and Se, Te replacing S) or nonstoichiometrically (e.g. As, Tl, Au, Mo).

Theoritical and experimental works on the inclusion of trace elements in authigenic pyrite was carried out particularly by the working group of J.W. Morse (Morse et al., 1987; Huerta-Diaz, 1989; Huerta-Diaz and Morse 1990; 1992; Kornicker and Morse, 1991; Morse, 1992, 1994; Akaraki and Morse, 1993; Morse and Akaraki, 1993; Cooper, 1998; Cooper and Morse 1998; Morse and Luther, 1999). Owing to the work of this group, there are not only numerous case studies, which document the different behavior of trace metals during pyritization, but also put the theoretical, physico-chemical bases of the adjustment of trace elements incorporation in iron sulfide during diagenesis (Kornicker and Morse, 1991; Akaraki and Morse, 1993; Morse and Akaraki, 1993; Morse and Luther, 1999). The experiments showed that the fixation of dissolved trace elements by mackinawit (the metastable precursor of the pyrite) are essentially linked to adsorption and coprecipitation processes. The adsorption takes place along a Langmuir isotherm. The surface affinity for bivalent cations, whose sulfides have a higher solubility than Mackinawit, is very similar (Mn^{2+}, Mg^{2+}, Ca^{2+}), whereas such with lower solubility (Cd^{2+}, Co^{2+}, Cr^{3+}, Cu^{2+}, Ni^{2+}, Zn^{2+}) show a surface affinity inversely proportional to the solubility of their sulfides. The adsorption constants of the elements at pyrite surfaces have been defined in the order Co>Cd>Mn>Ni>Ca>Zn (Kornicker and Morse, 1991).

The distribution coefficients of the most important elements e.g., which are included in pyrite by coprecipitation as "solid solution" (Mn, Co, Ni), have also been determined (Akaraki and Morse, 1993; Morse and Akaraki, 1993).

The distribution coefficient D is defined as:

$$D = \frac{\left(\frac{X_{Me}}{X_{Fe}}\right)_{Solid}}{\left(\frac{a_{Me^{2+}}}{a_{Fe^{2+}}}\right)_{Solution}}$$

where: - X_{Me} and X_{Fe} are the respective mol proportions in the solid phase

- a_{Fe}^{2+} and a_{Me}^{2+} are the activities of Fe^{2+} metals in the solution.

Similarly to the surface affinity, the distribution coefficients of the elements are inversely proportional to the solubility of their sulfides. The inclusion of different trace elements in pyrite is influenced apart from the metal availability and redox conditions also by the presence of other competitive mineral phases. In order to parameterize and characterize the uptake behavior of the elements, Huerta Diaz and Morse (1990) defined, in analogy to the degree of pyritization (Berner, 1970), the degree of trace metal pyritization (DTMP).

It is defined as follow:

$$DTMP(\%) = \frac{Pyrit_{Me}}{Pyrit_{Me} + Reactives_{Me}}$$

Pyrite $_{Me}$ = metal content in pyrite

Reactive $_{Me}$ = metal content in reactive (i.e. not silicate) phases

The DOP shows in which proportion non-silicate (reactive) iron is pyritised. Similarly to DOP, the DTMP is a measure for the proportion, of the non-silicate bound trace element in pyrite. These parameters permit a quantification of the transfer of Fe or of trace elements into pyrite, and in comparison to the total element concentrations they consider only the reactive proportion of elements.

The trace elements incorporated in pyrite can be separated in three different groups (Huerta Diaz and Morse, 1992):

1) As, Hg and Mo show a high affinity for pyrite and are almost completely taken up by pyrite, independently of the DOP and sedimentation environment. These elements are clearly enriched in pyrite in comparison to the total sediment.

2) The DTMP of the metals Co, Ni, Cu and Mn show a clear linear dependency on DOP and are approximately similarly distributed between pyrites and the other reactive mineral phases.

3) The elements Pb, Zn, Cd and Cr form their own sulfide inclusions and are generally depleted in pyrite in comparison to the bulk sediment.

The different DTMP is not only due to element-specific thermodynamic characteristics, but is also linked to differences in kinetics of the ligand exchange reactions and to the variety of the possible redox reactions (Rickard et al., 1995; Morse and Luher, 1999). So, because the water exchange kinetics of hydrolysed Pb, Zn and Cd complexes (elements only slightly pyritised) are higher than those of the hydrolysed Fe^{2+}, these elements will already form independent sulfides before the precipitation of Fe-sulfides. In the opposite way, Co and Ni with slower water exchange kinetics are incorporated to higher degree into pyrite. Elements such as Mo and As, which are present as oxyanions, must be first reduced by sulfides before they are built in pyrite.

Between DOP or the DTMP values and the sedimentation conditions exists a complex connection, which requires still further research. In a recent study, the trace element content of pyrite was used successfully as proxy for modifications of redox conditions in Holocene sediments (Sternbeck et al., 2000). Even with well-known distribution coefficients and adsorption isotherms the trace element contents in the authigenic pyrite do not permit an accurate reconstruction of element contents in pore or in seawater. However relative changes in concentration, which are of key importance in the “Event research”, should be sensitively

marked by elements with high DTMP, because these are built in pyrite completely, i.e. only as a function of availability (Huerta-Diaz and Morse, 1992; Stüben et al., 2002).

Thus, with the help of this approach it should be possible to get additional information on the hydrogeochemical changes at the Frasnian/Famennian boundary. Unfortunately, the presence of pyrites only in a few banks in Steinbruch Schmidt (23, 55, 56) and the absence of pyrites in late Frasnian and early Famennian at Kowala did not permit to systematically investigate these sections.

2. Methods

2.1. Inductively Coupled Plasma Mass Spectrometry (ICP-MS) analysis

Trace elements in pyrite:

Trace element contents in pyrite were determined in grains (different morphology) and pyritized fossils. About 10 mg of cleaned and fine ground pyrite grains was digested in 2 ml of subboiled HNO_3 (65% vol.) and 50 µl of bromine over night. After complete dissolution, the solution was evaporated to almost dryness and was taken up in 10 ml of 1% vol. HNO_3. In all steps, only suprapur quality chemicals and bi-distilled water were used. Trace element concentrations were analysed by high resolution ICP-MS (AXIOM).

Reactive trace elements:

Based on literature data and on results of preliminary tests, a modified method of Berner (1970) and Anderson et al. (1987) wad used. Reactive part of the elements was extracted from 100 mg of sample using 5 ml of hot 12 N HCl. After boiling the solution was added with 5 ml of bidestilled water, centrifuged and 2 ml removed and filled up with bidestilled water in a 100 ml volumetric flask. Trace element concentrations in the reactive part were analysed by high resolution ICP-MS (AXIOM). The degree of pyritization (DOP) was calculated as DOP = $Fe_{pyrite}/(Fe_{pyrite} + Fe_{reactive})$. Pyrite bound Fe ($Fe_{pyrite}$) was approximated by multiplying the S content with 0.871.

Standard solutions with known elements concentrations were used for calibration. Rh, In, Tm and Bi were used as internal standard to correct for physical matrix and oscillations in signal intensity. Solutions with 5 ppb or 25 ppb concentrations and blank solutions were analysed after every 5 samples. A procedurial blank was prepared for all analysis and the result substracted from the samples results. Each sample was analysed three times and the raw counts were processed and transformed to concentration values using the Thermo Elemental PlasmaLab software. The accuracy of the ICP-MS measurement was cheked with the certified standard sample TDMW (HPS, USA) and was found to be within ± 5%. The precision of the analysis, as determined by repeated measurements of the samples was found to be < 5%. A more detailed example is given in the following table, which illustrates the variability of the different element results in terms of accuracy and precision (5 ppb standard solution).

	Mg	V	Cr	Mn	Fe	Co	Ni	Cu	Zn	As	Se	Sr	Mo	Ag	Cd	Sb	Ba	Tl	Pb	Th	U
Standard deviation (ppb)	0.13	0.14	0.07	0.13	0.29	0.18	0.13	0.30	0.27	0.20	0.29	0.12	0.30	0.22	0.33	0.18	0.33	0.24	0.12	0.12	0.02
Accuracy (±%)	7.9	2.8	1.4	1.3	1.9	3.2	5.4	8.6	8.6	2.3	7.2	0.5	3.0	7.7	1.6	10.1	1.8	5.9	2.8	3.1	0.7
Precision (±%)	2.4	2.9	1.4	2.5	6.0	3.5	2.4	5.6	4.9	3.8	5.3	2.4	5.9	4.2	6.6	3.2	6.4	4.5	2.3	2.4	0.4

Table 6. Example of the ICP-MS trace elements results characteristics from 5 ppb standard solutions.

2.2. Isotope Ratio Mass Spectrometry

The isotopic composition of S in pyrite was measured in splits of samples used for trace element determination. For that a technique was applied in which an elemental analyser in continuous-flow mode was connected by an open split to the mass spectrometer. This method is detailed in Leosson (1999) and Berner et al. (2002).

$$\delta^{34}\mathrm{S}\ (\text{per mille CDT}) = \left(\frac{\left(34S/32S\right)sample}{\left(34S/32S\right)standard} - 1 \right) \times 1000$$

CDT (Canion Diablo Triolite) was used as standard.

The internal laboratory standard used was a cadmium sulfide (CdS) with a δ^{34}S value of 10.8 ‰ relative to the Canion Diablo Triolite (CDT). Each sample was analysed three times and standard deviation was generally < 0.2‰. The standard deviation of the internal standard is about 0.1‰. The accuracy of the analysis is about ± 0.05‰.

2.3. Synchrotron µ-XRF (ANKA, Karlsruhe)

Pyrites of different morphologies were prepared for the synchrotron measurement. The pyrites aggregates or fossils were fixed in an epoxy resin and polished to a precise thickness of 100 µm. The semi-quantitative concentration of the elements was evaluated by Dr. Utz. Kramar according to the following procedure. The calibration line was established using the STHS6 (Saint-Helene andesitic ash glass) and the ATHO-G (Iceland rhyolite glass) standards. The KL2-G (Kilauea tholeitic basalt glass) standard was also used for checking. The slope of

missing elements was obtained by interpolation. A correction of the pyrite matrix effect was applied. Finally, the ICP-MS results were compared to the synchrotron μ-XRF analysis results (the mean of the points measurement) for the same sample.

2.4. Statistical methods

The software package STATISTICA (StatSoft Inc., USA) was used to assess the relationship between the trace elements in pyrites and parameters like the DOP, the DTMP and the environmental proxies used in the first part. For that multivariate statistics was performed using the factor analysis. To facilitate the interpretation of the loadings the factor axis were rotated by the normalized Varimax method. The cluster analysis method was also used with the complete linkage and 1 Pearson-r options.

3. Results and interpretation

This chapter presents the results of the pyrite geochemistry in the Büdesheimer Bach section. The parameters studied are the reactive fraction, the degree of pyritization (DOP), the trace element contents in pyrites, the degree of trace metal pyritization (DTMP) and the sulphur isotopic composition of pyrites.

3.1. Discrimination between authigenic and epigenetic pyrite

In order to obtain possible paleoenvironmental information from the trace element pattern of pyrite, it was necessary to discriminate authigenic and epigenetic pyrite. Three different methods were used. The first method considers the relationship between the Corg and S contents (Fig. 43). A high content of S not correlated to the Corg content reflects a late enrichment of S and the presence of epigenetic pyrites, which must be excluded when expecting to acquire information based on the trace element content in pyrites. Such discrimination is particularly important in calculating the DOP, because a late enrichment in S and Fe leads to an overestimation of the DOP. Secondly, normally correlated to the S (Belzile and Lebel, 1986), it is presumed that epigenetic pyrite contains less amounts of some trace elements (like As), because at the time of their formation these trace elements were already incorporated in the sediment (Fig. 44). Lastly, a simultaneous high DOP and high reactive iron indicate also the presence of late diagenetic pyrites (Fig. 45). Based on these criteria only 23 pyrite samples have been considered for environmental interpretation out of 47. A comparison of the different discrimination methods revealed that the samples considered as containing late diagenetic pyrites are the same in the three cases. These methods are a useful tool for any study that focus on pyrites or trace elements in pyrites as a mean to differentiate the primary signal from the late or post-diagenetic signal in the sediment record.

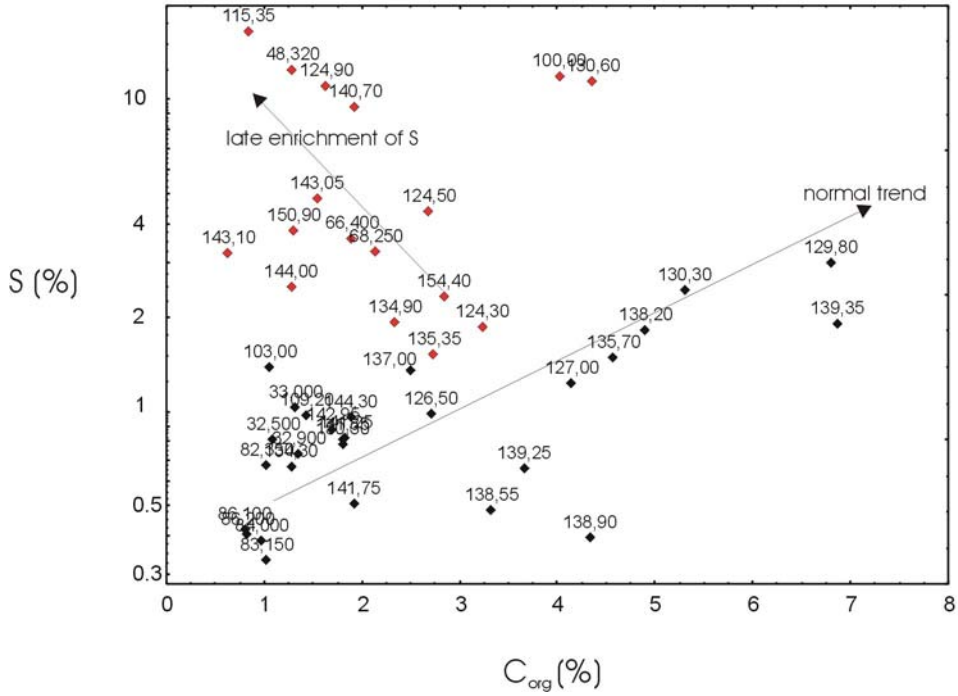

Figure 43. Crossplot of C_{org} (%) content vs. S content (%) in the host rock used to discriminate authigenic and epigenetic pyrites. The red dots correspond to the samples not considered for pyrite investigations.

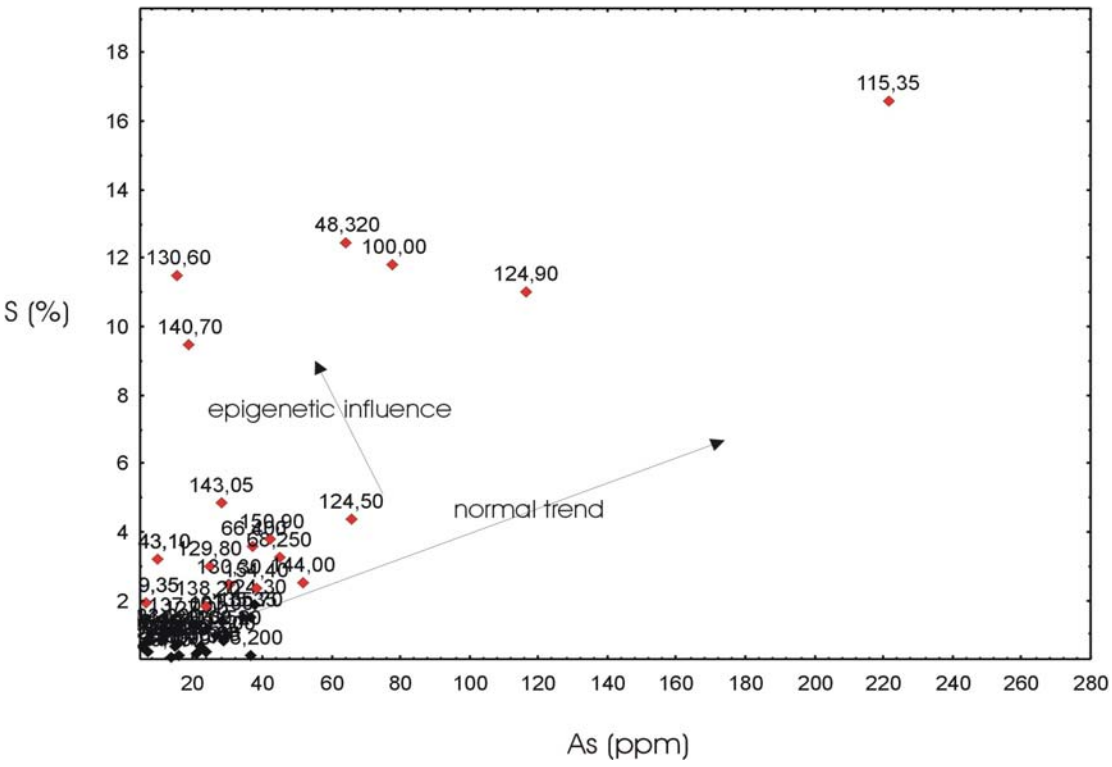

Figure 44. Crossplot of As content (ppm) vs. S content (%) used to discriminate authigenic and epigenetic pyrites. The red dots correspond to the samples not considered for pyrite investigations.

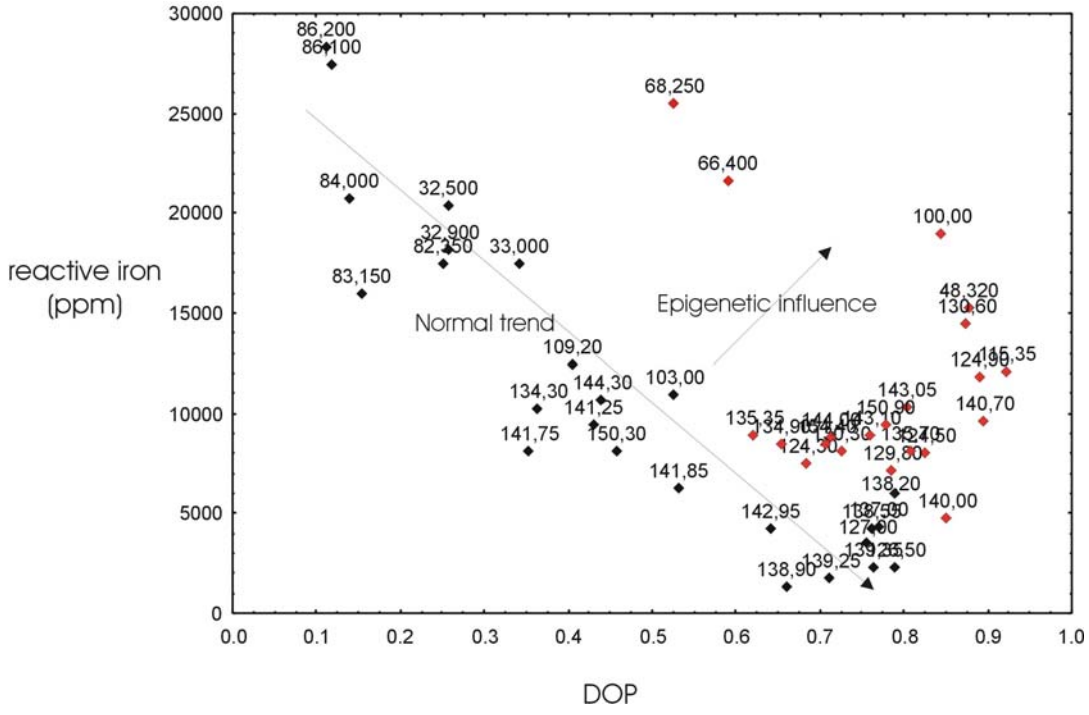

Figure 45. Crossplot of DOP vs. reactive iron content (ppm) used to discriminate authigenic and epigenetic pyrites. The red dots correspond to the samples not considered for pyrite investigations.

3.2. Morphology of pyrite

Several types of pyrites were extracted from the host rock in terms of morphology. The pyrite samples from the Kellwasser Horizons are mainly tiny cubic crystals, veins or aggregates of cubic crystals, whereas the other samples contains essentially pyritized fossils (Fig. 46). This observation is important because of the different mechanisms of formation involved in each case. Indeed the pyrites samples from the Kellwasser Horizons are supposed to have precipitated under anoxic conditions principally at or below the water/sediment interface, given that no framboidal pyrites were investigated because of their scarcity and their reduced sizes. This authigenic pyrites can be formed either through the intermediate stage of metastable Fe-sulfide-phases (Mackinawit, Greigit, Shoonen et al., 1991) leading finally to the formation of framboidal to euhedral crystals or crystal aggregates (Sawlowicz, 1993; Wilkin et al., 1997) or by the sulfidisation of Fe oxides (Morse and Arakaki, 1993; Huston et al., 1995). The pyritized fossils have precipitated in early stages of the diagenesis under normal marine conditions when due to bacterial mineralization of their organic remainders in the sediment a reducing microenvironment suitable for sulfate-reducing bacteria develops. They should therefore reflect partly the geochemical signal of the organic matter. In the

publications dealing with pyrite geochemistry including the S-isotope investigation, it is surprising that the morphology of the pyrites studied as well as an attempt to discriminate between authigenic and late diagenetic pyrites is often missing (see the previous paragraph). In the articles concerning the F/F boundary an increase of $\delta^{34}S$ was observed in the Kellwasser Horizons in several sections (Wang et al., 1996; Joachimski et al., 2001, etc..). The interpretation of this isotopic signal should take into account the information given by the morphology of pyrite concerning the site and mechanism of the pyrite formation.

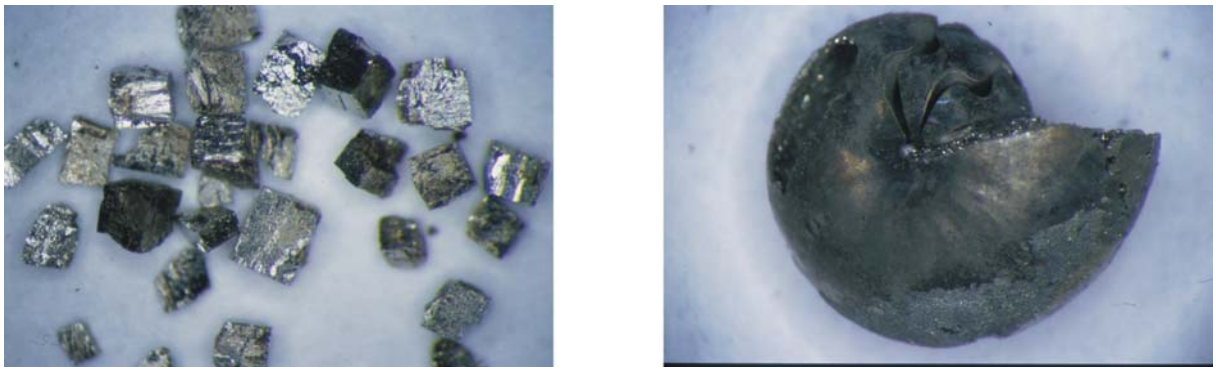

Figure 46. Example of cubic pyrite crystals present in the LKWH (depth 138.2 m, left) and of pyritized fossils (depth 86.1 m, right).

3.3. Reactive trace element

The reactive trace element contents were investigated essentially to calculate the degree of pyritization and the degree of trace metal pyritization. The reactive fraction corresponds mainly to the non-silicate bound iron, including amorphous iron oxides and oxi/hydroxides, some crystalline iron oxides as well as iron monosulfides, carbonates, manganese oxi/hydroxides and hydrous aluminosilicates (Canfield, 1989; Huerta-Diaz and Morse, 1992). The fraction adsorbed to organic matter is recovered in the reactive or HCl fraction. The statistical tool was used to assess the relationship of this extracted fraction with different parameters.

3.3.1. Inter-element dependency

To characterize the reactive fraction 20 elements (Mg, V, Cr, Mn, Fe, Co, Ni, Cu, Zn, As, Sr, Mo, Ag, Cd, Sb, Ba, Tl, Pb, Th, U) were analysed by ICP-MS.

The inter-element relationship was obtained by cluster analysis (Fig. 47). It is important to notice here that the cluster analysis links only the elements positively correlated, consequently a factor analysis was necessary to take into account inverse correlation among elements.

The elements grouped with reactive Fe are enriched in Fe oxides and oxi/hydroxides phase, whereas the elements grouped with Sr represent the elements enriched in the carbonate fraction and those grouped with Mn must be enriched in the Mn oxides fraction.

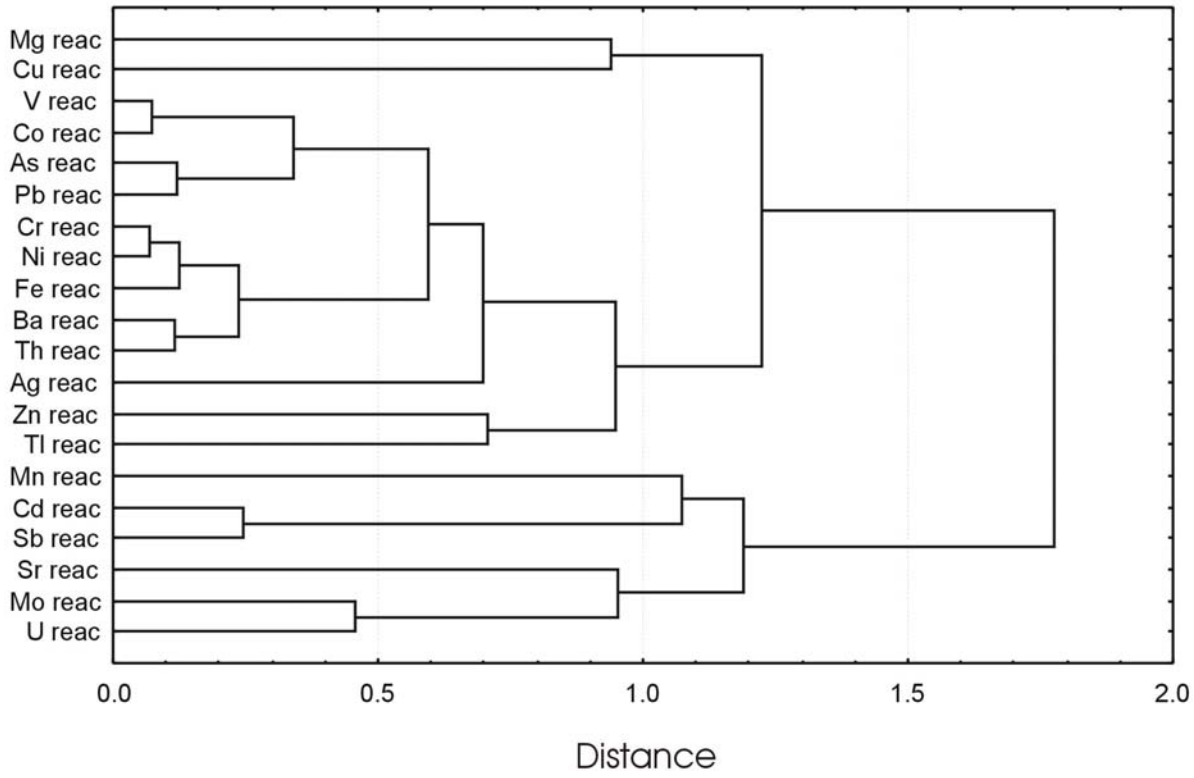

Figure 47. Tree diagram of the reactive elements fraction by complete linkage and 1-r Pearson methods.

3.3.2. DOP relationship

The inverse correlation observed between reactive Fe and reactive Sr by factor analysis indicates that the onset of anoxic conditions was coupled with enhanced carbonate deposition. Consequently, the decrease in the reactive element contents associated with the decrease in reactive Fe reflects either more reducing conditions (implying a higher degree of pyritization)

or a decrease in the detrital input (lower input of reactive phases). We have already shown in the paleoenvironmental study (chapter II.4) that relative sea-level rise and onset of anoxic condition were coupled.

The increase of the Mo/Al and U/Th ratios in the host rock are commonly used as indicator of reducing conditions (Algeo and Maynard, 2004; Cruse and Lyons, 2004). These both elements are associated in the reactive fraction with Sr and DOP (Fig. 48). The U reactive contents are sometimes increasing due to the deposition of phosphate (e.g., samples 84 and 86.1), but are also enriched in some samples of the LKWH. The increase of U in black shales has been ascribed recently to low and fluctuating oxygen regime and extremely low sedimentation rates (Fisher and Wignall, 2001). The U reactive versus Th reactive ratio presents an increase in samples with high DOP values (Fig. 48). Associated to the Sr reactive, it could mean that the carbonate fraction of the LKWH is enriched in U relative to the Th. However we cannot be sure of the U origin, which is present in the form of Uraninite (UO_2) or a metastable precursor under anoxic conditions, without knowing if the extraction procedure can dissolve such phases. Fisher and Wignall (2001) ascribed also the enrichement of U in anoxic sediment to the presence of francolite or other calciumfluoroapatite.

Two dominating processes supply U to surface sediments (Sternbeck et al., 2000), the first being the uptake by plankton in the photic zone followed by burial and preservation within the sediments and the second the diffusion at the sediment-water interface and precipitation within the sediments (Anderson et al., 1989). A study of the Baltic Sea waters shows that biogenic particles were enriched in U (Andersson et al., 1998) and that the U concentration was positively correlated to salinity (Prange and Kremling, 1985). The Molybdenum reactive is also moderately well correlated with the DOP value (r=0.47; Fig. 48). Among the pathways suggested for the incorporation of Mo in anoxic sediments is the adsorption on humic substances (Helz et al., 1996) or on particulate Mn-Fe-oxi/hydroxides and in that case is linked with the redox cycling of Mn and Fe (Adelson et al., 2001). The enrichment of Mo in the reactive part of anoxic sediments could be due to the presence of Fe monosulfides (Algeo and Maynard, 2004), which are dissolved by the extraction process. Indeed in anoxic porewaters, MoO_4^{2-} can be released from organic matter through decay by sulfate-reducing bacteria and be deposited after reduction as organic thiomolybdates or, after further reduction to MoS_4^{2-}, in solid solution with Fe-sulfides (Huerta-Diaz and Morse, 1992; Helz et al., 1996; Adelson et al., 2001; Algeo and Maynard, 2004). As the HCl fraction recovered also the

fraction adsorbed to the organic matter and as the DOP is correlated to the organic matter and S content (Fig. 49), the desorption from organic matter and the dissolution of Fe monosulfides could have been the major causes for the enrichment of the reactive Mo in the anoxic part of the section.

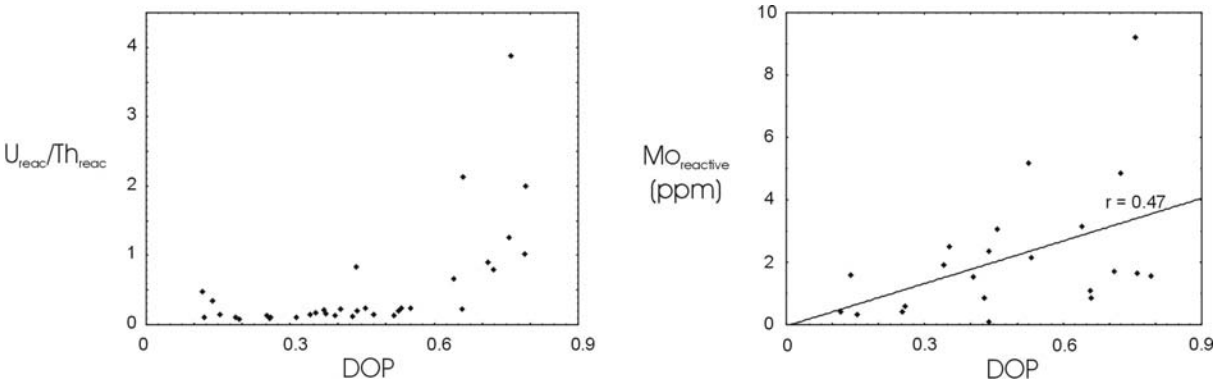

Figure 48. Crossplot of DOP vs. U $_{reactive}$/Th $_{reactice}$ ratio and Mo $_{reactive}$ (ppm).

3.3.3. Link with other parameters

Different characteristic paleoenvironmental indicators, like the Ba* and the P_2O_5* for the nutrient input/paleoproductivity or the C_{org} content for the biogenic input (see 4.1 paleoenvironmental factors for more details), and the reactive fraction were compared by statistic methods in order to obtain a general view on the relationship among these parameters (Fig. 49). There are two distinct groups of parameters. The first group consists of carbonate deposition (CaO) associated with the reactive Sr, the anoxic condition (DOP, Corg, S) associated with the reactive U and Mo and the increase of nutrient input or paleoproductivity coupled with sea-level rise (Na/K reflecting the volcaniclastic background versus detrital input). The second group includes essentially the detrital input controlling the Al content, but also most of the reactive part of the elements adsorbed or precipitated on Fe oxi/hydroxides and/or Mn oxides. The interdependency between the different factors as already mentioned is a major difficulty for the interpretation of the geochemical data.

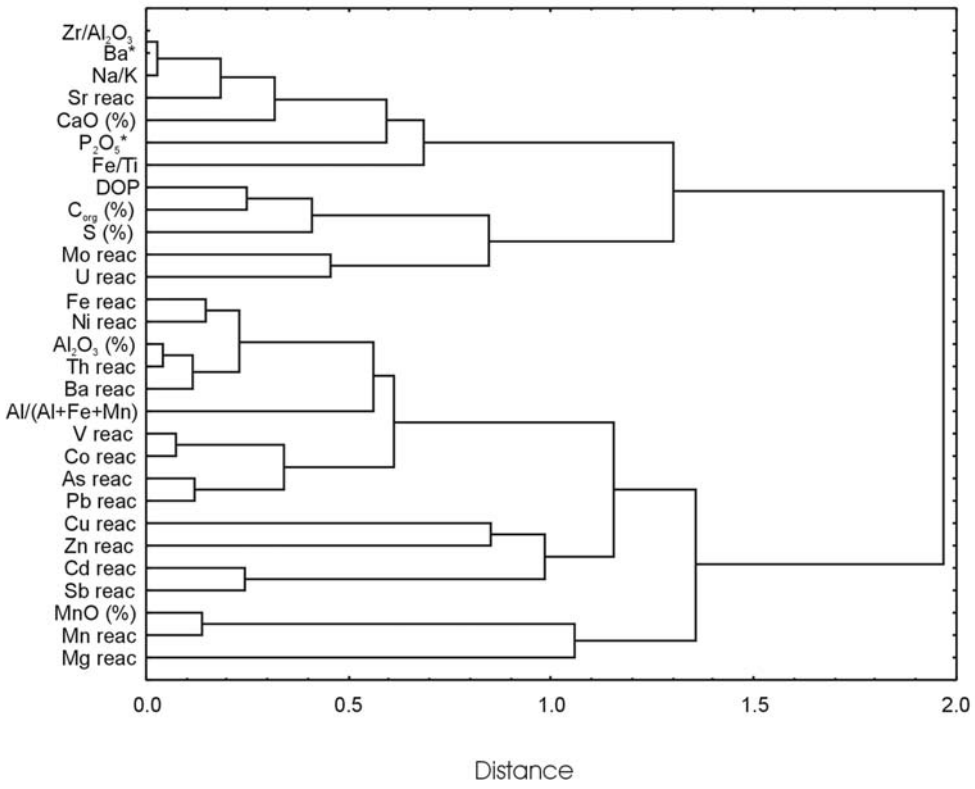

Figure 49. Tree diagram of the reactive elements fraction and some paleoenvironmental factors (DOP, Ba*, etc..) by complete linkage and 1-r Pearson methods

3.4. Trace elements in pyrite

To characterize the trace elements incorporation in pyrites, 18 elements (Mg, V, Mn, Co, Ni, Cu, Zn, As, Se, Sr, Mo, Ag, Cd, Sb, Ba, Pb, Th, U) were measured by ICP-MS.

3.4.1. Inter-element dependency

It is rather difficult to interpret directly the meaning of the relationship between the different trace elements incorporated in pyrites (Fig. 50) because of the complexity and the multitude of the factors are involved like the mechanism of incorporation, the redox conditions, the mechanism and site of the pyrite formation, etc…Assumptions could be done based on the literature, but some preliminary discriminations are still necessary to obtain meaningful information as it will be shown in the following paragraphs.

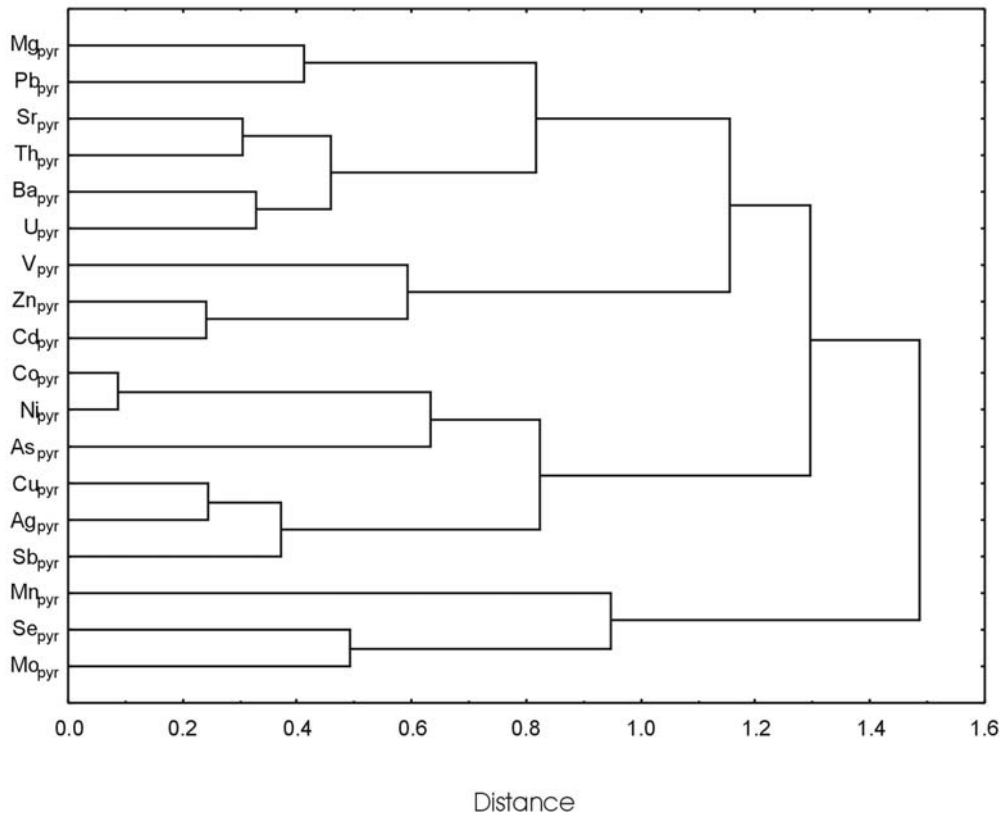

Figure 50. Tree diagram of the trace element contents in pyrites by complete linkage and 1-r Pearson methods.

3.4.2. DOP relationship

Factor and cluster analysis provided some starting points to interpret the significance of the trace elements incorporated in pyrites.

The DOP is inversely correlated to elements previously grouped with Ni (Fig. 51), Co, Cu, Ag, As and Sb in the pyrites and positively correlated to the content of Mn in pyrites. However according to the literature, we would have expected a positive correlation between the DOP and elements like As, Mo or Cd in pyrites (Huerta-Diaz and Morse, 1992; Sternbeck et al., 2000). The significance of these inconsistencies with the theoretical (Huerta-Diaz and Morse, 1992) and environmental (Sternbeck et al., 2000) reference studies must be consequently discussed. As introduced in the paragraph 3.2, the morphology of pyrites is directly linked to their formation process. It is therefore necessary to verify in the first place how the trace element content of the pyrites can be influenced by genetic conditions as expressed by their morphology in order to avoid misinterpretations.

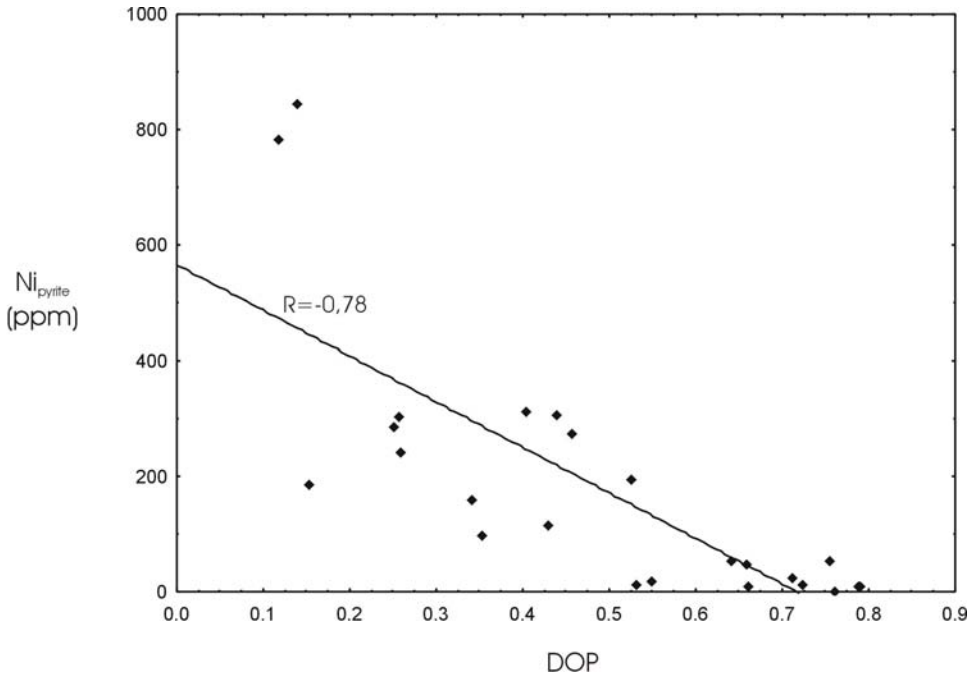

Figure 51. Crossplot of DOP vs. Ni content in pyrite.

3.4.3. Link with other parameters

The negative correlation (r =-0.78) between DOP and the content of Ni in pyrites shown previously (Fig. 51) could be interpreted as a direct consequence of the redox conditions prevailing at the time of pyrites formation, while it appears that the contents of the elements Ag, Cu, Sb, V, Zn, Cd, Co, Ni in pyrites are correlated mainly to their morphology (Fig. 52). The parameter morphology was included in the statistic by giving a different value to pyritized fossils (=3) and group aggregates, cubic crystal and veins (=1). The content of Ni in pyrites (Fig. 53), though not the closer to the morphology parameter in the tree diagram (Fig. 52), exemplifies the role of morphology in the incorporation of the trace elements mentioned previously in pyrite. The fact that elements like As are included in the same group as the elements particularly influenced by morphology, lead to reconsider the meaning of the enrichment of these elements in pyrite along the section. The redox conditions and the morphology of pyrites are obviously linked but the content of these elements in the pyrites reflect more the mechanism of formation than the environmental conditions (Fig. 53). The pyritized fossils are enriched in elements grouped with the morphology parameter, which could be ascribed to the sulfidisation of the organic matter, which contains e.g., a higher Ni and Co concentration.

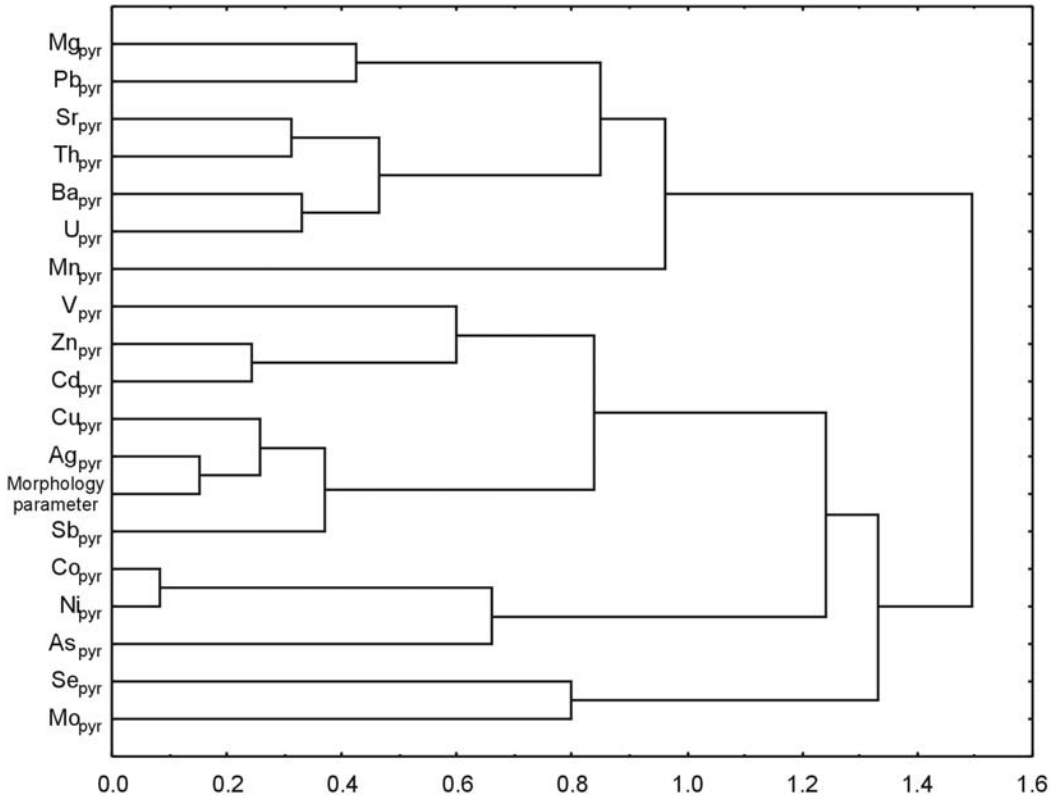

Figure 52. Tree diagram of the trace element contents in pyrites and the morphology parameter by complete linkage and 1-r Pearson methods.

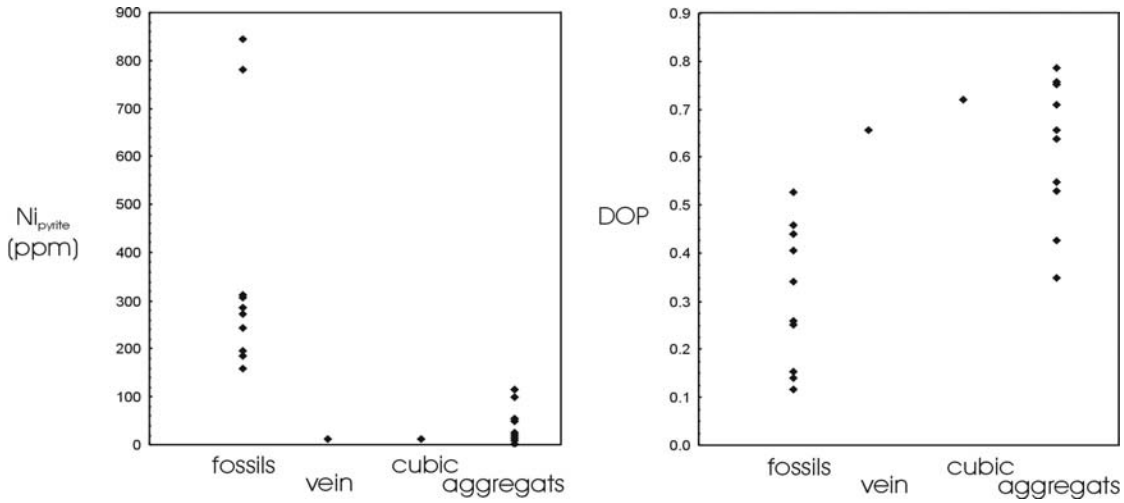

Figure 53. Crossplot of the pyrite morphology vs. Ni content in pyrite and DOP.

Other characteristic enrichments of trace elements in pyrites were recognized which cannot be explained only by the morphology of pyrites. Of particular interest are those related to the deposition of the Kellwasser Horizons. In that sense, Mn, As and U in pyrites present an

increase in the Kellwasser Horizons, particularly in the upper one (Fig. 54). The signal is more significant for the U content in pyrites, with the three highest values corresponding to both Kellwasser Horizons. This enrichment cannot be explained only based on the morphology of pyrites (Fig. 55) or the redox conditions because the upper Kellwasser horizon presents DOP values which indicate dysoxic environment and secondly, because all samples with high DOP values do not show high U_{pyrite} content (Fig. 55). As noticed previously, the increase of As or Mo in pyrites, due to anoxic environment described in the literature (Huerta-Diaz and Morse, 1992), cannot be generalized. Similarly the use of Cd enrichment in pyrites as proxies for reducing conditions (Sternbeck et al., 2000) was not successful.

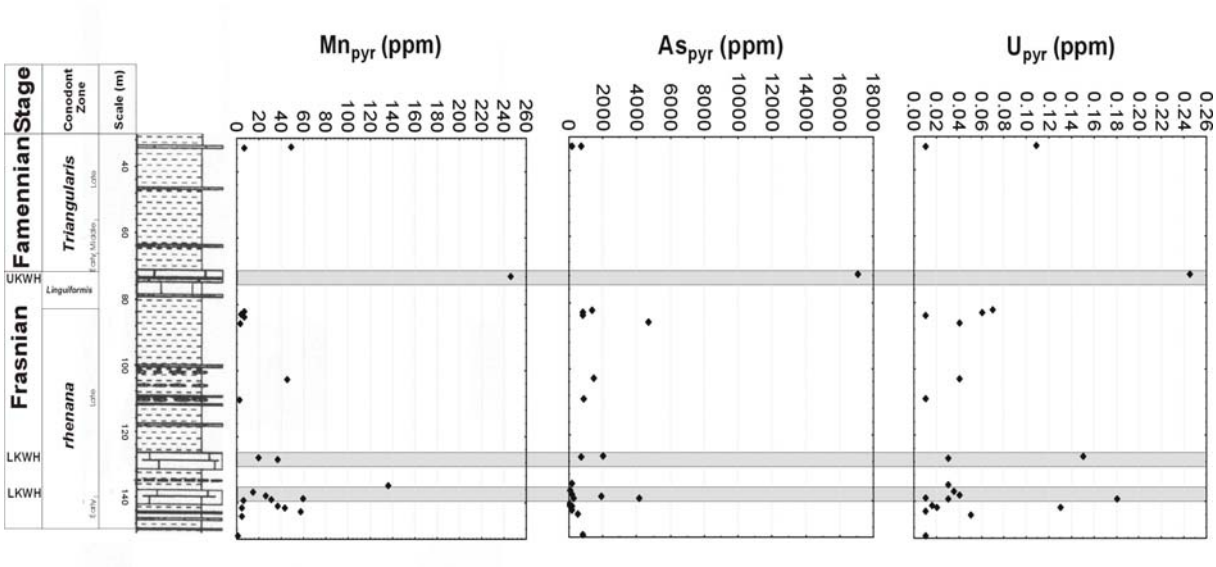

Figure 54. Distribution of the Mn, As, U in pyrite along the Büdesheimer Bach section. The grey zones correspond to the Kellwasser Horizons position. Litholog modified after Joachimski et al., 2001 (see Fig. 2 for details).

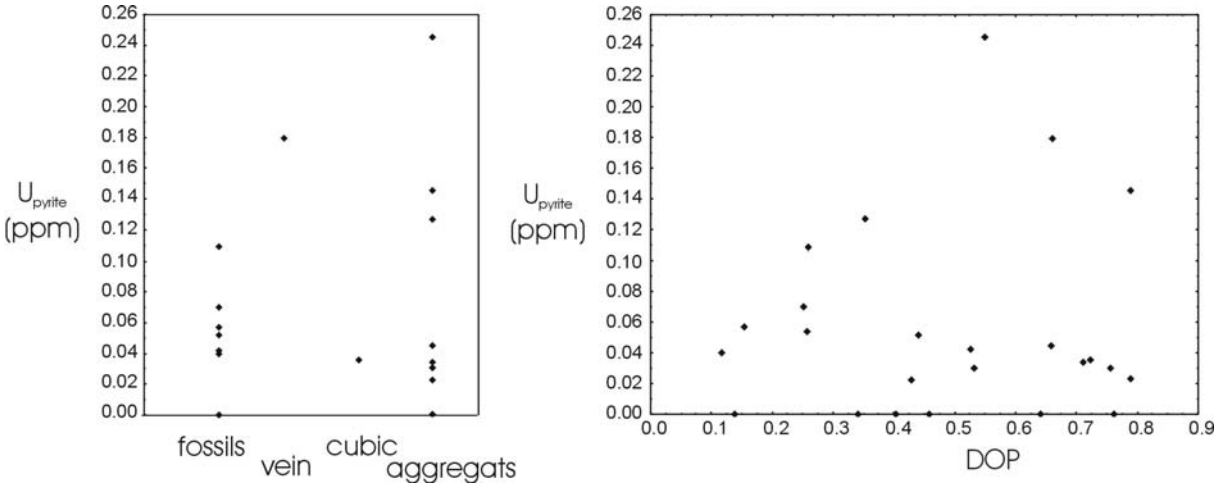

Figure 55. Crossplot of U content in pyrite vs. morphology and DOP.

3.4.4. The non-fossil pyrite fraction

Taking into account the effect induced by the pyrite morphology (Fig. 52), the trace element content in pyritized fossils were excluded in the following comparison between paleoenvironmental factors and trace element content in pyrites. The discriminations in function of the epigenetic influence (3.1) and pyrites morphology lead to a reduction of pyrites samples considered from 46 to 11. This is a rather low number of samples to allow generalizations but still permits a better interpretation of data than the mixture of pyrites of different genesis. The information after this discrimination are closer to results of previous works.

Indeed e.g., As and Cd are enriched in the group containing the anoxia factor DOP (Fig. 56). Arsenic is known to substitute in pyrite for both S (Huerta-Diaz and Morse, 1992; Bostick and Fendorf, 2003), and also for Fe (Thomas and Saunders, 1998). The uptake of As by pyrite is mainly ascribed to the sorption (adsorption, co-precipitation) of As on Fe- mineral phases from As-enriched water (Bostick and Fendorf, 2003). The dissolution of Mn-/Fe-oxihydroxides (scavenging As) by reduction can lead to the enrichment of As in anoxic bottom water or pore water (Peterson et al., 1986; Sullivan and Aller, 1996). Arsenic can also be bound to the organic fraction of anoxic sediments via different processes like the uptake and production of organo-arsenicals by phytoplankton followed by subsequent deposition with organic matter, or via scavenging by particulate organic matter. However, the very high content of these elements in pyrites of the upper Kellwasser horizon cannot be explained only by DOP values or by the C_{org} content. Whereas for the other samples the As and Cd in pyrites are well correlated with the C_{org} content or the DOP values, the upper Kellwasser horizon sample shows the highest values with a relative low C_{org} content and a DOP value corresponding to dysoxic conditions (Fig. 57). The content of Corg should not have changed significantly and can be considered as constant. By contrast the DOP value could have decreased due to either a decrease of the S content or an increase of reactive iron. Investigations with the SEM and microprobe revealed that the pyrites of the upper Kellwasser horizon have in majority framboidals morphology and are lower in size than 5 µm, which would suggest that this sample was deposited under anoxic bottom waters (Wilkin et al., 1996, 1997, Wilkin and Arthur, 2000) and should have consequently a higher DOP value. However, in spite of the results of the cluster analysis (Fig. 56), the correlation coefficients

show that As in pyrites is better correlated to the productivity indicators, like P_2O_5* and Ba* (Fig. 59). Indeed, whereas the correlation coefficient between As and Cd in pyrites and DOP and/or C_{org} is close to 0 due to the high content of As and Cd in pyrites in the upper Kellwasser Horizon (Fig. 57-58), the correlation coefficient between As content in pyrite and and P_2O_5* and Ba* attains value of 0.9 and 0.6, respectively (Fig. 59). Productivity, redox conditions and C_{org} deposition are normally coupled, but parameters as sea level oscillations or detrital input can also exert a controle on redox conditions or C_{org} preservation. The upper Kellwasser Horizon in the Büdesheimer Bach section represents the only sample with simultaneously high detrital input and high productivity indicators. Interruptions in the upward increasing trend of detrital input (as indicated e.g., by the Al_2O_3 content, Fig. 17 Paragraph 4.1.1) were noticed at the level of the two KWH, but the upper one is less pronounced due to its deposition during a phase of enhanced detrital input. This observation may become relevant in explaining the differences observed between the two Kellwasser Horizons in terms of redox conditions and C_{org} deposition.

The productivity factor P_2O_5* and Ba* seems to be linked to the content of Sr, U, Ba, V and Sb in the pyrites although they are coupled also to carbonate deposition and the sea-level rise as indicated by the volcaniclastic background versus detrital input factor. The link between Ba* and Ba_{pyrite} could be interpreted as reflecting micro-inclusions of barite in the pyrite aggregates. Similarly the link between CaO content and Sr_{pyrite} could be ascribed to micro-inclusion of calcite. A closer look on the data shows that among the elements of this group the U_{pyrite} content is stronger correlated to the P_2O_5* and Ba* parameters (Fig. 60). The increase of the U_{pyrite} content could be also assigned to the co-precipitation and micro-inclusions of minerals like uraninite under reducing conditions. As mentioned previously, Fisher and Wignall (2001) ascribed the enrichement of U in anoxic sediments to the presence of francolite or other carbonate fluoroapatite, which are known to incorporate U (Starinsky et al., 1982). Consequently micro-inclusions of francolite or uraninite in the pyrite aggregates could explain the correlation between U in pyrite (and Sr) and the CaO or the P_2O_5* contents. To find out the mineral phase at the origin of the high U_{pyrite} content in the Kellwasser Horizons, more detailed investigations would be necessary.

The element group linked to the Al content is mainly related to detrital input and oxic conditions as indicated by the inverse correlation between Al content and DOP values. This relationship was already observed in the reactive fraction (see 3.3.3). Consequently taking Ni

as an axample, the Ni content in pyrite aggregates increases with low DOP values (Fig. 61) or with increasing reactive Fe content (Fig. 61) and high detrital input. A high reactive Fe content is supposed to reflect mainly a high content of Fe oxi/hydroxides, which are typically enriched in transition metals. This could reflect the formation of Ni rich pyrites by sulfidisation of iron oxides (Morse and Arakaki, 1993; Huston et al., 1995). Moreover the pyrites enriched in transition metals like Ni or Co are localized just below the anoxic lower Kellwasser Horizon and could have been affected by descending sulfidisation fronts.

The S content of the bulk rock is linked to the incorporation of Se content of pyrites in the last group. A lattice substitution in pyrite can take place stoichiometrically with Se replacing S (Huston et al., 1995).

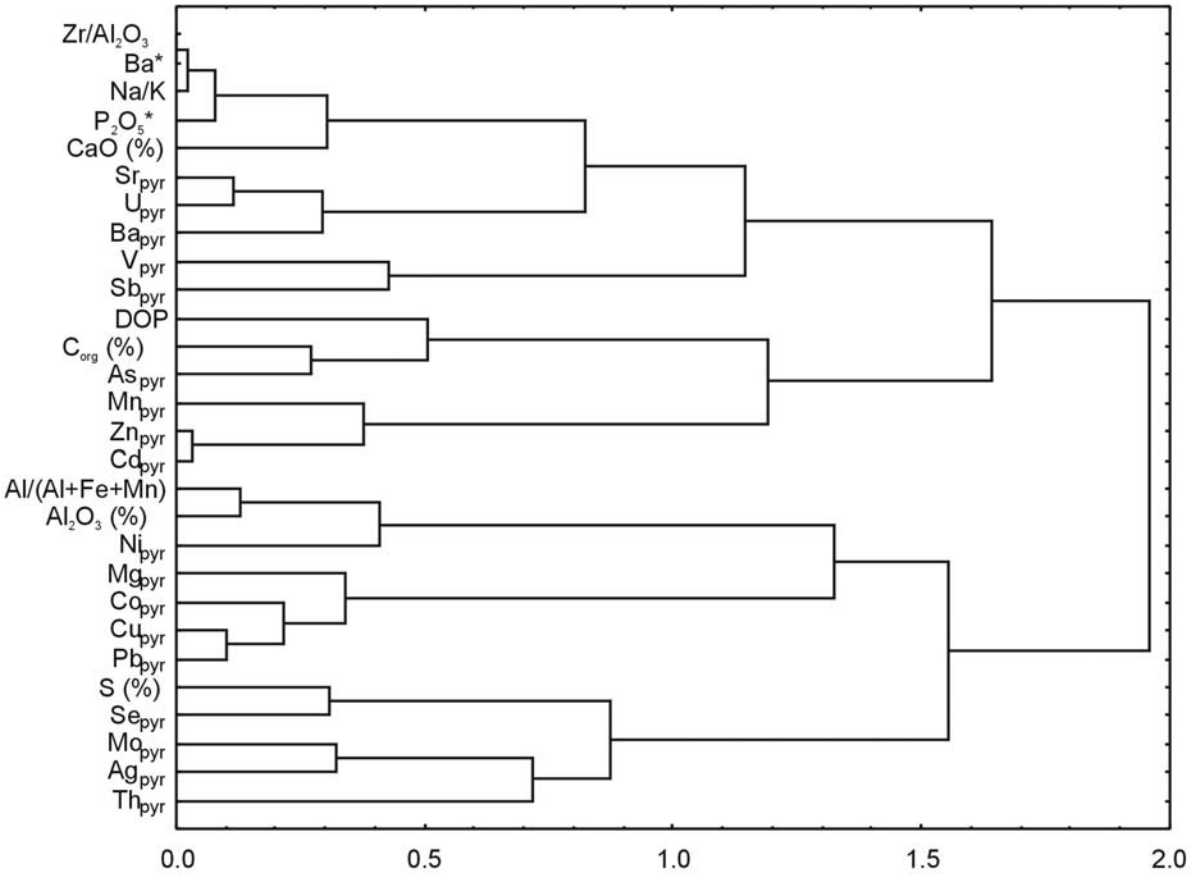

Figure 56. Tree diagram of the trace element contents in pyrites and the paleoenvironmental factors (after exclusion of the pyritized fossils samples) by complete linkage and 1-r Pearson methods.

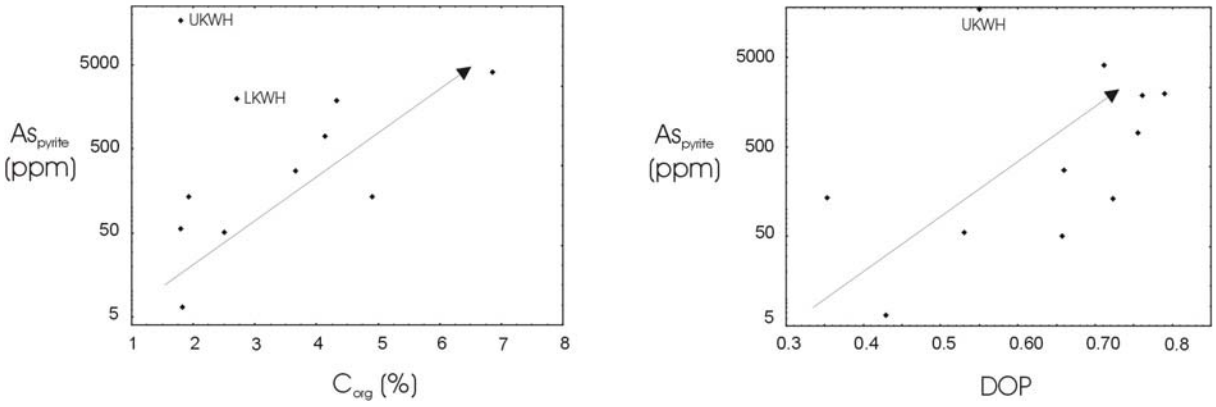

Figure 57. Crossplot of the As content in pyrite (ppm) vs. Corg content (%) and DOP.

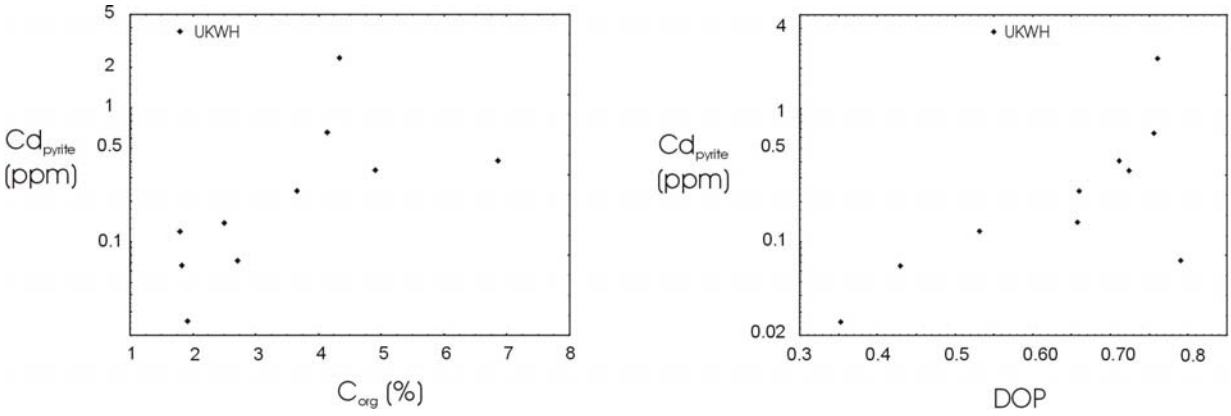

Figure 58. Crossplot of the Corg content (%) and DOP vs. Cd content in pyrite (ppm).

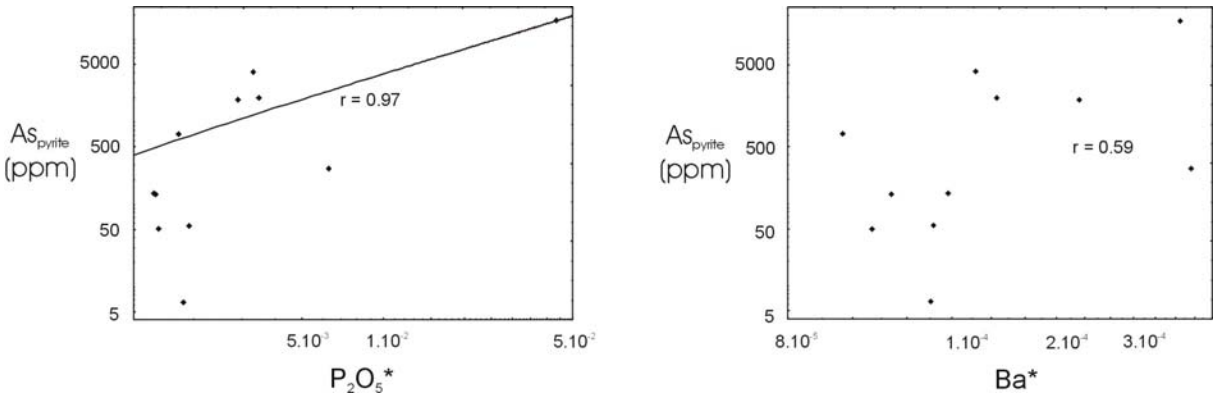

Figure 59. Crossplot of P_2O_5* and Ba* vs. As content in pyrite (ppm).

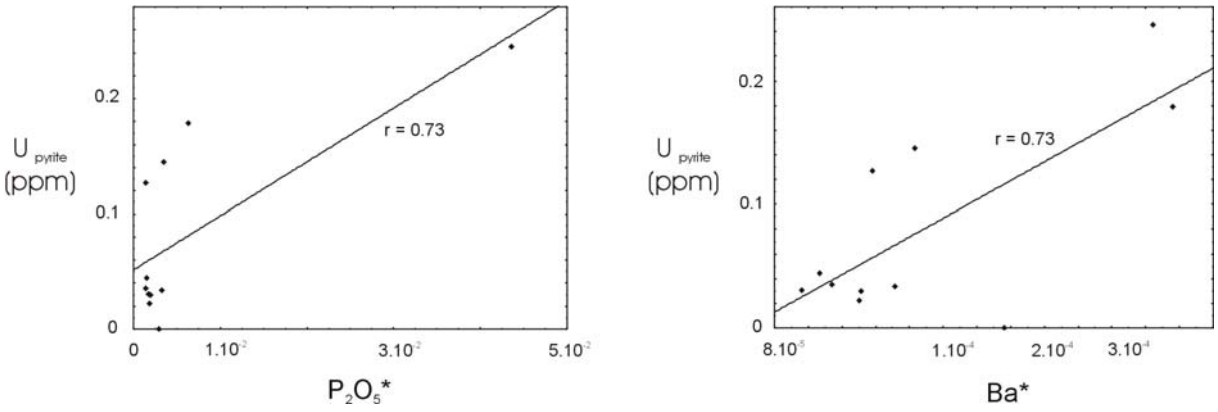

Figure 60. Crossplot of P_2O_5* and Ba* vs. U content in pyrite (ppm).

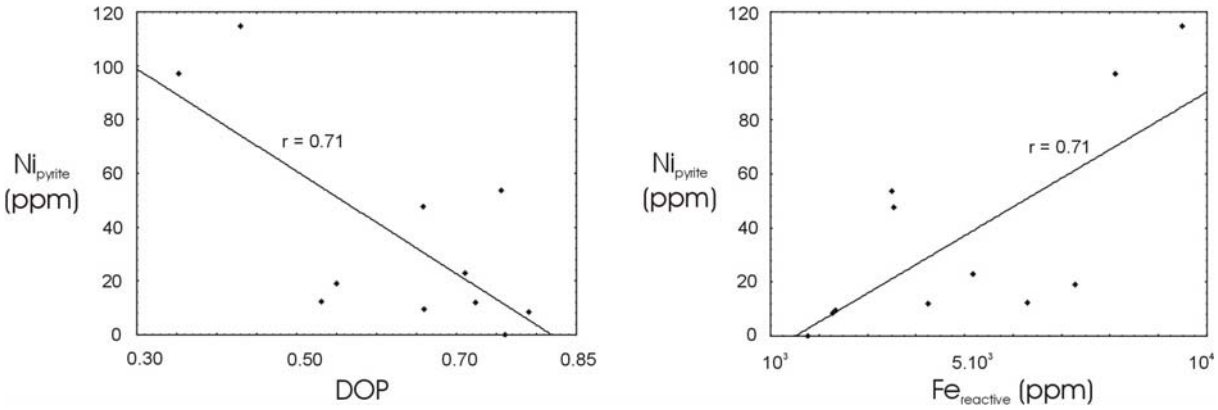

Figure 61. Crossplot of Ni content in pyrite (ppm) vs. DOP and reactive iron (ppm).

3.5. The degree of trace metal pyritization

Before interpreting the data on the degree of trace metal pyritization, the results on the reactive fraction and the trace element contents in pyrite must be considered in order to assess the meaning of this signal. As shown before the DTMP is calculated as follow:

$$DTMP(\%)=\frac{Pyrit_{Me}}{Pyrit_{Me}+Reactives_{Me}}$$

with pyrite $_{Me}$ = metal content in the pyrite and reactive $_{Me}$ = metal content in reactive (i.e. not silicate) phases. It amounts to saying that the DTMP depend, for the content of trace elements in pyrites, mainly on the morphology parameter relative to the detrital input and/or oxic conditions (for most of the elements) or anoxic conditions (for U and Mo) for the metal content in the reactive fraction. It means that for pyritized fossils, the DTMP of elements like Ni will express in a way the ratio between the enrichment of Ni in pyrite due to the

sulfidisation of organic matter and the enrichment of Ni in the reactive fraction due to a higher amount of reactive Fe (as a consequence of higher detrital input and oxic conditions)(Fig. 64). Whereas for pyrites aggregates the DTMP of Ni will represent the comparison between the variation in Ni content due to changes in DOP and the variations in Ni content in the reactive fraction due to the detrital input and redox parameters (Fig. 65-66). This demonstrates that similar to the trace elements content of pyrites (see 3.4.3), the DTMP of samples containing pyrites of different morphologies cannot be compared. Moreover, in the reference study of Huerta-Diaz and Morse (1992) on the degree of trace metal pyritization, the lithology of the investigated sediments was more homogenous than in the Büdesheimer Bach section in which the Kellwasser Horizons are characterized by the deposition of carbonate rocks intercalated between calcareous shales (Fig. 3). This difference in lithology makes more difficult the interpretation of the DTMP because of the difference in the reactive Fe fraction, which is not only dependent on the redox conditions, but it is also related to the detrital input. An additional factor, which can also be involved in the content of reactive Fe and related elements (see 3.3) is the amount of Fe bearing carbonates like siderite or ankerite (formed by carbonate dissolution and reprecipitation). Indeed, based on the X-ray diffraction the Büdesheimer Bach core contains a non-negligible fraction of ankerite. Taken as an example the aggregat samples illustrate well the influence of this mineral phase on the reactive iron content and also on the DOP values (Fig. 62). According to the definition of the DOP and DTMP, which are a function of reactive iron or reactive elements contents, the presence of iron-bearing carbonates can also lead to misinterpretation of the results. The formation of ankerite during the diagenesis or due to anoxic condition will increase the reactive iron content and finally decrease the DOP values. This mechanism could explain the discrepancy of the results obtained for the upper Kellwasser Horizon using different methods. The microscopic observation showed that most of the pyrites are framboidal with grains less than 5 μm in size, which speak for deposition under anoxic condition, while the DOP values are in the range characteristic for dysoxic conditions. The reactive fraction is consequently a function of the detrital input and/or the redox condition, but also of the Fe bearing carbonates content.

Considering the multitude of parameters controlling the incorporation of trace elements in pyrites and in the reactive fraction, the DTMP results of the pyrites cannot give always conclusive results. The variability of pyrite morphology analysed coupled with the difference in lithology and detrital input in the Kellwasser Horizons can explain the difference between

the presented results and those e.g., of Huerta-Diaz and Morse (1992) or Sternbeck et al. (2000). A good example to demonstrate the ambiguity of these results can be illustrated by the DTMP of the elements Ni and Co. As reviewed in paragraph 1.2, trace elements can be incorporated in pyrite by different processes. Heavy metals like Co and Ni can readily substitute in pyrite because of their similar ionic radii to Fe (II) and because they both form octahedral coordination just like Fe in pyrites with sulfides ligands (Sternbeck et al., 2000). Other invoke kinetic constrains (Morse and Arakaki, 1999). Opposite to the positive correlation observed in other studies between the DOP and the DTMP of Ni and Co (Huerta-Diaz and Morse, 1992; Sternbeck et al., 2000) in this study there was found a negative correlation between DOP and DTMP of these elements (Fig. 63). The sulfidisation of organic matter and of iron oxides (enriched in these elements) common in oxic calcareous shales, seems to be the main reason for these differences. Consequently it would be uncorrect to interpret these results in terms of environmental changes or to use them as indicators for hydrogeochemical variations.

We can try also to assess the meaning of the aggregates pyrites DTMP knowing already the behavior of each parameter (see before, 3.3 and 3.4.3). Taking again the example of Ni, it was shown that the Ni content in pyrites decreases with increasing DOP values (Fig. 61). This behavior was interpreted as indicating a sulfidisation of iron oxides at low DOP values. The amount of reactive iron and of related elements, like Ni (Fig. 49), increases with increasing detrital input and/or oxic condition, but also possibly with the amount of Fe-bearing carbonates as e.g., ankerite. Consequently, under anoxic conditions and high DOP values, the Ni content in pyrite and the amount of reactive Ni will be low due to the deposition of the Kellwasser Horizons under lower detrital input and anoxic conditions and/or due to the presence of lower ankerite content (Fig. 66). In this case both Ni_{pyrite} and $Ni_{reactive}$ will be low and their ratio will be hard to predict and to interpret. Similarly, under oxic conditions both parameters will increase and the results of the ratio (the DTMP) will be hard to interpret.

Based on the presented results, it is clear that, in the presented case study, the content of trace elements in pyrites is easier to interpret than the DTMP values due to the multiple parameters involved in the incorporation of trace elements in the pyrites and in the reactive fraction, which can have antagonistic or additional effects not only in the case of the pyritized fossils but also for aggregates.

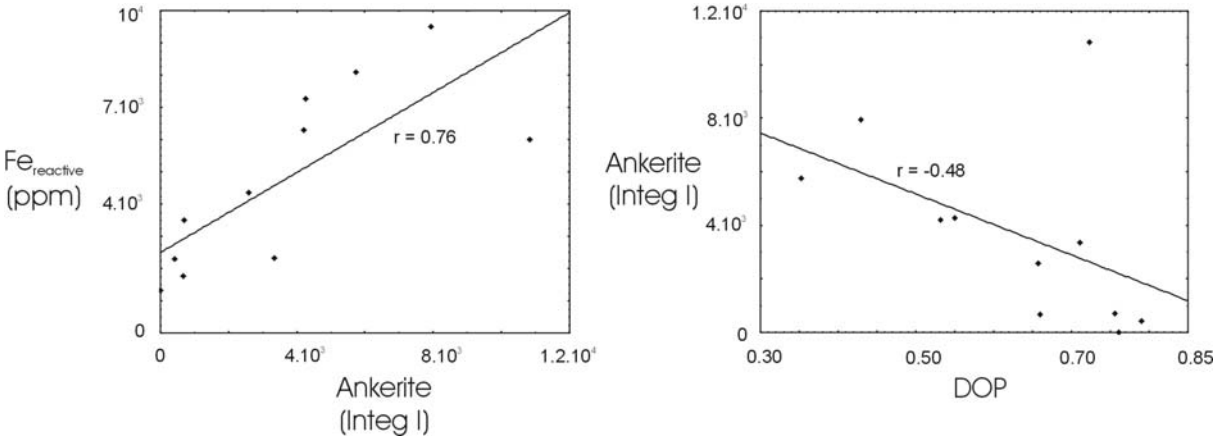

Figure 62. Crossplot of the ankerite integrated intensity (XRD) vs. reactive iron (ppm) and DOP values in the aggregates pyrites samples.

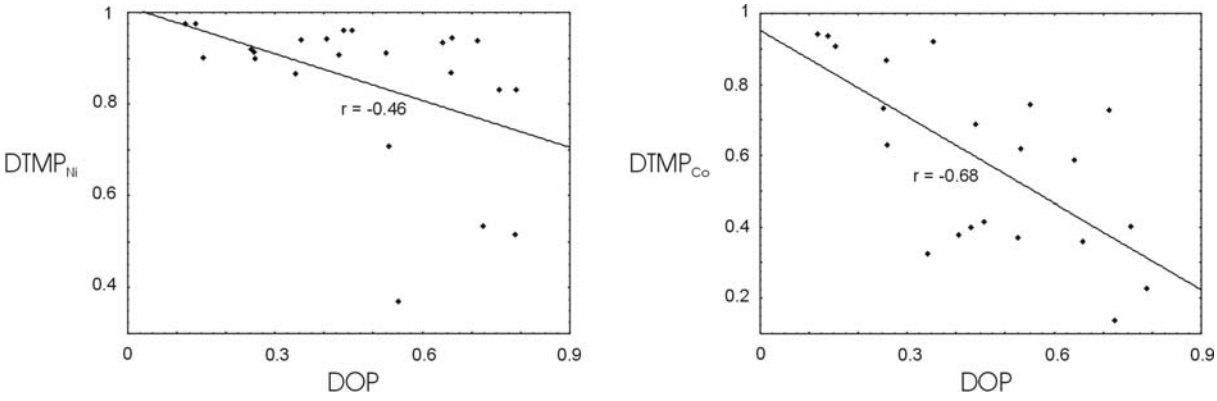

Figure 63. Crossplot of the DOP vs. DTMP of Ni and Co including all pyrites samples.

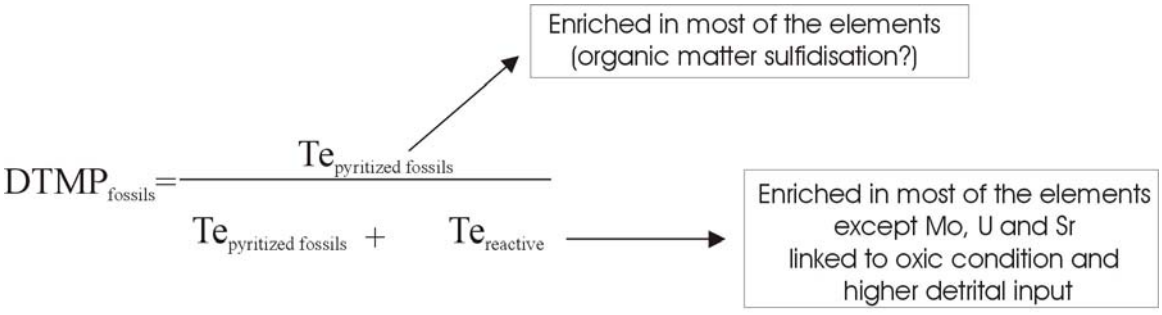

Figure 64. Model showing the parameters involved in the DTMP of the pyritized fossils.

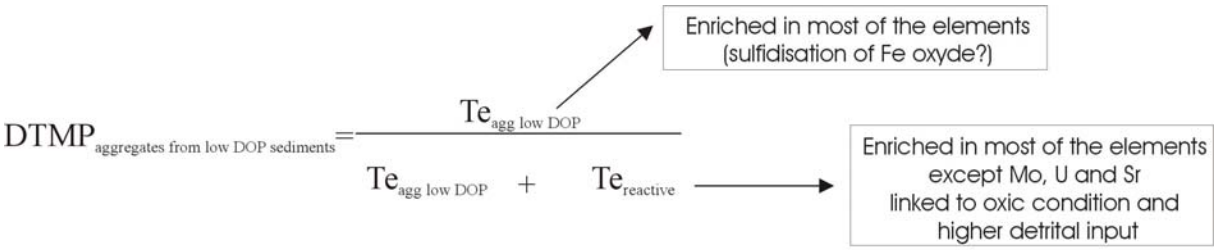

Figure 65. Model showing the parameters involved in the DTMP of the pyrites aggregates from low DOP sediments.

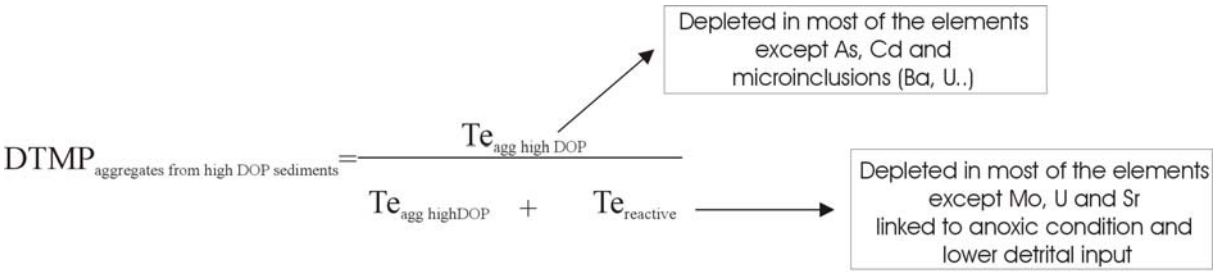

Figure 66. Model showing the parameters involved in the DTMP of the pyrites aggregates from high DOP sediments (LKWH).

3.6. Sulphur isotope geochemistry

The $\delta^{34}S_{pyrite}$ depends on several parameters which control the formation of sedimentary iron sulfides, notably the availability of metabolisable organic carbon (Morse and Berner, 1995) and/or reactive iron (Canfield, 1989) as well as on parameters which affect the fractionation of S isotopes essentially including the rate of sulfate reduction, but also sulfate concentration, temperature, pH, the bacterial species and growth conditions (Habicht et al., 1997).

The $\delta^{34}S_{pyrite}$ increase in the LKWH up to values around +20 ‰, which contrast sharply with the much lower values (-3 to –26 ‰) registered before and after (Fig. 64). Similar high values were found close to the F/F boundary in the Kowala Section (Joachimski et al., 2001) as well as in the Medicine Lake and the Cinquefoil Sections in Canada (Geldsetzer et al., 1987; Wang et al., 1996). According to a widely accepted model (e.g., Anderson et al., 1987; Joachimski et al., 2001) such high $\delta^{34}S$ values in pyrites can be explained either by their formations below the water/sediment interface under closed system conditions (i.e., limited sulfate supply) and iron limitation or by a higher sulfate reduction rate. The high $\delta^{34}S_{pyrite}$ values could be due to

higher fraction of metabolisable organic carbon due to an enhanced input of photoautotroph biomass during the deposition of the LKWH leading to an increase of the sulfate reduction rate and consequently lower ^{34}S depletion in the sedimentary pyrite. This could also explain the positive correlation found between the $\delta^{34}S_{pyrite}$ and the Corg content (Fig. 65). The correlation of the $\delta^{34}S_{pyrite}$ values correlated also with anoxia proxies, like the DOP values or the C_{org}/P ratio (Fig. 64) suggests the interdependency of these factors. Indeed the following sequence of events is conceivable: higher supply of nutrients (see 4.1.3) > increase of productivity > development of bottom water anoxia > higher organic carbon burial > higher sulfate reduction rate > high $\delta^{34}S_{pyrite}$.values. The $\delta^{34}S_{pyrite}$ vary also with the pyrite morphology (Fig. 65). Supposed to reflect changes in environmental parameters during the deposition of the lower Kellwasser Horizon, the $\delta^{34}S_{pyrite}$ of the pyritized fossils might be linked more to microscale and pore water conditions. This emphasizes once again (see.3.4.2) that the trace element content in pyrites of different morphology cannot be compared in quantitative terms because they do not represent the same site and mechanism of formation. During sulfidisation of organic matter, like in case of the formation of pyritized fossils, the isotope fractionation is normally low (Mossmann et al., 1991; Raiswell et al., 1993), but a preferential diffusion of ^{32}S can also occur (Chanton et al., 1987) and lead to low $\delta^{34}S_{pyrite}$ values. The influence of these two mechanisms during the sulfidisation of the organic matter could explain the high variability of the $\delta^{34}S_{pyrite}$ values observed in fossils (-3 to -26 ‰). As mentioned previously other parameters affecting the fractionation of S isotopes like the rate of sulfate reduction, but also the sulfate concentration, temperature, pH, the bacterial species and growth conditions, which cannot be measured in such paleoenvironmental study, could have also be involved (Habicht et al., 1997).

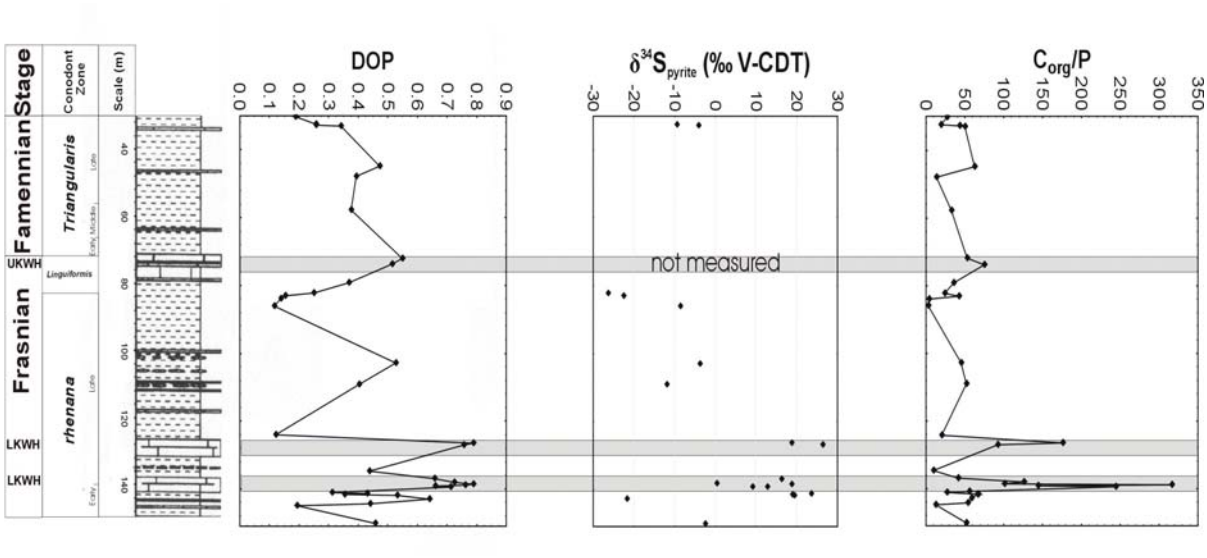

Figure 67. Distribution of the DOP, the $\delta^{34}S_{pyrite}$ (‰ V-CDT) and the C_{org}/P ratio along the Büdesheimer Bach section. The grey zones correspond to the Kellwasser Horizons position. Litholog modified after Joachimski et al., 2001 (see Fig. 2 for details).

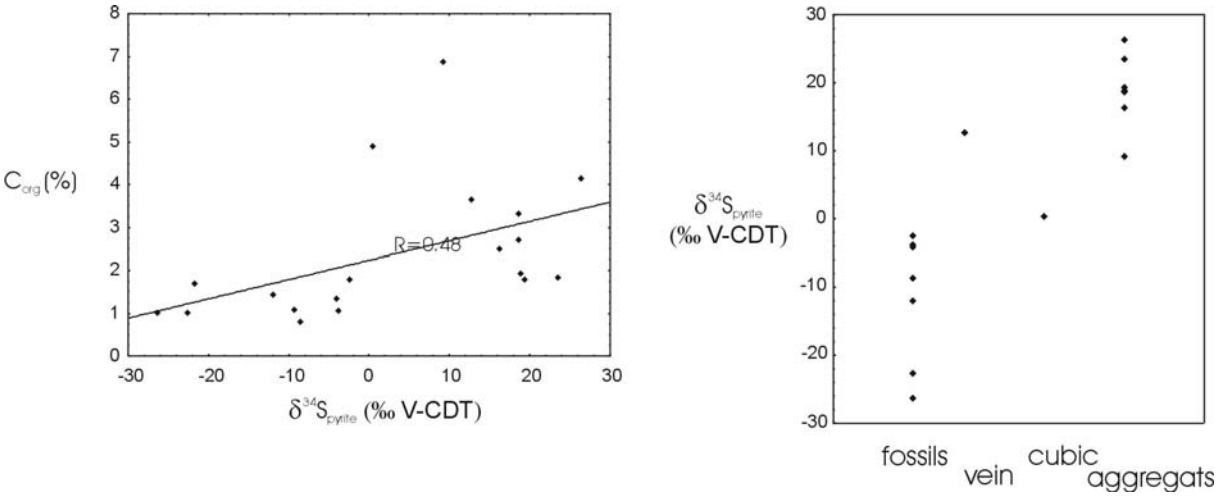

Figure 68. Crossplot of $\delta^{34}S_{pyrite}$ (‰ V-CDT) vs. Corg (%) and pyrite morphology.

3.7. µ-XRF synchrotron results on pyrites

The µ-XRF synchrotron measurements (Tab. 7) confirmed the difference already observed by ICP-MS analysis between the concentration of elements like Ni or Cu in the pyritized fossils and idiomorphic crystals. These elements are indeed enriched in pyritised fossils (table.7; see also 3.4.3). Some sections across pyrite grains were prepared in order to verify the homogeneity of the trace elements pattern in individual grains. The results show that the concentration of elements may fluctuate within the same fossil or aggregate; particularly the As contents have proved to be highly variable.

sample depth (m)		Ni (ppm)	Cu (ppm)	Zn (ppm)	As (ppm)	Pb (ppm)	
103 - pyritized fossils							
Grain 1 - homogenous point in a Goniatite							
	ghp_01	458	396	99	1640	1283	
Grain 1 - profil from the center to the border of a Goniatite							
	gcbs_002	301	466	70	2047	2138	
	gcbs_003	234	441	95	1064	1356	
	gcbs_004	208	354	79	1171	1625	
	gcbs_005	290	398	85	1203	1280	
	gcbs_006	310	300	107	1187	1235	
	gcbs_007	643	403	96	0	1315	
	gcbs_008	775	449	92	514	1137	
	gcbs_009	688	503	98	501	1130	
	gcbs_010	700	537	122	261	1196	
	gcbs_011	812	456	226	576	811	
Grain 2 - cross section across a tentaculid							
	vp_01	59	1129	128	9024	1634	center
	vp_03	474	1114	959	22835	11	In between
	vp_02	81	276319	2150	17174	1132	fringe
109.2 - inner part of a tentaculid							
Grain 1 - transversal section							
	-2_fp_01	1600	567	46	991	771	yellow-reddish
	-2_fp_02	3280	899	74	901	850	white-blueish
	-2_fp_03	1578	570	62	882	837	dark yellow
	-2_fp_04	1021	787	86	3584	979	light yellow
124.3 - pyritized Goniatite							
Grain 1	3_fp_01	485	176	70	623	673	
Grain 2	3_f2p_01	715	625	80	929	590	
127 - idiomorphic aggregate							
Cross section from center to border							
	as_001	0	177	127	917	1047	
	as_002	0	135	97	1860	1181	
	as_003	162	252	87	3305	1438	
	as_004	0	137	105	336	998	
	as_005	208	291	146	0	559	
	as_006	45	122	80	105	1084	
	as_007	41	212	75	13	1251	
	as_008	0	155	128	608	384	
139.25 - idiomorphic aggregate							
	25ap01	50	174	55	556	781	
	25ap_02	42	143	50	438	1100	
	25ap_03	47	282	107	2262	1073	
139.35 - idiomorphic grain							
Grain 1	35ap_01	44	139	56	7530	815	
	35_ap02	0	111	66	14121	924	
Grain 2	35ap2_01	51	138	74	20796	1833	
	35ap2_02	46	94	85	20569	881	
	35ap2_03	168	154	61	26116	921	greenish, infilling?

Table 7. Results of the synchrotron μ-XRF analysis on different pyrite grains.

3.8. Environmental implications - Discussion

Based on the results presented before, it seems that several arguments speak against the use of the trace element content in pyrites for paleoenviromental reconstruction. First of all, the interpretation of this signal is difficult due to the complexity and the number of processes involved in the trace element incorporation in the pyrites like the redox conditions, the detrital input, the biogenic input, the mechanism and site of pyrite formation as expressed by the pyrite morphology. Discrimination is necessary between authigenic, syngenetic and early diagenetic as well as epigenic pyrite. Moreover the method can be rarely applied given that only seldom sections present anoxic conditions throughout a long period of time (in the case of the F/F boundary limited mainly to the Kellwasser Horizons). Consequently, no comparison can be done due to the fact that the pyrites studied do not represent the same site or mechanism of formation. Lastly, the procedure is very time consuming.

Nevertheless, the results provide some new constraints on the depositional conditions of the Kellwasser Horizons in the Büdesheimer Bach section, but also possibly new indicators for anoxic conditions. The analysis of the reactive fraction proved to be interesting not only for the reactive iron fraction (for DOP calculation), but also by showing the possible use of the reactive Mo and U as indicator for anoxic conditions. However, a high U content can be also related to low sedimentation rate (Fisher and Wignall, 2001), an increase in planktonic deposition (Anderson, 1989) or in salinity (Prange and Kremling, 1985).

Although hardly applicable for the F/F boundary, the study on the trace element content of pyrite allowed to establish a geochemical link between the mechanism/site of pyrite formation and its trace element content. The enrichment of elements like Ni, Co or Cu in pyrites may be a useful tool to identify its mechanism of formation and the nature of its precursor. Indeed, the concentration of these elements is higher in the pyritised fossils and possibly in the pyrites formed by iron oxides sulfidisation. This could be of interest for future studies aiming to assess the enrichment of metals relative to aluminium, commonly used in paleoenvironmental studies as an indicator of redox conditions, which could be due to a descending sulfidisation front and late diagenetic pyrites formation.

This work emphasizes also that studies on pyrite geochemistry, including such on its isotopic composition, should cautiously discriminate among different types of pyrites formation in

order to obtain paleoenvironmental information. After discriminating among authigenic and epigenetic pyrites and those with different morphologies, a positive correlation between As_{pyrite}, Cd_{pyrite} and DOP was observed, which is in agreement with previous works (e.g., Sternbeck et al., 2000). The mineral phase at the origin of the high U_{pyrite} in the Kellwasser Horizons should be investigated more precisely. Micro-inclusions of francolite or other carbonate fluoroapatite could explain the correlation between U (and Sr) in pyrite and the $CaO\text{-}P_2O_5$* contents.

The high $\delta^{34}S_{pyrite}$ in the LKWH has been interpreted as reflecting a higher sulfate reduction rate although other processes could have been involved like the sulfate concentration, the temperature, the pH, the bacterial species and growth conditions (Habicht et al., 1997). The high $\delta^{34}S_{pyrite}$ values could be due to a higher supply of metabolisable organic carbon or to an enhanced input of photoautotroph biomass during the deposition of the LKWH, which could have lead to an increase of the sulfate reduction rate and consequently less ^{34}S depletion in the sedimentary pyrite. This could explain the correlation between the $\delta^{34}S_{pyrite}$ and the C_{org} content. The fact that the $\delta^{34}S_{pyrite}$ is correlated also with anoxia proxies as the DOP values or the C_{org}/P ratio suggests the interdependency of these factors. Indeed the following sequence of processes could have occured: higher supply of nutrients (see 4.1.3) > increase of productivity > development of bottom water anoxia > higher organic carbon burial > higher sulfate reduction rate > high $\delta^{34}S_{pyrite}$.values. This sequence is in concert with the model presented at the end of the section, which discusses the paleoenvironmental changes at the F/F transition (see 4.2).

IV. Conclusions - Perspectives

1. Conclusions

The study brings new geochemical evidences which emphasize the role of tectono-magmatic processes, like volcanism, hydrothermalism and major tectonic movements in the development of the particularities of the Kellwasser Horizons deposited close to the southern shores of Laurussia and the northern parts of Gondwana. The adopted geochemical multiproxy approach revealed a relative sea-level rise coupled with higher nutrient input, the intensification of magmatic activity (as indicated by increased hydrothermal and volcanic influence) as well as the development of a generally more oxygen deficient depositional environment during the deposition of the Kellwasser Horizons. Among the environmental changes at the origin of the geochemical variations recorded in the Kellwasser Horizons, the rapid sea-level fluctuation seems to be the most important parameter. Indeed, long-term (like the semi-closed configuration of the Paleotethys in the late Devonian) and short-term processes must be distinguished.

The results also show that conventionally used indicators like the organic matter content or the oxygenation level of bottom waters does not have always-diagnostic values for recognizing the Kellwasser Horizons. Moreover, some of the proxies, like the V/Cr and Ni/Co ratios, turned out to be not representative in the Kellwasser Horizons for the environmental conditions to which they are generally associated. By its ability to discern among different processes, a multiparametric geochemical approach, as used in the present study, allows to draw more reliable paleo-environmental conclusions.

Finally the observed enrichment in metals, in nutrients and the lowering of the oxygen level in the sea water during the deposition of the Kellwasser Horizons, coupled with an enhanced bacterial activity, must have played a decisive role in the major biotic crisis which affected the Frasnian – Famennian transition (Pujol et al. revised).

The study of the trace element spectrum of pyrite as a source for supplementary information on depositional conditions, proved to be hardly applicable in the sections studied. The main

reason was the lack of appropriate Frasnian-Famennian sections with continuous and long lasting anoxic conditions, which would have yielded a sufficiently high sampling resolution of authigenic pyrites to permit a detailed comparative study in terms of trace element contents in pyrite. The DTMP of pyrites with different morphologies cannot be quantitatively compared and interpreted due to the multiple parameters involved in the incorporation of trace elements in pyrite and in the reactive fraction.

The results of this work emphasize that studies on pyrite geochemistry, including such on sulphur isotopic composition, should cautiously discriminate among pyrites formed at different sites and under different mechanisms in order to obtain reliable paleoenvironmental information.

The content of elements like Ni, Co or Cu in pyrites may be a useful tool to identify the mechanism of pyrite formation and the nature of its precursor. This could be of interest for future studies to assess the enrichment of metals relative to aluminium, content commonly used in paleoenvironmental studies as an indicator for redox conditions, because such enrichments could be due to a descending sulfidisation front and formation of diagenetic pyrites.

After eliminating epigenetic pyrites and those formed by pyritization of organic rests, a positive correlation between As_{pyrite}, Cd_{pyrite} and DOP was observed, which is in agreement with previous works (Huerta-Diaz and Morse, 1992; Sternbeck et al., 2000). The importance of this study also includes, its contribution to the small number of existing publications dealing with the potential of trace element pattern of pyrite as an indicator for depositional conditions.

2. Perspectives

This study brought new insights regarding the causes of the biotic crisis at the Frasnian-Famennian transition, but also emphasized the complexity of the geochemical record in terms of metal enrichment due mostly to the overlapping of different factors like the redox conditions, the hydrothermalism or the sea-level variations leading to possible misinterpretations. In regard of this finding, new research strategies could be applied to solve this problem.

- The use of a similar multiproxy approach to a F/F transition deposited under oxic condition, like the Australian Canning basin section (George and Chow, 2002), could prove to be interesting allowing to eliminate the effect of low redox conditions in the enrichment of trace metals.

- The study of a F/F transition with less variation in detrital input variations would be also helpful to eliminate the influence of dilution effect. If such variations are important, they may lead to enrichment of metal relative to Al by increasing the volcaniclastic background relative to the detrital input.

The analysis of Pb isotope ratios in the Frasnian/Famennian sections studied could strengthen the hypothesis on the hydrothermal influence postulated in this work.

The investigation of Moroccan sections, deposited on the northern shore of Gondwana, using the same multi-proxy approach, would be interesting to put constraints on the regional character of the observations provided by this study.

A comparison between the paleontological data and the results of the different proxies by a statistical study could also give some additional information about the relation between the environmental changes and their effects on the biota. The comparison on several locations of various families, genera and species, which were differently affected, could provide new clues in that matter.

References

Abbas, S., Abbas, A., 1998. Volcanogenic dark matter and mass extinctions. Astroparticle physics 8, 317-320.

Achterberg, E.P., van der Berg, C.M.G., Boussemart, M., Davison, W., 1997. Speciation and cycling of trace metals in Esthwaite water: a productive English lake with seasonal deep-water anoxia. Geochim. Cosmochim. Acta 61, 5233-5255.

Adelson, J.M., Helz, G.R., Miller, C.V., 2001. Reconstructing the rise of recent coastal anoxia; molybdenum in Chesapeake Bay sediments. Geochim. Cosmochim. Acta 65, 237-252.

Alaasm, I.S., Morad, S., Durocher, S., Muir, I., 1996. Sedimentology, C-S-Fe relationships and stable isotopic compositions in devonian black mudrocks, Mackenzie Mountains, Northwest Territories, Canada. Sediment. Geol.106 (3-4), 279-298.

Alberdi-Genolet, M., Tocco, R., 1999. Trace metals and organic geochemistry of the Machiques Member (Aptian-Albian) and La Luna Formation (Cenomanian-Campanian), Venezuela. Chem. Geol.160, 19-38.

Algeo, J.T., Berner, R.A., Maynard J.B., Scheckler, S.E., 1995. Late Devonian oceanic anoxic events and biotic crises; "rooted" in the evolution of vascular land plants?. GSA Today 5, 64-66.

Algeo, J.T., 1996. Geomagnetic polarity bias patterns through the Phanerozoic. J. Geophys. Res. 101, 2785-2814.

Algeo, J.T., Maynard, J.B., 2004. Trace-element behavior and redox facies in core shales of the Upper Pennsylvanian Kansas-type cyclothems. Chem. Geol. 206, 289-318.

Anderson, T.F., Kruger, .J., Raiswell., R., 1987. C-S-Fe relationships and the isotopic composition of pyrite in the New Albany Shale of the Illinois Basin, U.S.A. Geochim. Cosmochim. Acta 51, 2795-2805.

Anderson, R.F., LeHuray, A.P., Fleisher, M.Q., Murray, J.W., 1989. Uranium deposition in Saanich Inlet sediments, Vancouver Island. Geochim. Cosmochim. Acta 53, 2215-2224.

Anderson, R.F., Fleisher, M.Q., LeHuray, A.P.,1989. Concentration, oxidation state, and particulate flux of Uranium in the Black Sea. Geochim. Cosmochim. Acta 53, 2205-2213.

Andersson, P.S., Porcelli, D., Wasserburg, G.J., Ingri, J., 1998. Particle transport of ^{234}U-^{238}U in the Kalix River and in the Baltic Sea. Geochim. Cosmochim. Acta 62, 385-392.

Arakaki, T., Morse, J.W., 1992. Coprecipitation and adsorption of Mn (II) with mackinawite (FeS) under conditions similar to those found in anoxic sediments. Geochim. Cosmochim. Acta 57, 9-14.

Bai, S.L., Bai, Z.Q., Ma, X.P., Wang., D.R., Sun, Y.L., 1994. Devonian events and Biostratigraphy of south China. Peking Univ. Press, Beijing, 303 pp.

Barker, W.W., Parks, T.C., 1986. The thermodynamic properties of pyrrhotite and pyrite: a re-evaluation. Geochim. Cosmochim. Acta 50, 2185-2194.

Barton, P.B.Jr., Skinner, B.J., 1979. Sulfide Mineral Stabilities. In: H.L. Barnes (Ed.): Geochemistry of hydrothermal ore deposits. John Wiley & Sons, New York - Chichester - Brisbane – Toronto, p. 278-403.

Barton, E.S, Hallbauer, D.K., 1996. Trace metals and U-Pb isotope compositions of pyrite types in the Proterozoic Black Reef, Transvall Sequence, South Africa: Implications on genesis and age. Chem. Geol. 133, 173-199.

Beck, C.B., 1981. *Archaeopteris* and its role in vascular plant evolution. In: Niklas, K.J., (ed.): Paleobotany, Paleoecology, and evolution, Volume 1: New York, Praeger, 193-230.

Becker, R.T., 1993. Anoxia, eustatic changes, and Upper Devonian to lowermost Carboniferous global ammonoid diversity. Syst. Assoc. Spec. 47,115-163.

Becker, R.T., House, M.R., 1994. Kellwasser events and goniatite successions in the Devonian of the montagne noire, with comments on possible causations. Cour. Forsch. Inst. Senckenberg 169, 45-77.

Belzile, N. Lebel, J., 1986. Capture of arsenic by pyrite in near-shore marine sediments. Chem. Geol. 54, 279-281.

Berner, R. A., 1970. Sedimentary pyrite formation. Amer. J. Sc. 268, 1-23.

Berner, R.A., 1984. Sedimentary pyrite formation: an update. Geochim. Cosmochim. Acta 48, 605-615.

Berner, R.A., Raiswell, R., 1984. C/S method for distinguishing freshwater from marine sedimentary rocks. Geology 12, 365-368.

Berner, Z., 1993. S-Isotopengeochemie in der KTB-Vorbohrung und Beziehungen zu den Spurenelementmustern der Pyrite. Karlsruher Geochemische Hefte, Schriftenreihe des Instituts für Petrographie und Geochemie (IPG) der Universität Karlsruhe (TH) 2:1-167.

Berner, Z., Puchelt, H., 1995. Konzentrationen und Bindungsformen von Spurenelementen in Abhängigkeit vom Ausgangsgestein und der Entwicklung der Bodenbildung (hier Posidonienschiefer - Lias-Epsilon). Abschlussbericht zum Forschungsvorhaben PW 86014, Institut für Petrographie und Geochemie (IPG) der Universität Karlsruhe (TH).

Berner, Z., Stüben, D., Leosson, M., Klinge, H., 2002. S- and O-isotopic character of dissolved sulphate in the cover rock aquifers of a Zechstein salt dome. Appl. Geochem. 17, 1515-1528.

Bertrand, P., Shimmield, G., Martinez, P., Grousset, F., Jorissen, F., Pujol, C.J., Bouloubassi, I., Buat Menard, P., Peypouquet, J.P., Beaufort, L., Sicre, M.A., Lallier-Verges, E., Foster, J.M., Ternois, Y., 1996. The glacial ocean productivity hypothesis: the importance of regional temporal and spatial studies. Mar. Geol. 130, 1-9.

Bond, D., Wignall, P.B., Racki, G., 2004. Extent and duration of marine anoxia during the Frasnian-Famennian (Late Devonian) mass extinction in Poland, Germany, Austria and France. Geol. Mag. 141, 173-193.

Bostick, B.C., Fendorf, S., 2003. Arsenite sorption on troilite (FeS) and pyrite (FeS_2). Geochim. Cosmochim. Acta 67, 909-921.

Boström, K., 1983. Genesis of ferromanganese deposit - diagnostic criteria for recent and old deposits. In: Rona, P.A., Boström, K., Laubier, L., Smith, K.L., (eds.), Hydrothermal Processes at Seafloor Spreading Centers. Plenum Press, New York, pp. 473-489.

Bralia, A., Sabatini, G., Troja, F., 1979. A Revaluation of the Co / Ni Ratio in Pyrite as Geochemical Tool in Ore Genesis Problems. Miner. Depos.14, 353-374.

Bratton, J.F., Berry, W.B.N., Morrow, J.R., 1999. Anoxia pre-dates Frasnian-Famennian boundary mass extinction horizon in the Great Basin, USA. Palaeogeogr., Palaeoclimatol., Palaeoecol. 154, 275-292.

Buggisch, W., 1991. The global Frasnian-Fammenian „Kellwasser Event“. Geol. Rundsch. 80, 49-72.

Burns, S.J., McKenzie, J.A., Vasconcelos, C., 2000. Dolomite formation and biogeochemical cycles in the Phanerozoic. Sedimentology 47, 49-61.

Burnett, B.R., Nealson, K.H., 1981. Organic films and microorganisms associated with manganese nodules. Deep-Sea Res. 28, 637-645.

Calvert, S.E., Petersen, T.F., 1993. Geochemistry of recent oxic and anoxic marine sediments: implications for the geologic record. Mar. Geol. 113, 67-88.

Canfield, D.E., 1989. Reactive iron in marine sediments. Geochim. Cosmochim. Acta 53, 619-632.

Caplan, M.L., Bustin, R.M., Grimm, K.A., 1996. Demise of a Devonian-Carboniferous carbonate ramp by eutrophication. Geology 24, 715-718.

Caputo, M.V., 1985. Late Devonian glaciation in South America. Palaeogeogr., Palaeoclimatol., Palaeoecol. 51, 291-317.

Caroll, R., 1995. Between fish and amphibian. Nature 373, 389-390.

Carpenter, S.J., Lohmann, K., 1997. Carbon isotope ratios of Phanerozoic marine cements: Re-evaluating the global carbon and sulfur systems. Geochim. Cosmochim. Acta 61, 4831-4846.

Casier, J.G., Lethiers, F., 1998. Ostracods late Devonian mass extinction; the Schmidt Quarry parastratotype (Kellerwald, Germany). CR. Acad. Sci. II. A. 326, 71-78.

Cathles, L.M., Hallam, A., 1991. Stress-induced changes in plate density, Vail sequences, epeirogeny, and short lived global sea level fluctuations. Tectonics 10, 659-671.

Chambers, L.A., 1982. Sulphur isotope study of a modern intertidal environment, and the interpretation of ancient sulphides: Geochim. Cosmochim. Acta 46, 721-728.

Chanton, J.P., Martens, C.S., Goldhaber, M. B., 1987. Biogeochemical cycling in an organic-rich coastal marine basin. A sulphur isotopic budget balanced by differencial diffusion across the sediment-water interface. Geochim. Cosmochim. Acta 51, 1201-1228.

Chaloner, W.G., Sheering, A., 1979. Devonian macrofloras. In: House, M.R., Scrutton, C.T., Basset, M.G. (eds.): The Devonian system. Spec. Paper Palaeont. 23. London, 145-161.

Chen, D., Qing, H., Li, R., 2005. The Late Devonian Frasnian-Famennian (F/F) biotic crisis: Insights from $\delta^{13}C_{carb}$, $\delta^{13}C_{org}$ and $^{87}Sr/^{86}Sr$ isotopic systematics. Earth Planet. Sci. Lett. Vol. 235, 151-156.

Chen, X.P., Gao, Y.U., 1988. Thermal water deposition and Pb-Zn barite deposits in the Devonian System Central Guangxi. Chin. J. Geochem. 7, 321-328.

Chowdhury, A.H, Noble, J.P.A., 1996. Organic carbon and pyrite sulphur relationships as evidence of bottom water conditions of sedimentation, Albert Formation fine-grained lacustrine sediments, New Brunswick, Canada. Marine and Petroleum Geology 13 (1), 79-90.

Claeys, P; Casier, J.G., 1994. Microtektite-like impact glass associated with the Frasnian-Famennian boundary mass extinction. Earth Planet. Sci. Lett. Vol. 122, 303-315.

Coffin, M.F., Eldholm, O., 1994. Large igneous provinces: crustal structure, dimensions, and external consequences. Rev. Geophys. 32, 1-36.

Cooper, D.C., 1998. Trace metal diagenesis in anoxic marine sediments Ph.D. dissertation, Texas A&M University, College Station, TX.

Cooper, D.C., Morse, J.W., 1998. Extractibility of metal sulfide minerals in acidic solutions: Applications to environmental studies of trace metal contamination. Environ. Sci. Technol. 32, 1076-1078.

Copper, P., 1986. Frasnian/Fammenian mass extinction and cold-waters oceans. Geology 14, 835-839.

Copper, P., 2002. Reef development at the Frasnian/Famennian mass extinction boundary. Palaeogeogr., Palaeoclimatol., Palaeoecol. 181, 27-65.

Crick, R.E., Ellwood, B., Feist, R., El Hassani, A., Schindler, E., Dreesen, R., Over, D.J., Girard, C., 2002. Magnetostratigraphy susceptibility of the Frasnian/Famennian boundary. Palaeogeogr., Palaeoclimatol., Palaeoecol. 181, 67-90.

Cruse, A.M., Lyons, T.W., 2004. Trace metal records of regional paleoenvironmental variability in Pennsylvanian (Upper Carboniferous) black shales. Chem. Geol. 206, 319-347.

Davis, C., Pratt, L.M., Sliter, W.V., Mompart, L., Murat, B., 1999. Factors influencing organic carbon and trace metal accumulation in the Upper Cretaceous La Luna Formation of the western Maracaibo basin, Venezuela. In: Barerra, E. and Johnson, C. (eds.), Evolution of the cretaceous ocean-climate system. Geol. Soc. Am. Spec. Pap. 332, Boulder, pp. 203-230.

De Baar, H.J.W., de Jong, J.T.M., Bakker, D.C.E., loscher, B.M., Veth, C., Bathmann, U., Smetacek, V., 1995. Importance of iron for plakton blooms and carbon dioxide drawdown in the southern Ocean. Nature 273, 412-415.

DeBoer, P.L., 1986. Changes in organic carbon Burial during the Early Cretaceous. In: Summerhayes, C.P., Shackleton, N.J. (eds), North Atlantic Palaeoceanography. Geol. Soc. London. Spec. Pub. 21, pp. 321-331.

Devleeschouwer, X., 1999. La transition Frasnien-Famennien (Dévonien Supérieur) en Europe: Sédimentologie, stratigraphie séquentielle et susceptibilité magnétique. Unpublished PhD Thesis, Free University, Brussels.

Devleeschouwer, X., Herbosch, A., Préat, A., 2002. Microfacies, sequence stratigraphy and clay mineralogy of a condensed deep-water section around the Frasnian-Famennian boundary (Steinbruch Schmidt, Germany). Palaeogeogr., Palaeoclimatol., Palaeoecol. 181, 171-193.

Diester-Haass, L., Zahn, R., 1996. Eocene-Oligocene transition in the Southern Ocean: History of water mass circulation and biological productivity. Geology 24, 163-166.

Dill, H., Kemper, E., 1990. Crystallographic and chemical variations during pyritization in the Upper Barremian and Lower Aptian dark claystones from the Lower Saxonian Basin (NW Germany). Sedimentology 37, 427-443.

Dill, H. G., Eberhard, E., Hartmann, B., 1996. Use of variations in unit cell length, reflectance and hardness for determining the origin of Fe disulphides in sedimentary rocks. Sedimentary Geology 107, 281-301.

Donnelly, T.H., Shergold, J.H., Southgate, P.N., 1988. Pyrite and organic matter in normal marine sediments of Middle Cambrian age, southern Georgina Basin, Australia sediments. Geochim. Cosmochim. Acta 52, 259-263.

Dvorak, J., Frakova, O., Kullman, J., 1988. Influence of volcanism on Upper Devonian black limestone and shale deposition, Czechoslovakia. In: McMillan, N.J., Embry, A.F., Glass, D.J. (eds.), Devonian of the World, 2. Can. Soc. Pet. Geol. Mem. 14, pp. 377-391.

Echarfaoui, H., Hafid, M., Aït Salem, A., 2002. Seismic structure of the Doukkala Basin, Paleozoic basement, Western Marocco: a hint for an Eovariscan fold-and-thrust belt. C.R. Geosci. 334, 13-20.

Eckhardt, J-D., Glasby, G.P., Puchelt, H., Berner, Z., 1997. Hydrothermal manganese crusts from Enarete and Palinuro seamounts in the Tyrrhenian Sea. Mar. Georesour. Geotechnol. 15, 175-208.

Ehrlich, H.L., 1990. Geomicrobiology of iron. In: Ehrlich, H.L. (ed.), Geomicrobiology, 2nd ed. Marcel Dekker, New York, pp. 283-346.

Feist, R., (edit) 1990. The Frasnian-Famennian boundary and adjacent strata of the Eastern Montagne Noire, France. Guide book of the Field Meeting, Montagne Noire, 1990. Int. Union. Geol. Sc., Subcomm. Dev. Str., Montpellier, 1-69.

Filipiak, P., 2002. Palynofacies around the Frasnian/Famennian boundary in the Holy Cross Mountains, southern Poland. Palaeogeogr., Palaeoclimatol., Palaeoecol. 181, 313-324.

Filippeli, G.M., 1999. Effects of climate and landscape development on the terrestrial phosphorus cycle. Geology 27, 171-174.

Fisher, Q.J., Wignall, P.B., 2001. Paleoenvironmental controls on the uranium distribution in an Upper Carboniferous black shale (*Gastrioceras listeri* Marine Band) and associated strata; England. Chem. Geol. 175, 605-621.

Frogner, P., Gislason, S.R., Oskarsson, N., 2001. Fertilizing potential of volcanic ash in ocean surface water. Geology 29, 487-490.

Garzanti, E., 1993. Himalayan ironstones, 'superplumes', and the breakup of Gondwana. Geology 21, 105-108.

Geldsetzer, H.H.J, Goodfellow, W.D., McLaren, D.J, Orchard, M.J., 1987. Sulfur-isotope anomaly associated with the Frasnian/Fammenian extinction, Medecine Lake, Alberta, Canada. Geology 15, 393-396.

George, A.D., Chow, N., 2002. The depositional record of the Frasnian-Famennian interval in a fore-reef succession, Canning Basin, Western Australia. Palaeogeogr., Palaeoclimatol., Palaeoecol. 181, 347-374.Giles, K.A., McMillan, N.J., McCarson, B.L., 2002. Geochemical analysis and paleoecological implications of phosphatic microspherules (otoliths?) from Frasnian-Famennian boundary strata in the great basin, USA. Palaeogeogr., Palaeoclimatol., Palaeoecol. 181, 111-125.

Gillan, D.C., Cadée, G.C., 2000. Iron-encrusted diatoms and bacteria epibiotic on *Hydrophobia ulvae* (Gastropoda: Prosobranchia). J. Sea Res. 43, 83-91.

Gillan, D.C., De Ridder, C., 2001. Accumulation of a ferric mineral in the biofilm of Montacuta ferruginosa (Mollusca, Bivalvia). Biomineralization, bioaccumulation, and inference of paleoenvironments. Chem. Geol. 177, 371-379.

Gillan, D.C., Ribesse, J., De Ridder, C., 2004. The iron encrusted community of *Urothoe poseidonis* (Crustacea, Amphiboda). J. Sea Res. 52, 21-32.

Girard, C., Albarede, F., 1996. Trace elements in conodonts phosphates from the Frasnian/Famennian boundary. Palaeogeogr., Palaeoclimatol., Palaeoecol. 126, 195-209.

Girard, C., Robin, E., Rocchia, R., Froget, L., Feist, R., 1997. Search for impact remains at the Frasnian-Famennian boundary in the stratotype area, southern France. Palaeogeogr., Palaeoclimatol., Palaeoecol. 132, 391-397.

Girard, C., Lécuyer, C., 2002. Variations in Ce anomalies of conodonts through the Frasnian-Famennian of Poland (Kowala- Holy Cross Mountains); implications for the redox state of seawater and biodiversity. Palaeogeogr., Palaeoclimatol., Palaeoecol. 181, 299-311.

Goddéris, Y., Joachimski, M.M., 2004. Global change in the late Devonian: modelling the Frasnian-Famennian short term carbon isotope excursions. Palaeogeogr., Palaeoclimatol., Palaeoecol. 202, 309-329.

Goldhaber, M. B., Kaplan, I. R., 1974. The sulfur cycle. In: E. D. Goldberg (Ed.) The Sea, Vol. 5. Marine Chemistry, John Willey & Sons, New York - London - Sydney - Toronto, p. 569-655.

Goodfellow, W.D., 1987. Anoxic stratified oceans as a source of sulphur in sediment-hosted stratiform Zn-Pb deposits (Selwyn Basin, Yukon, Canada). Chem. Geol. 65, 359-382.

Golonka, J., Ross, M.I., Scotese, C.R., 1994. Phanerozoic paleogeographic and paleoclimatic modelling maps. In: A.F. Embry, B. Beauchamp, and D.J. Glass (eds.), Pangea; global environments and resources. Can. Soc. Pet. Geol. Mem. 17, pp. 1-47.

Govindaraju, K., 1994. Special issue Geostandard newsletters. Vol. XVIII.

Gurnis, M., 1990. Ridge spreading, sudduction, and sea level fluctuations. Science 250, 970-972.

Graham, U.M., Robertson, J.D., 1995. Micro-PIXE analysis of framboidal pyrite associated maceral types in oil shale. Fuel 74 (4), 530-535.

Habicht, K.S., Canfield, D.E., 1997. Sulfur isotope fractionation during bacterial sulfate reduction in organic-rich sediments. Geochim. Cosmochim. Acta 61, 5351-5361.

Hallock, P., 1988. The role of nutrient availability in bioerosion: consequences to carbonate buildups. Palaeogeogr., Palaeoclimatol., Palaeoecol. 63, 275-291.

Harrison, W.J., 1991. Trace elements in pyrites of the Green River Formation oil shales, Wyoming, Utah, and Colorado. In: Tuttle M.L. (ed.), Geochemical, biogeochemical and sedimentological studies of the Green River Formation, Wyoming, Utah and Colorado. Geol. Surv. Bull. Rep. No B. 1973-A-G p.D1-D23.

Helz, G.R., Miller, C.V., Charnock, J.M., Mosselmans, J.F.W., Pattrick, R.A.D., Garner, C.D., Vaughan, D.J., 1996. Mechanism of molybdenum removal from the sea and its concentration in black shales: EXAFS evidence. Geochim. Cosmochim. Acta 60, 3631-3642.

Hladil, J., 2002. Geophysical records of dispersed weathering products on the Frasnian carbonate platform and early famennian ramps in Morovia, Czech Republic: proxies for eustasy and paleoclimate. Palaeogeogr., Palaeoclimatol., Palaeoecol. 181, 213-250.

Ho, S. E., McQueen, K. G., McNaughton, N. J., Groves, D. I., 1995. Lead isotope systematics and pyrite trace element geochemistry of two granitoid-associated mesothermal gold deposits in the Southeastern Lachlan Fold Belt. Economic Geology & the Bulletin of the Society of Economic Geologists 90 (6), 1818-1830.

Hoffman, D.L., Algeo, T.J., Maynard, J.B., Joachimski, M.M., Hower, J.C., Jaminski, J., 1998. Regional and stratigraphic variation in bottom water anoxia in offshore core shales of Upper Pennsylvanian cyclothems from the eastern Midcontinent Shelf (Kansas), U.S.A. In: Schieber, J., Zimmerle, W., Sethi, P.S., (eds.), Shales and mudstones. I. Basin Studies, Sedimentology, and Paleontology. E. Schweizer-bart'sche Verlag, Stuttgart, pp. 243-269.

House, M.R., Becker, R.T., Feist, R., Klapper, G., 1988. Stratotype proposal for the Frasnian/Famennian boundary in the Montagne Noire. Doc. Subm. to the Subcommm., IUGS, Rennes.

House, M.R., 2002. Strength, timing, setting and cause of mid-Palaeozoic extinctions. Palaeogeogr., Palaeoclimatol., Palaeoecol. 181, 5-25.

Hübner, A., Rahders, E., Rahner, S., Halbach, P., Varnavas, S.P., 2004. Geochemistry of hydrothermally influenced sediments of Methana (western Hellenic volcanic arc). Chem. Erde-Geochem. 64, 75-94.

Huerta-Diaz, M.A., 1989. Geochemistry of trace metals associated with sedimentary pyrite from anoxic marine environments: Ph.D. dissertation, Texas A&M Univ.

Huerta-Diaz, M.A., Morse, J.W., 1990. A quantitative method for determination of trace metal concentration in sedimentary pyrite. Mar. Chem. 29, 119-144.

Huerta-Diaz, M.A., Morse, J.W., 1992, Pyritization of trace metals in anoxic marine sediments : Geochim. Cosmochim. Acta 56, 2681-2702.

Huston, D. L., Sie, S. H., Suter, G. F., Cooke, D. R., Both, R. A., 1995. Trace elements in sulfide minerals from eastern australian volcanic-hosted massive sulfide deposits. 1. Proton microprobe analyses of pyrite, chalcopyrite, and sphalerite, and 2. selenium levels in pyrite - comparison with delta-s-34 values and implications for the source of sulfur in volcanogenic hydrothermal systems. Economic Geology & the Bulletin of the Society of Economic Geologists, v. 90(5), p.1167-1196.

Ingall, E., Jahnke, R., 1997. Influence of water-column anoxia on the elemental fractionation of carbon and phosphorus during sediment diagenesis. Mar. Geol. 139, 219-229.

Jewell, W.P., 1995. Geologic consequences of globe-encircling currents. Geology 23, 117-120.

Joachimski, M.M., Buggisch, W., 1993. Anoxic event in the late Frasnian-causes of the Frasnian-Fammenian faunal crisis?. Geology 21, 675-678.

Joachimski, M.M., Ostertag-Henning, C., Pancost, R.D., Strauss, H., Freeman, K.H., Littke, R., Sinninghe Damsté, J.P., Racki, G., 2001. Water column anoxia, enhanced productivity and concomitant changes in delta (super 13) C and delta (super 34) S across the Frasnian-Famennian boundary (Kowala-Holy Cross Mountains/Poland). Chem. Geol. 175, 109-131.

Joachimski, M.M., Pancost, R.D., Freeman, K.H., Ostertag-Henning, C., Buggisch, W., 2002. Carbon isotope geochemistry of the Frasnian-Fammenian transition. Palaeogeogr., Palaeoclimatol., Palaeoecol. 181, 91-109.

Joachimski, M.M., Buggisch, W., 2002. Conodont apatite delta (super 18) O signatures indicate climatic cooling as a trigger of the late Devonian mass extinction. Geology 30, 711-714.

Johnson, J.G., Klapper, G., Sandberg, C.A., 1985. Devonian eustatic fluctuations in Euramerica. Geol. Soc. Am. Bull. 96, 567-587.

Jones, B., Manning, A.C.D., 1994. Comparaison of geochemical indices used for the interpretation of paleoredox conditions in ancient mudstones. Chem. Geol. 111, 111-129.

Jones, C.E., Jenkyns, H.C., 2001. Seawater strontium isotopes, oceanic anoxic events, and seafloor hydrothermal activity in the Jurassic and the Cretaceous. Am. J. Sci. 301, 112-149.

Karl, D.M., Mc Murty, G.M., Malahoff, A., Garcia, O., 1988. Loihi seamount, Hawaii: a mid-plate volcano with a distinctive hydrothermal system. Nature 335, 532-535.

Kemp, A.L.W.,Thode, H.G., 1968. The mechanism of the bacterial reduction of sulphate and of sulphite from isotope fractionation studies: Geochim. Cosmochim. Acta 32, 71-91.

Kerr, A., 1998. Oceanic plateau formation: a cause of mass extinction and black shale deposition around the Cenomanian-Turonian boundary?. J. Geol. Soc. London. 155, 619-626.

Kirsten S. Habicht and Donald E. Canfield, 1997. Sulfur isotope fractionation during bacterial sulfate reduction in organic-rich sediments : Geochim. Cosmochim. Acta 24, 5351-5361.

Klapper, G., Feist, R., Becker, R.T., House, M.R., 1993. Definition of the Frasnian/Famennian Stage boundary. Episodes 16, 433-441.

Klapper, G., Becker, R.T., 1999. Comparison of Frasnian (Upper D evonian) Conodont zonations. B. Soc. Paleontol. Ital. 37, 339-348.

Knauth-Köhler, K., Albers, B.P., Krumbein, W.E., 1996. Microbial mineralization of organic carbon and dissolution of inorganic carbon form mussel shell (*Mytilus edulis*). Senckenb. Marit. 26, 157-165.

Kornicker, W.A., Morse, J.W., 1991. Interactions of divalent cations with the surface of pyrite: Geochim. Cosmochim. Acta, 55, 2621-2625.

Kramar, U., 1997. Advances in energy-dispersive x-ray fluorescence. J. Geochemical Exploration 58, 73-80.

Kramm, V., Kogarko, L.N., Kononova, V., Vartiainien, H., 1993. The Kola alkaline province of the CIS and Finland, precise Rb-Sr ages define 380-360 Ma range for all magmatism, Lithos 30, 23-32.

Kuhn, T., Burger, H., Castradori, D., Halbach, P., 2000. Volcanic and hydrothermal history of ridge segments near the Rodrigues Triple Junction (Central Indian Ocean) deduced from sediment geochemistry. Mar. Geol. 169, 391-409.

Kuhn, T., Bostick, B.C., Koschinsky, A., Halbach, P., Fendorf, S., 2003. Enrichment of Mo in hydrothermal Mn precipitates: possible Mo sources, formation process and phase associations. Chem. Geol. 199, 29-43.

Leitch, E., Vasisht, G., 1998. Mass extinctions and the sun's encounters with spiral arm. New astronomy 3, 51-56.

Leosson, M.A., 1999. A contribution to the Sulphur Isotope Geochemistry of the Upper Continental Crust: The KTB Main Hole- A Case study. Karlsruher Geochem. H., 12.

Lethiers, F., 1998. Evolution de la biosphere et événements géologiques. Gordon and Breach Science Publishers, Amsterdam.

Lethiers, F., Baudin, F., Casier, J.G., 1998. Ostracods from the Frasnian-Famennian boundary in anoxic environment (La Serre, Montagne Noire, France). Rev. Micropal. 41, 331-336.

Lethiers, F., Casier, J.G., 1999. Autopsie d'une extinction biologique. Un exemple: la crise de la limite Frasnien-Famennien (364 Ma). CR. Acad. Sci. II. A. 329, 303-315.

Leventhal, J.S., 1983. An interpretation of carbon and sulfur relationships in Black Sea sediments as indicators of environments of deposition. Geochim. Cosmochim. Acta 47, 133-137.

Leventhal, J.S., 1987. Carbon and sulfur relationships in Devonian shales from Appalachian Basin as indicators of environments of deposition. Am. J. Sci. 287, 33-49.

Leventhal, J., Taylor, C., 1990. Comparaison of methods to determine degree of pyritization. Geochim. Cosmochim. Acta 54, 2159-2171.

Loftus-Hills, G., Solomon, M., 1967. Cobalt, nickel, and selenium in sulfides as indicators of ore genesis. Miner. Depos. 2, 228-242.

Lüschen H., Schnetger, B., Brumsack, H.J., 2001. Spurenelementsignaturen silurischer bis pleistozäner Schwarzschiefer. Berichtskolloquim des Schwerpunktprogrammes 1054, p.32-33.

Lyons, T.W., Berner, R.A., 1992. Carbon-sulfur-iron systematics of the uppermost deep-water sediments of the Black Sea. In Geochemistry of Metalliferous Black Shales. Chem. Geol. (special issue) 99, 1-27.

Ma, X.P., Bai, S.L., 2002. Biological, depositional, microspherule, and geochemical records of the Frasnian-Famennian boundary beds, South China. Palaeogeogr., Palaeoclimatol., Palaeoecol. 181, 325-346.

Mahmudy Gharaie, M.H., Matsumoto, R., Kakuwa, Y., Milroy, P.G., 2004. Late Devonian facies variety in Iran: volcanism as a possible trigger of the environmental perturbation near the Frasnian-Famennian boundary. Geol. Quaterly. 48, 323-332.

Matte, P., 2001. The Variscan collage and orogeny (480-290 Ma) and the tectonic definition of the Armorica microplate: a review. Terra Nova 13, 122-128

McGhee, G.R., 1982. The Frasne-Famenne extinction event: A preliminary analysis of Appalachian marine ecosystems. Geol. Soc. Amer. Spec. Pap. 190, 491-500.

McGhee, G.R., Orth, C.J., Quintana, L.R., Gilmore, J.S., Olsen, E.J., 1986. Late devonian "Kellwasser Event" mass-extinction horizon in Germany: No geochemical evidence for a large-body impact. Geology 14, 776-779.

McGhee, G.R., 2001. The `multiple impacts hypothesis' for mass extinction: a comparison of the Late Devonian and the late Eocene. Palaeogeogr., Palaeoclimatol., Palaeoecol. 176, 47-58.

McLaren, D.J., 1970. Time, life and boundaries. Journal of Paleontology 44, 801-815.

McManus, J., Berelson, W.M., Coale, K.H., Johnson, K.S., Kilgore, T.E., 1997. Phosphorus regeneration in continental margin sediments. Geochim. Cosmochim. Acta 61, 2891-2907.

McManus, J., Berelson, W.M., Klinkhammer, G.P., Johnson, K.S., Coale, K.H., Anderson, R.F., Kumar, N., Burdige, D.J., Hammond, D.E., Brumsack, H.J., McCorkle, D.C., Rushdi, A., 1998. Geochemistry of barium in marine sediments: implications for its use as a paleoproxy. Geochim. Cosmochim. Acta 62, 3453-3473.

Meyers, S., sageman B., Hinnov L., 2001. Integrated quantitative stratigraphy of Cenomanian-Turonian Bridge Creek Limestone Member using Evolutive Harmonic Analysis and stratigraphic modelling. J. Sedim. Res. 71, 628-644.

Middelburg, J.J., 1991. Organic carbon, sulphur, and iron in recent semi-euxinic sediments of Kau Bay, Indonesia. Geochim. Cosmochim. Acta 55, 815-828.

Mongenot, TH., Tribovillard, N.-P., Desprairies, A., Lallier-Vergès, E., Laggoun-Defarge, F. , 1996. Trace elements as paleoenvironmental markers in strongly mature hydrocarbon source rocks: the Cretaceous La Luna Formation of Venezuela. Sedimentary Geology 103, 23-37.

Morgan, J.P., Reston, T.J., Ranero, C.R., 2004. Contemporaneous mass extinctions, continental flood basalts, and "impact signals": are mantle plume-induced lithospheric gas explosions the causal link?. Earth Planet. Sci. Lett. 217,. 263-284.

Morse, J.W., Millero, F.J., Cornwell, J.C., Rickard, D., 1987. The Chemistry of Hydrogen Sulfide and Iron Sulfide Systems in Natural Waters. Earth Sc. Rev. 24, 1-42.

Morse, J.W., Emeis, K.C., 1990. Controls on C/S ratios in hemipelagic sediments. Amer. J. Sci. 285, 1117-1135.

Morse, J.W., 1992. Pyritization of metals in anoxic sediments. Journal of Geochemical Exploration 46 (2), 238

Morse, J.W., Arakaki, T., 1993. Adsorption and coprecipitation of divalent metals with mackinawite (FeS). Geochim. Cosmochim. Acta 57, 3635-3640.

Morse, J.W., 1994. Interactions of trace metals with authigenic sulfide minerals: Implications for their bioavailability, Mar. Chem. 46, 1-6.

Morse, J.W., Berner, R.A., 1995. What determines sedimentary C-S Ratios?. Geochim. Cosmochim. Acta. 59, 1073-1077.

Morse, J.W., Luther, G.W., 1999. Chemical influences on trace metal-sulfide interactions in anoxic sediments. Geochim. Cosmochim. Acta 63, 3373-3378.

Mossmann, J.R., Aplin, A.C., Curtis, C.D., Coleman, M.L., 1991. Geochemistry of inorganic and organic sulphur in organic-rich sediments from the Peru Margin. Geochim. Cosmochim. Acta 55, 3581-3595.

Moyer, C.L., Dobbs, F.C., Karl., D.M., 1995. Phylogenic diversity of the bacterial community from a microbial mat at an active, hydrothermal vent system, Loihi Seamount, Hawaii. Appl. Environ. Microbiol. 61, 1555-1562.

Muchez, P., Boulvain, F., Dreesen, R., Hou, H.F., 1996. Sequence stratigraphy of the Frasnian-Famennian transitional strata: a comparaison between South China and southern Belgium. Palaeogeogr., Palaeoclimatol., Palaeoecol. 123, 289-296.

Murao, S., Sie, S. H., Suter, G. F., 1996. Distribution of rare metals in Kuroko-type ore - a pixeprobe study. Nuclear Instruments & Methods in Physics Research Section B - Beam Interactions with Materials & Atoms 109, 627-632.

Murphy, A.E., Sageman, B.B., Hollander, D.J., 2000. Eutrophication by decoupling of the marine biogeochemical cycles of C, N, and P; a mechanism for the Late Devonian mass extinction. Geology 28, 427-430.

Murphy, J.B., Keppie, J.D., 1998. Late Devonian palinspastic reconstruction of the Avolon-Meguma terrane boundary: implication for terrane accretion and basin development in the Appalachian orogen. Tectonophysics 284, 221-231.

Murphy A.E., Sageman B.B., Hollander D.J., Lyons T.W., Brett, C.E., 2000. Black shale deposition in the Devonian Appalachian Basin: siliciclastic starvation, episodic water-column mixing, and efficient recycling of biolimiting nutrients. Paleoceanography 15, 280-291.

Nikishin, A.M., Ziegler, P., Stephenson, R.A., Cloetingh, S.A.P.L., Furne, A.V., Fokin, P.A., Yershov, A.V., Bolotov, S.N., Koratayev, M.V., Alekseyev, A.S., Gorbachev, V., Shipilov, E.V., Lankreijer, A., Bembinova, E.Y., Shalimov, I.V., 1996. Late Precambrian to Triassic history of the East European Craton; dynamics of sedimentary basin evolution. Tectonophysics 268, 23-63.

Over, D.J., Conaway, C.A., Katz, D.J., Goodfellow, W.D., Gregoire, D.C., 1997. Platinum group element enrichments and possible chondritic Ru:Ir across the Frasnian-Famennian boundary, western New York State. Palaeogeogr., Palaeoclimatol., Palaeoecol. 132, 399-410.

Paris, F., Girard, C., Feist, R., Winchester-Seeto, T., 1996. Chitinozoan bio-event in the Frasnian-Famennian boundary beds of La Serre (Montagne Noire, Southern France). Palaeogeogr., Palaeoclimatol., Palaeoecol. 121, 131-145.

Passier, H.F., Middelburg, J.J., van Os, B.J.H., de Lange, G.J., 1996. Diagenetic pyritization under eastern Mediterranean sapropels caused by downward sulphide diffusion. Geochim. Cosmochim. Acta 60, 751-763.

Peterhänsel, A., Pratt, R.B., 2001. Nutrient-triggered bioerosion on a giant carbonate platform masking the postextinction Famennian benthic community. Geology 29, 1079-1082.

Peterson, M.L., Carpenter, R., 1986. Arsenic distribution in porewaters and sediments of Puget Sound, Lake Washington, the Washington coast and Saanich Inlet, B.C. Geochim. Cosmochim. Acta 50, 353-369.

Piecha, M., 1994. Untersuchungen am Kernmaterial der Bohrung “Büdesheimer Bach“ (Kernbohrung 1) aus dem Oberdevon der Prümer Mulde (Eifel)-Stratigraphische, sedimentpetrographische und mikrofazielle Zusammenhänge. Cour. Forsch. Inst. Senckenberg 169, 329-349.

Piecha, M., 2002. A considerable hiatus at the Frasnian/Famennian boundary in the Rhenish Shelf region of northwest Germany. Palaeogeogr., Palaeoclimatol., Palaeoecol. 181, 195-211.

Pierret, M.C., Clauer, N., Blanc, G., 2000. Influence hydrothermale dans les sédiments de fosses de la mer rouge par l’étude de quelque éléments traces. Oceanol. Acta 23, 783-792.

Piper, D.Z., 1994. Seawater as the source of minor elements in Black shales, phosphorites and other sedimentary rocks. Chem. Geol. 114, 95-114.

Piqué, A., Bossiere, G., Bouillin, J.P., Chalouan, A., Hoepffner, C., 1993. Southern margin of the Variscan belt – the north-western Gondwana mobile zone (eastern Morocco and northern Algeria). Geol. Rdsch. 82, 432-439.

Poty, E., 1999. Famennian and Tournaisian recoveries of shallow water Rugosa following late Frasnian and late Strunian major crises, southern Belgium and surroundings areas, Hunan (South China) and the Omolon region (NE Siberia). Palaeogeogr., Palaeoclimatol., Palaeoecol. 154, 11-26.

Prange, A., Kremling, K., 1985. Distribution of dissolved molybdenum, uranium and vanadium in Baltic Sea waters. Mar. Chem. 16, 259-274.

Préat, A., Mamet, M., Bernard, A., Gillan, D., 1999. Bacterial mediation, red matrices diagenesis, Devonian, Montagne Noire (Southern France). Sediment. Geol. 126, 223-242.

Pujol, F., Berner, Z., Stüben, D. Paleoenvironmental changes at the Frasnian/Famennian boundary in key European sections: chemostratigraphic constraints. Palaeogeogr. Palaeoclimatol. Palaeoecol. (Reviewed and revised).

Pye, K., Krinsley, D.H., 1986. Diagenetic carbonate and evaporite minerals in Rotlieglend Aeolian sandstones of the southern North Sea: their nature and relationship to secondary porosity. Clay Min. 21, 443-457.

Racki, G., 1998. Frasnian-Famennian biotic crisis; undervalued tectonic control?. Palaeogeogr., Palaeoclimatol., Palaeoecol.141, 177-198.

Racki, G., 1999a. Silica-secreting biota and mass extinctions: survival patterns and processes. Palaeogeogr., Palaeoclimatol., Palaeoecol. 154, 107-132.

Racki, G., 1999b. The Frasnian-Famennian biotic crisis: How many (if any) bolide impact?. Geol. Rundsch. 87, 617-632.

Racki, G., Cordey, F., 2000. Radiolarial paleoecology and radiolarites: is the present the key to the past?. Earth-Sci. Rev. 52, 83-120.

Racki, G., Racka, M., Matyja, H., Devleeschouwer, X., 2002. The Frasnian/Famennian boundary interval in the South Polish-Moravian shelf basins; integrated event-stratigraphical approach. Palaeogeogr., Palaeoclimatol., Palaeoecol. 181, 251-297.

Raiswell, R., Plant, J., 1980. The incorporation of trace elements into pyrite during Diagenesis of Black Shales, Yorkshire, England. Economic Geology 75, 684-699.

Raiswell, R., Berner, R.A., 1985. Pyrite formation in euxinic and semi-euxinic sediments. Amer. J. Sc. 285, 710-724.

Raiswell, R., Berner, R.A., 1986. Pyrite and organic matter in Phanerozoic normal marine shales. Geochim. Cosmochim. Acta 50, 1967-1976.

Raiswell, R., Buckley, F., Berner, R.A., Anderson, T.F., 1988. Degree of pyritization of iron as a paleoenvironmental indicator of bottom-water oxygenation. Journal of Sedimentary Petrology 58, 812-819.

Raiswell, R., Al-Biatty, H.J., 1989. Depositional and diagenetic C-S-Fe signatures in early Paleozoic normal marine shales. Geochim. Cosmochim.Acta 53, 1147-1152.

Raiswell, R., Bottrell, S.H., Al -Biatty, H.J., Tan, M., 1993. The influence of bottom water oxygenation and reactive iron content on sulfur incorporation into bitumens from Jurassic marine shales. Am. J. Sci. 293, 569-596.

Rickard, D., Shoonen, M.A.A., Luther, G.W., 1995. Chemistry of iron sulfides in sedimentary environments. In: M.A. Vairavamurthy and M.A.A. Schoonen (eds.) Geochemical Transformations of Sedimentary Sulfur. ACS Symposium Series 612, ACS Washington, D.C. p. 168-193.

Riquier, L., Tribovillard, N., Averbuch, O., Joachimski, M., Racki, G., Devleeschouwer, X., El Albani, A., Riboulleau, A., in press. Productivity and bottom water redox conditions at the Frasnian-Famennian boundary on both sides of the Eovariscan Belt: constraints from trace-element geochemistry. Palaeogeogr., Palaeoclimatol., Palaeoecol. in press.

Sageman, B.B., Murphy, A.E., Werne, J.P., Ver Straeten, C.A., Hollander, D.J., Lyons, T.W., 2003. A tale of shales: the relative roles of production, decomposition, and dilution in the accumulation of organic-rich strata, Middle-Upper Devonian, Appalachian basin. Chem. Geol. 195, 229-273.

Sageman, B.B., Lyons, T.W., 2004. Geochemistry of Fine-Grained Sediments and Sedimentary Rocks. In: Mackenzie, F.T., Holland, H.D., Turekian, K.K. (eds.), Sediments, Diagenesis, and Sedimentary Rocks. Treatise on Geochemistry 7, Elsevier, Amsterdam, pp. 116-148.

Sander, S., Koschinsky, A., 2000. Onboard –ship redox speciat ion of chromium in diffuse hydrothermal fluids from the North Fiji Basin. Mar. Chem.. 71, 83-102.

Sawlowicz, Z., 1993. Pyrite framboids and their development: a new conceptual mechanism. Geol. Rundschau 82, 148-156.

Schaller, T., Morford, J., Emerson, S.R., Feely, R.A., 1999. Oxyanions in metalliferous sediments: tracers for paleoseawater metal concentrations?. Geochim. Cosmochim. Acta 64, 2243-2254.

Schieber, J., Krinsley, D., Riciputi, L., 2000. Diagenetic origin of quartz silt in mudstones and implications for silica cycling. Nature 406, 981 – 985.

Schindler, E., 1990. Die Kellwasser Krise (Hohe Frasne-Stufe, Ober-Devon). Gott. Arb. Geol. Palaontol. 46, 1-117.

Schmitz, B., Charisi, S.D., Thompson, E.I., Speijer, R.P., 1997. Barium, SiO_2 (excess), and P_2O_5 as proxies of biological productivity in the Middle East during the Palaeocene and the latest Palaeocene benthic extinction event. Terra Nova 9, 95-99.

Schoonen, M. A. A., Barnes, H. L., 1991. Reactions forming pyrite and marcasite from solution: I. Nucleation of FeS_2 below 100°C. II. Via FeS precursors below 100°C. Geochim. Cosmochim. Acta, v. 55, p. 1495-1504 and 1505-1514.

Scotese, C.R., McKerrow, W.S., 1990. Revised worl maps and introduction. In: McKerrow, W.S., Scotese, C.R., (eds.), Palaeozoic palaeogeography and biogeography, Geol. Soc. Mem. 12, pp. 1-21.

Sengör, A.M.C., Cakir, Z., Eris, K., 1998. Continental elevation as indicator of mantle plume activity: Late Devonian East Europe as a taste case. Geol. Soc. Am. Abstr. Pr. 30. pp. 343.

Sepkoski, J.J., 1986. Phanerozoic overview of mass extinction. In: Raup, D.M., Jablonski, D., (eds.): Patterns and progresses in the history of life. Berlin, Springer, 277-295.

Sheridan, R.E., 1997. Pulsation tectonics as a control on the dispersal and assembly of supercontinents. J. Geodyn. 23, 173-196.

Starinsky, A., Katz, A., Kolodny, Y., 1982. The incorporation of uranium into diagenetic phosphorite. Geochim. Cosmochim. Acta 46, 1365-1374.

Stearn, C.W., 1987. Effect of the Frasnian-Fammenian extinction event on the stromatoporoids. Geology 15, 677-679.

Stephens, N.P., Sumner, D.Y., 2003. Late Devonian carbon isotope stratigraphy and sea level fluctuations, Canning Basin, Western Australia. Palaeogeogr., Palaeoclimatol., Palaeoecol. 191, 203-219.

Sternbeck, J., Sohlenius, G., Hallberg, R.O., 2000. Sedimentary trace elements as proxies to depositional changes induced by a Holocene fresh-brackish water transition. Aquatic Geochemistry 6, 325-345.

Strauss, H., 1999. Geological evolution from isotope proxy signals – sulfur. Chem. Geol. 161, 89-101.

Streel, M., Caputo, M.V., Loboziak, S., Melo, J.H.G., 2000. Late Frasnian-Famennian climates based on palynomorph analyses and the question of the late Devonian glaciations. Earth-Sci. Rev. 52, 121-173.

Stüben, D., Berner, Z., Puchelt, H., Noeltner, T., 2002. Trace Element Pattern of Authigenic Pyrite: A Promising Proxy for the Redox State of Depositional Environment. EOS Trans. AGU, 83(47), Fall Meet. Suppl., Abstract PP51A-0267.

Sullivan, K.A., Aller, R.C., 1996. Diagenetic cycling of arsenic in Amazon shelf sediments. Geochim. Cosmochim. Acta 60, 1465-1477.

Suzuki, N., Ishida, K., Shinomiya, Y., Ishiga, H., 1998. High productivity in the earliest Triassic ocean: blach shales, Southwest Japan. Palaeogeogr., Palaeoclimatol., Palaeoecology. 141, 53-65.

Tait, J., Bactadse, V., Franke, W., Sofel, H., 1997. Geodynamic evolution of the European Varisacn fold belt: paleomagnetic and geological constraints. Geol. Rdsch. 86, 585-598.

Tertian, R., Claisse, F., 1982. Principle of Quantitative X-Ray Fluorescence Analysis, Heyden & Sons, London.

Thomas, R.C., Saunders, J.A., 1998. Arsenic coprecipitation in low-temperature pyrite; implications for bioremediation via sulfate reducing bacteria. Geol. Soc. Am. Abst. Progr. 30, 58

Thomson, J., Higgs, N. C., Wilson, T. R. S., Croudace, I. W., de Lange, G. J. and van Santvoort, P. J. M., 1995. Redistribution and geochemical behaviour of redox-sensitive elements around S1, the most recent eastern Mediterranean sapropel. Geochim. Cosmochim. Acta 59, 3487-3501.

Tribovillard, N., Averbuch, O., Devleeschouwer, X., Racki, G., Riboulleau, A., 2004. Deep water anoxia over the Frasnian-Famennian boundary (La Serre, France): a Tectonically induced oceanic anoxic event?. Terra Nova 16, 288-295.

Tonguç Uysal, I., Golding, S.D., Glikson, A.Y., Mory, A.J., Glikson, M .,2001. K-Ar evidence from illitic clays of a Late Devonian age for the 120 km diameter Woodleigh impact structure, Southern Carnarvon Basin, Western Australia. Earth Planet. Sci. Lett. 192, 281-289.

Tucker, R.D., Bradley, D.C., Ver Straeten, C.A., Harris, A.G., Ebert, J.R., McCutcheon, S.R., 1998. New U-Pb zircon ages and the duration and division of the Devonian time. Earth Planet. Sci. Lett. 158, 175-186.

Turner, R.J.W., 1992. Formation of the Phanerozoic stratiform sediment-hosted Pb-Zn deposits: evidence for the critical role of ocean anoxia. Chem. Geol. 99, 165-188.

Veimarn, A.B., Kuzmin, A.V., Vorontsova, T.N., 1997. Geologicheskie sobytiya v Kazakhstanie na rubezhe franskogo i famenskogo vekov i ich znachene v ryadu global'nykh sobytii etogo vremenii. Biul. Mosk. Obsch. Ispyt. Prirody. Otd. Geol. 72, 35-46.

Vermeij, G.J., 1995. Economics, volcanoes, and Phanerozoic revolutions. Paleobiology 21, 125-152.

Vicente, J.C., 1975. Essai d'organisation paléogéographique et structurale du Paléozoïque des Andes méridionales. Geol. Rdsch. 64, 343-394.

Vishnevskaya, V., Pisera. A., Racki, G., 2002. Siliceous biota (radiolarians and sponges) and the Late Devonian crisis: The Polish reference. Acta Palaeontol. Pol. 47, 211-226.

Vismann, B., 1991. Sulfide tolerance: physiological mechanisms and ecological implications: Ophelia 34, 1-27.

Vogt, P.R., 1989. Volcanogenic upwelling of anoxic, nutrients-rich water, a possible factor in carboate-bank/reef demise and benthic faunal extinctions?. Geol. Soc. Am. Bull. 101, 1225-1245.

Von Damm, K.L., 1995. Controls of the chemistry and temporal variability of sea floor hydrothermal systems. In: Humphris, S.E., Zierenberg, R.A., Mullineaux, L.S., Thomson, R.E. (eds.), Seafloor Hydrothermal Systems: Physical, Chemical, Biological and Geological Interactions. Geophysical monograph 91, AGU, Washington DC, pp. 222-247.

Wang, K., Orth, C.J., Attrep, M., Chatterton, B.D.E., Hou, H., Geldsetzer, H.H.J., 1991. Geochemical evidence for a catastrophic biotic event at the, Frasnian/Fammenian boundary in south China. Geology 19, 776-779.

Wang, K., Geldsetzer, H.H.J., Goodfellow, W.D., Krouse, H.R., 1996 Carbon and sulfur isotope anomalies across the Frasnian-Famennian extinction boundary, Alberta, Canada. Geology 24, 187-191.

Watling, J.R., Herbert, H.K., Abell, I.D., 1995. The application of laser ablation-inductively coupled plasma-mass spectrometry (LA-ICP-MS) to analysis of selected sulphide minerals. Chem. Geol. 124, 67-81.

Werne, J.P., Sageman B.B., Lyons T., Hollander D.J., 2002. An integrated assessment of a "type euxinic" deposit: evidence for multiple controls on black shale deposition in the Middle Devonian Oatka Creek Formation. Am. J. Sci. 302, 110-143.

Whalen, M.T., Day, J., Eberli, G.P., Homewood, P.W., 2002. Microbial carbonates as indicators of environmental change and biotic crises in carbonate systems: examples from the late Devonian, Alberta basin, Canada. Palaeogeogr., Palaeoclimatol., Palaeoecol. 181, 127-151.

Wheat, C.G., Jannasch, H.W., Kastner, M., Plant, J.N., Heinen DeCarlo, E., 2003. Seawater transport and reaction in upper basaltic basement: chemical data from continuous monitoring of sealed boreholes in a ridge flank environment. Earth Planet. Sci. Lett. 216, 549-564.

Whyte, M.A., 1977. Turning points in Phanerozoic history. Nature 267, 679-682.

Williams, K. L., 1987. An Introduction to X-Ray Spectrometry, Allen & Unwin, London.

Wilkin, R.T., Barnes, H.L., Brantley, S.L., 1996. The size distribution of framboidal pyrite in modern sediments: An indicator of redox conditions. Geochim. Cosmochim. Acta 60, 3897-3912.

Wilkin, R.T., Arthur, M.A., Dean, W.E., 1997. History of water-column anoxia in the Black Sea indicated by pyrite framboid size distributions. Earth Planet. Sci. Lett 148, 517-525.

Wilkin, R.T., Barnes, H. L., 1997. Formation process of framboidal pyrite. Geochim. Cosmochim. Acta 60, 323-339.

Wilkin, R.T., Arthur, M.A., 2000. Variations in pyrite texture, sulfur isotope composition, and iron systematics in the Black Sea; evidence for late Pleistocene to Holocene excursions of the O (sub 2) -H (sub 2) s redox transition. Geochim. Cosmochim. Acta 65, 1399-1416.

Wilson, M., Lyashkevitch, Z.M., 1996. Magmatism and the geodynamics of rifting of the Pripyat-Dnieper-Donets Rift, East European Platform. Tectonophysics 268, 65-81.

Young, C.G., Moody, J.M., Casas, J.E., 2000. New discoveries of Devonian vertebrated from South America, and implications for Gondwana-Euramerica contact. CR. Acad. Sci. II. A. 331, 755-761.

Yudina, B.A., Racki, G., Savage, N.M., Racka, M., Malkowski, K., 2002. The Frasnian-Famennian events, Subpolar Urals: biotic, depositional, and geochemical records. Acta Palaeontol. Pol. 47, 355-372.

Zakowa, H., Radlicz, K., 1990. Makro- i mikrofauna oraz petrographia famenu z otworu wiertniczego Kowala 1. Kwart. Geol. 34, 243-270.

Ziegler, W., 1971. A field trip guidebook; post-symposium excursion, Sept. 15-18, 1971 to Rhenish Slate Mountains and Harz Mountains. Phillips-University of Marburg, Symposium on conodont taxonomy, 47 pp.

Ziegler, W., Sandberg, C.A.,1990. The Late Devonian standard conodont zonation. Cour. Forsch. Inst. Senckenberg. 121, 115 pp, 17 pls.

Zimmerle, W., 1985. New aspects on the formation of hydrocarbon source rocks. Geol.Rundsch. 74, 385-416.

Appendix

Table 8. Results of the Kowala section analysis.

Sample name	Depth (m)	Na_2O (%)	MgO (%)	Al_2O_3 (%)	SiO_2 (%)	P_2O_5 (%)	CaO (%)	K_2O (%)	TiO_2 (%)	MnO (%)	Fe_2O_3 (%)	V (ppm)	Cr (ppm)	Ni (ppm)	Co (ppm)	Zr (ppm)	Ba (ppm)	Cu (ppm)	Zn (ppm)	As (ppm)	Ag (ppm)	Pb (ppm)	Corg (%)	S (%)	Quartz (integ I)
K65	3.1	0.02	0.84	1.71	6.67	0.08	47.6	0.49	0.09	0.02	1.20	14	24	19	6	20	48	17	238	11	<0.7	8	1.7	0.88	1995
K64	3.3	0.02	0.89	1.91	7.85	0.06	47.0	0.56	0.10	0.02	1.04	14	22	21	6	20	33	19	125	6	1.3	9	1.8	0.61	2587
K63	3.5	0.04	0.83	1.72	7.62	0.07	48.1	0.53	0.09	0.03	1.05	14	26	21	5	19	37	12	206	9	<0.7	<5	1.1	0.56	2683
K62	4	0.03	0.76	1.43	5.72	0.07	49.3	0.42	0.08	0.03	0.91	18	20	14	5	16	33	23	143	8	<0.7	6	1.0	0.50	1954
K61	4.4	0.02	0.85	1.82	7.16	0.15	47.5	0.56	0.10	0.03	1.68	24	18	28	8	20	28	76	132	12	<0.7	25	1.6	1.23	1920
K60	5	0.03	0.98	2.33	10.22	0.16	45.4	0.70	0.12	0.03	0.93	17	18	15	6	25	46	18	54	7	0.8	<5	1.7	0.38	3404
K59	5.7	0.05	1.88	4.34	16.39	0.14	38.6	1.34	0.22	0.03	1.32	53	35	25	9	43	96	16	146	7	<0.7	16	2.3	0.29	5556
K58	5.8	0.03	0.73	1.38	6.14	0.05	48.9	0.41	0.08	0.03	1.44	19	19	25	8	16	23	13	291	11	1.0	18	1.7	1.07	1987
K57	6.15	0.03	0.97	1.79	6.92	0.10	47.8	0.53	0.09	0.03	0.99	22	20	22	6	22	29	11	145	10	1.0	<5	1.7	0.62	2158
K56	6.3	0.02	0.83	1.39	5.87	0.09	48.8	0.41	0.07	0.03	1.18	24	17	20	7	16	36	24	321	13	<0.7	6	1.7	0.88	2276
K55	6.6	0.03	0.90	1.42	5.72	0.07	49.0	0.43	0.08	0.02	1.02	15	21	17	9	16	19	13	121	10	<0.7	9	1.6	0.67	2029
K54	6.9	0.03	0.63	0.85	4.46	0.06	50.9	0.24	0.05	0.02	0.62	21	22	15	7	14	19	17	389	5	<0.7	11	1.9	0.49	1561
K53	7.4	0.03	1.20	2.41	9.70	0.07	45.7	0.72	0.12	0.03	0.88	33	27	14	6	26	56	13	226	8	0.7	12	1.8	0.36	2954
K52	7.7	0.03	1.24	3.00	12.11	0.06	43.3	0.90	0.14	0.03	0.89	47	28	22	9	28	62	98	197	9	<0.7	15	2.4	0.22	4016
K50	8.1	0.10	2.86	8.15	29.59	0.19	25.7	2.48	0.39	0.03	2.11	139	60	46	9	68	177	25	421	17	0.8	56	3.1	0.55	10064
K49	8.15	0.05	0.83	1.79	7.21	0.14	47.7	0.55	0.10	0.03	1.04	26	22	15	7	19	24	17	559	9	0.5	19	1.7	0.72	2042
K48	8.2	0.08	2.60	7.31	27.12	0.23	28.3	2.24	0.35	0.03	2.05	124	63	49	12	65	159	27	494	24	1.1	75	3.0	0.63	9442
K47	8.4	0.04	1.10	2.54	10.28	0.13	45.5	0.77	0.14	0.03	1.28	44	31	30	9	29	49	28	461	12	0.7	21	2.2	0.70	3010
K46	8.55	0.09	2.49	8.15	30.44	0.62	23.4	2.51	0.40	0.03	3.01	127	54	70	16	76	181	34	464	46	2.1	44	2.9	1.56	10787
K45	8.65	0.04	0.76	1.60	6.56	0.09	48.1	0.49	0.09	0.03	2.05	20	18	44	9	19	35	16	488	28	<0.7	12	0.7	1.83	2163
K44	8.8	0.03	0.85	1.80	7.82	0.08	48.5	0.55	0.09	0.03	1.22	20	25	18	10	22	42	19	322	16	1.5	14	1.6	0.81	2338
K43	9	0.03	0.68	1.28	5.98	0.14	49.7	0.36	0.07	0.03	1.26	11	20	23	8	15	27	18	278	12	1.3	15	1.7	1.06	1944
K42	9.25	0.07	1.11	2.18	9.26	0.07	46.1	0.66	0.11	0.04	1.17	17	21	48	8	18	45	17	415	8	0.5	10	1.6	0.63	3077
K39	10.3	0.01	0.89	1.17	12.03	0.15	46.6	0.35	0.07	0.04	0.34	30	18	29	5	16	20	14	29	7	<0.7	<5	1.3	0.04	5927

Sample name	Depth (m)	Na_2O (%)	MgO (%)	Al_2O_3 (%)	SiO_2 (%)	P_2O_5 (%)	CaO (%)	K_2O (%)	TiO_2 (%)	MnO (%)	Fe_2O_3 (%)	V (ppm)	Cr (ppm)	Ni (ppm)	Co (ppm)	Zr (ppm)	Ba (ppm)	Cu (ppm)	Zn (ppm)	As (ppm)	Ag (ppm)	Pb (ppm)	Corg (%)	S (%)	Quartz (integ I)
K38	10.7	0.02	3.62	3.63	18.14	0.11	36.3	1.04	0.18	0.11	2.12	175	44	15	4	37	62	6	27	8	<0.7	<5	1.3	0.12	8142
K37	11.2	0.03	3.43	3.52	23.26	0.15	34.4	1.07	0.18	0.19	1.26	131	34	10	6	35	70	12	88	5	<0.7	27	1.0	0.03	12093
K36	11.35	0.03	0.51	0.92	12.94	0.08	47.3	0.25	0.05	0.04	0.28	13	23		6	20	30	10	30	4	<0.7	<5	1.1	0.02	7260
K35	11.8	0.03	0.96	1.35	14.83	0.06	44.2	0.43	0.08	0.05	0.39	110	19	5	2	15	17	10	25	4	0.6	<5	1.4	0.001	4154
K34	12.3	0.01	0.72	0.98	10.65	0.06	55.0	0.30	0.06	0.03	0.30	69	19	4	6	21	59	5	62	7	<0.7	6	0.9	0.001	17182
K33	12.6	0.05	2.79	5.51	36.22	0.09	26.4	1.66	0.28	0.14	1.69	386	65	20	6	51	120	12	98	4	0.6	154	0.6	0.02	19319
K31	13.2	0.05	0.71	1.21	44.12	0.24	28.3	0.36	0.07	0.05	2.21	201	28	8	7	14	34	21	41	24	0.5	12	0.6	0.02	23245
K30	13.3	0.06	0.77	1.14	14.79	0.14	46.0	0.34	0.07	0.03	0.38	40	24	5	6	16	44	12	32	1	0.9	<5	1.3	0.002	7065
K29	13.15	0.03	0.39	0.22	9.50	0.09	50.3	0.07	0.03	0.02	0.28	24	17	3	5	11	<10	13	16	4	1.2	<5	0.9	0.001	4546
K28	13.6	0.07	0.16		69.04	0.08	16.9	0.11	0.04	0.02	0.17	9	31		7	7	21	13	18	4	0.8	<5	0.2	0.01	52853
K27	13.75	0.05	1.27		28.29	0.10	33.5	0.47	0.09	0.07	0.65	121	27	2	2	16	26	16	15	0	0.9	35	1.2	0.02	6320
K26	14	0.06	0.45		7.63	0.07	52.7	0.10	0.03	0.03	0.18	0	18	14	4	14	<10	10	15	1	<0.7	7	1.6	0.02	3397
K25	15	0.01	0.39	0.18	7.50	0.05	49.0	0.06	0.02	0.03	0.14	4	11	1	5	10	<10	13	14	4	<0.7	<5	1.1	0.02	3549
K24	15.1	0.03	0.39		8.87	0.05	48.4	0.07	0.03	0.03	0.17	-1	15	2	4	10	25	10	19	6	0.8	<5		0.01	4441
K23	15.25	0.04	0.74	0.79	38.12	0.12	32.4	0.24	0.06	0.06	0.43	14	21		3	13	31	3	24	3	<0.7	<5	0.6	0.0002	22122
K22	15.35	0.02	0.97		16.97	0.13	43.6	0.30	0.06	0.07	0.49	23	20	1	3	15	22	36	33	4	<0.7	5	1.2	0.2	8350
K21	15.45	0.02	0.66		18.10	0.05	43.6	0.14	0.04	0.05	0.33	6	24	3	4	12	<10	6	14	5	<0.7	<5	1.2	0.002	8778
K20	15.9	0.04	1.12		13.95	0.11	43.7	0.27	0.06	0.10	0.56	9	21	3	4	19	24	0	34	5	0.6	9	1.2	0.01	6554
K19	16.05	0.02	0.69	0.46	10.90	0.06	47.4	0.14	0.03	0.04	0.28	7	12	3	3	11	<10	17	26	1	<0.7	5	1.1	0.0005	4854
K18	16.2	0.04	1.24	1.05	17.03	0.08	43.2	0.31	0.07	0.08	0.44	14	17	1	5	13	24	9	39	4	<0.7	<5	0.9	0.003	7561
K17	16.3	0.02	3.72	3.03	21.26	0.18	35.9	0.89	0.16	0.16	1.57	30	36	12	5	31	68	7	172	10	<0.7	8	0.3	0.01	10325
K16	16.6	0.05	4.00	2.65	20.08	0.10	36.4	0.79	0.14	0.12	1.36	26	28	5	4	27	55	7	36	4	<0.7	13	0.9	0.03	10040
K15	17.5	0.02	3.56	1.96	10.86	0.06	42.1	0.57	0.10	0.03	0.80	21	18	14	10	26	37	14	40	11	0.8	55	2.1	0.32	4383
K13	18.4	0.07	2.68	4.00	16.40	0.09	36.3	1.23	0.20	0.03	1.70	48	34	40	13	43	101	62	532	24	0.6	136	2.6	0.91	6090
K12	18.65	0.02	0.74	1.51	7.18	0.04	48.5	0.45	0.09	0.02	1.15	52	23	20	5	19	37	15	268	9	<0.7	43	1.1	0.63	2698
K11	18.8	0.04	0.66	2.01	8.68	0.16	47.4	0.56	0.11	0.02	1.05	59	21	20	7	25	45	21	157	12	<0.7	47	1.8	0.66	3378
K10	19.7	0.03	1.11	1.57	7.13	0.18	48.2	0.47	0.09	0.02	0.88	43	18	11	6	20	46	12	68	9	1.7	58	1.5	0.51	2335
K9	19.85	0.02	1.04	1.38	6.24	0.10	49.1	0.42	0.08	0.02	1.03	70	16	16	9	20	28	15	74	13	0.7	47	0.9	0.44	1896

Sample name	Depth (m)	Na_2O (%)	MgO (%)	Al_2O_3 (%)	SiO_2 (%)	P_2O_5 (%)	CaO (%)	K_2O (%)	TiO_2 (%)	MnO (%)	Fe_2O_3 (%)	V (ppm)	Cr (ppm)	Ni (ppm)	Co (ppm)	Zr (ppm)	Ba (ppm)	Cu (ppm)	Zn (ppm)	As (ppm)	Ag (ppm)	Pb (ppm)	Corg (%)	S (%)	Quartz (integ I)
K8	20	0.03	0.67	1.90	8.34	0.26	47.6	0.55	0.10	0.03	1.10	28	22	15	10	21	46	5	36	15	<0.7	28	1.9	0.58	3451
K7	20.45	0.03	0.65	1.55	7.13	0.31	48.7	0.43	0.09	0.03	0.86	33	20	21	8	22	41	9	18	12	1.5	47	2.0	0.40	3097
K6	20.9	0.03	0.70	1.72	7.81	0.26	48.6	0.49	0.09	0.04	0.92	29	18	18	6	19	35	80	24	6	<0.7	62	1.5	0.42	3503
K5	21.4	0.04	0.69	2.10	9.58	0.04	46.2	0.61	0.11	0.03	0.87	24	15	12	8	24	43	16	30	8	<0.7	14	0.5	0.28	3734
K4	21.9	0.05	1.36	2.66	10.13	0.07	44.7	0.82	0.14	0.04	0.98	26	24	22	7	28	59	29	30	6	<0.7	34	1.2	0.22	3437
K3	22.6	0.03	1.04	2.72	11.18	0.10	45.9	0.84	0.15	0.04	1.24	35	25	19	11	39	84	10	27	5	<0.7	36	0.7	0.08	5653
K2	22.9	0.05	1.31	2.63	9.21	0.05	46.3	0.81	0.14	0.08	1.15	26	25	24	9	32	67	11	25	8	1.2	54	1.1	0.45	4202
KS2S7	25	0.04	1.16	3.34	13.66	0.11	40.6	1.04	0.19	0.05	1.03	46	29	19	8	29	55	20	85	7	<0.7	15	1.4	0.33	3323
KS2S6	25.15	0.05	1.21	3.31	12.89	0.07	43.0	1.00	0.18	0.07	1.37	28	29	21	9	36	81	17	118	13	<0.7	17	0.9	0.42	4719
KS2S4	25.45	0.05	1.17	4.81	18.15	0.10	38.3	1.42	0.25	0.07	1.70	42	33	32	14	45	123	22	225	15	0.1	31	1.4	0.46	7105
KS2S3	25.55	0.05	1.50	3.80	13.92	0.05	41.8	1.16	0.21	0.07	1.43	30	33	21	10	41	88	18	197	12	0.7	23	1.0	0.32	4608
KS2S2	25.65	0.07	1.60	4.57	16.82	0.06	39.1	1.40	0.24	0.10	1.75	41	35	24	10	48	105	18	616	17	<0.7	59	0.8	0.44	6149
KS2S1	25.75	0.04	0.80	2.64	9.74	0.06	45.7	0.73	0.15	0.08	1.37	22	25	23	12	27	77	36	152	13	0.9	26	1.2	0.59	4030
KS1S9	26.1	0.04	0.76	2.39	9.07	0.05	46.1	0.74	0.13	0.06	1.00	21	22	31	6	26	47	8	157	34	0.8	11	1.3	0.38	2989
KS1S8	26.2	0.05	0.77	2.27	8.15	0.05	46.6	0.63	0.12	0.07	1.57	36	26	69	9	25	56	22	498	141	<0.7	127	1.2	0.87	2823
KS1S7	26.3	0.04	0.73	2.41	9.02	0.06	46.1	0.67	0.12	0.12	0.78	33	20	13	7	28	65	16	303	23	0.6	14	1.3	0.33	4056
KS1S6	26.4	0.05	0.67	2.19	8.76	0.05	45.2	0.63	0.12	0.05	0.74	36	14	16	6	23	56	18	476	8	0.7	92	0.1	0.20	3207
KS1S5	26.5	0.03	0.77	2.52	9.88	0.06	44.8	0.72	0.13	0.05	0.89	35	26	21	7	25	55	9	97	8	0.5	50	1.0	0.18	3244
KS1S4	26.6	0.03	0.84	3.09	12.36	0.09	43.1	0.88	0.17	0.13	0.96	47	31	19	8	35	75	17	58	11	0.7	277	1.0	0.13	6157
KS1S3	26.7	0.04	0.82	2.69	10.78	0.07	44.1	0.77	0.14	0.09	1.19	36	33	21	10	29	68	21	34	10	1.2	18	1.3	0.44	4598
KS1S2	26.8	0.05	1.10	3.73	14.93	0.11	40.5	1.13	0.20	0.09	1.55	54	32	20	13	37	83	70	79	17	1.5	139	1.6	0.47	5817
KS1S1	26.9	0.05	0.79	2.36	9.29	0.07	44.2	0.69	0.13	0.14	1.35	20	17	15	13	26	49	20	350	13	1.4	25	1.1	0.67	4027

Table 9. Results of the Büdesheimer Bach section analysis.

Sample depth (m)	Na_2O (%)	MgO (%)	Al_2O_3 (%)	SiO_2 (%)	P_2O_5 (%)	CaO (%)	K_2O (%)	TiO_2 (%)	MnO (%)	Fe_2O_3 (%)	V (ppm)	Cr (ppm)	Ni (ppm)	Co (ppm)	Zr (ppm)	Ba (ppm)	Cu (ppm)	Zn (ppm)	As (ppm)	Ag (ppm)	Pb (ppm)	Corg (%)	S (%)	Quartz (integ I)
30.20	0.58	2.98	17.0	47.8	0.09	6.89	4.03	0.68	0.07	7.48	124	96	65	25	131	413	57	164	21	0.8	14	1.06	0.75	15779
32.50	0.63	2.86	17.7	48.7	0.13	5.15	4.21	0.71	0.07	7.46	156	87	58	22	140	460	51	123	29	1.7	15	1.09	0.81	16360
32.90	0.73	2.83	17.4	47.9	0.07	6.25	4.15	0.68	0.06	7.11	208	91	57	22	139	435	77	134	15	0.8	21	1.35	0.73	16479
33.00	0.65	2.83	18.0	48.8	0.06	5.13	4.21	0.71	0.06	7.39	281	87	66	23	129	458	57	123	13	1.2	29	1.32	1.04	15680
45.00	0.60	2.68	15.3	45.4	0.06	8.58	3.66	0.61	0.08	6.63	133	76	54	23	110	426	46	60	21	0.9	42	1.65	1.43	16627
47.90	0.72	2.97	17.9	50.6	0.13	4.25	4.28	0.72	0.07	6.96	221	77	56	17	123	489	47	86	13	1.2	21	0.74	1.09	17676
57.90	0.70	2.88	18.0	49.3	0.09	5.32	4.20	0.70	0.06	6.39	233	80	55	17	131	460	58	126	10	<0.7	23	1.24	1.07	16209
71.80	0.46	2.73	15.7	43.7	0.08	9.92	3.81	0.61	0.06	5.27	253	96	72	20	91	319	184	92	24	<1	23	1.80	1.01	13568
73.80	0.56	3.39	14.5	40.8	0.09	11.39	3.42	0.57	0.09	6.42	86	80	46	15	93	372	33	70	85	0.7	36	2.77	1.52	13668
79.35	0.66	3.09	16.5	46.6	0.07	6.86	3.75	0.69	0.07	6.41	283	67	55	20	131	460	47	120	16	0.8	20	1.04	1.02	16806
82.35	0.69	3.00	17.5	49.9	0.10	5.47	3.92	0.76	0.07	6.63	220	83	54	19	139	459	42	135	22	1.1	13	1.02	0.67	18376
83.15	0.69	2.95	17.2	50.3	0.06	5.94	3.87	0.76	0.07	6.20	196	83	54	16	139	471	40	127	14	1.1	15	1.02	0.33	19895
84.00	0.81	2.94	17.0	47.7	0.54	6.75	3.80	0.72	0.08	6.83	170	89	62	15	133	465	40	116	16	1.6	10	0.98	0.39	17275
86.10	0.65	3.04	17.2	45.4	0.67	7.29	3.80	0.70	0.09	8.50	130	124	74	19	131	468	38	127	21	0.8	13	0.80	0.42	14317
103.00	0.62	2.63	17.5	46.7	0.05	6.53	3.92	0.74	0.10	7.42	398	63	86	19	130	472	47	187	28	1.2	46	1.06	1.39	15035
109.20	0.66	2.71	16.3	43.9	0.06	9.85	3.68	0.66	0.14	6.89	428	45	92	29	121	451	23	106	30	1.6	42	1.44	0.97	13597
124.15	0.50	2.19	11.7	36.5	0.09	17.65	2.75	0.48	0.10	6.23	419	16	89	18	106	330	33	101	10	0.3	14	0.77	0.14	13509
126.50	0.10	0.64	1.5	6.5	0.04	48.07	0.30	0.05	0.07	1.48	34	33	11	2	17	51	8	103	27	1.7	19	2.71	0.99	2206
127.00	0.37	1.43	8.8	39.8	0.10	20.51	2.11	0.28	0.03	3.24	94	45	40	12	56	236	31	70	21	1.3	31	4.14	1.24	18764
134.80	0.47	2.09	10.1	32.4	0.50	22.92	2.32	0.41	0.09	4.71	139	67	53	14	77	248	29	136	32	<0.7	13	2.16	0.92	10462
137.00	0.54	2.93	14.0	46.6	0.14	10.79	3.51	0.53	0.04	4.17	163	75	49	13	99	330	48	123	16	<0.7	17	2.50	1.35	15716
138.20	0.37	4.42	9.2	45.4	0.09	11.44	2.37	0.38	0.04	4.56	96	56	41	17	70	186	45	74	24	1.5	31	4.90	1.83	20422
138.55	0.45	2.58	8.8	45.4	0.08	15.11	2.19	0.36	0.03	4.23	91	53	40	13	83	195	45	79	24	1.9	39	3.32	0.48	19797
138.90	0.12	0.56	1.6	8.1	0.03	46.91	0.32	0.05	0.03	0.92	14	33	11	6	23	26	11	105	16	<0.7	6	4.33	0.39	2376
139.25	0.19	0.73	1.4	6.5	0.06	46.71	0.25	0.05	0.03	1.03	13	31	10	6	29	28	13	10	5	1.5	5	3.66	0.66	1928
139.35	0.17	1.60	2.9	23.8	0.06	35.33	0.70	0.12	0.03	1.61	25	33	13	4	29	64	14	47	7	1.3	15	6.86	1.91	10497
141.00	0.51	5.58	11.7	38.6	0.08	14.18	3.00	0.54	0.07	4.86	126	64	37	12	106	266	42	46	6	<0.7	17	1.94	0.60	11302
141.25	0.56	4.44	12.8	42.1	0.16	12.75	3.24	0.59	0.06	5.00	151	68	42	16	111	314	49	65	7	1.5	18	1.83	0.82	13445
141.75	0.34	3.16	6.8	24.3	0.07	29.71	1.77	0.31	0.07	3.31	82	44	21	13	63	151	16	44	7	<0.7	10	1.92	0.51	6606
141.85	0.25	2.29	4.8	17.5	0.06	36.34	1.18	0.22	0.08	3.05	58	43	17	8	43	110	16	38	7	1.3	11	1.80	0.82	4706
142.95	0.26	1.45	4.1	15.1	0.07	39.92	0.99	0.19	0.12	2.61	61	36	15	10	41	97	11	34	7	<0.7	4	1.70	0.88	4190
144.30	0.68	3.72	12.9	42.2	0.08	12.59	3.22	0.61	0.07	5.94	339	40	62	22	127	323	39	131	12	<0.7	16	1.89	0.96	13278
144.90	0.68	3.66	14.4	47.8	0.10	9.71	3.49	0.70	0.07	5.53	94	79	40	16	151	367	38	91	10	<0.7	9	0.56	0.28	16838
150.30	0.73	3.19	13.5	44.5	0.08	11.42	3.33	0.64	0.05	5.86	388	38	60	19	132	356	44	106	11	1.4	17	1.80	0.79	15030

Sample depth (m)	$Fe_{reactive}$ (ppm)	DOP	$\delta 34S_{pyrite}$ (‰ V-CDT)	$Mg_{reactive}$ (ppm)	V_{reac}	Cr_{reac}	Mn_{reac}	Co_{reac}	Ni_{reac}	Cu_{reac}	Zn_{reac}	As_{reac}	Sr_{reac}	Mo_{reac}	Ag_{reac}	Cd_{reac}	Sb_{reac}	Ba_{reac}	Tl_{reac}	Pb_{reac}	Th_{reac}	U_{reac}
30.20	28568	0.19																				
32.50	20398	0.26	-9.37																			
32.90	18198	0.26	-4.09	8276	41	17	305	11	27	14	98	9	316	0.60	0.08	0.05	0.10	41	0.08	15	4.68	0.48
33.00	17433	0.34		7716	57	17	270	12	25	25	63	10	288	1.90	0.08	0.05	0.10	47	0.05	22	4.58	0.65
45.00	13831	0.47																				
47.90	14596	0.39																				
57.90	15563	0.37																				
71.80	7275	0.55		5840	14		250	3	32	7	271	7	357			1.79	1.26	46		16	4.10	1.00
73.80	12471	0.52																				
79.35	15096	0.37																				
82.35	17513	0.25	-26.33	8876	39	15	352	10	25	6	129	15	258	0.43	0.23	0.05	0.10	69	0.20	17	5.50	0.75
83.15	16011	0.15	-22.61	8493	34	14	349	4	20	6	122	14	260	0.33	0.05	0.05	0.10	67	0.05	29	4.25	0.63
84.00	20758	0.14		8294	37	19	438	11	22	15	75	8	351	1.58	0.55	0.05	0.33	77	0.05	15	5.33	1.83
86.10	27468	0.12	-8.62	7786	30	15	441	11	20	10	65	7	345	0.40	0.05	0.05	0.10	66	0.05	13	6.40	3.03
103.00	10906	0.53	-3.80	3359	52	8	468	15	19	3	135	23	320	5.18	0.28	3.05	2.35	72	0.05	40	4.80	0.95
109.20	12413	0.40	-11.92	4891	74	9	922	18	19	0	31	24	491	1.53	0.10	0.05	1.40	73	0.05	39	5.10	1.15
124.15	8613	0.12																				
126.50	2283	0.79	18.66	3436	12	1	624	1	2	1	111	5	792	1.55	0.05	0.60	0.10	10	0.05	3	0.50	1.00
127.00	3493	0.76	26.38	3013	7	3	255	4	11	5	65	13	699	9.20	0.05	0.05	0.90	35	0.05	20	2.50	3.15
134.80	10316	0.44		4699	10	5	392	4	8	19	125	5	440	0.10	0.05	0.10	0.10	38	0.05	15	3.45	0.35
137.00	3537	0.66	16.28	6386	9	4	218	3	7	5	109	6	401	1.10	0.05	0.05	0.10	40	0.05	7	4.85	1.10
138.20	4254	0.72	0.41	19176	8	3	239	4	10	4	75	6	350	4.85	0.05	0.65	1.35	23	0.05	19	3.60	2.85
138.55	1318	0.79	18.66																			
138.90	1762	0.76		2977	3	1	252	0	0	1	148	2	856	1.65	0.05	1.00	0.10	6	0.05	5	0.40	1.55
139.25	2333	0.66	12.74	2636	3	1	245	1	1	2	0	0	1274	0.85	0.05	0.05	0.10	9	0.05	4	0.40	0.85
139.35	5172	0.71	9.20	7271	3	0	250	1	2	1	34	1	938	1.70	0.05	0.10	0.10	9	0.05	6	0.95	0.85
141.00	11477	0.31																				
141.25	9487	0.43	23.46	14256	16	5	379	6	12	9	36	0	432	0.85	0.05	0.20	0.10	33	0.05	10	4.10	0.50
141.75	8102	0.35	18.88	13956	18	3	627	3	6	5	8	0	427	2.50	0.05	0.10	0.75	18	0.05	7	2.55	0.45
141.85	6297	0.53	19.31	9776	17	3	703	3	5	3	38	0	411	2.15	0.05	0.15	0.10	14	0.05	7	1.85	0.45
142.95	4266	0.64	-21.77	5631	18	2	1010	3	4	4	22	0	410	3.15	0.05	0.25	0.25	14	0.05	4	1.50	1.00
144.30	10642	0.44		9186	40	4	424	9	12	19	105	0	459	2.35	0.05	2.50	2.10	35	0.05	14	4.40	0.85
144.90	10232	0.19																				
150.30	8127	0.46	-2.42	5024	40	4	615	9	11	19	112	0	451	2.68	0.05	2.58	1.85	33	0.05	13	3.88	1.13

Sample depth (m)	$DTMP_U$	$DTMP_{Th}$	$DTMP_{Pb}$	$DTMP_{Ni}$	$DTMP_{Cu}$	$DTMP_{As}$	$DTMP_{Mo}$	$DTMP_{Ba}$	$DTMP_{Co}$	$DTMP_{Mn}$	$DTMP_V$	$DTMP_{Mg}$
30.20												
32.50	0.09	0.03	0.78	0.91	0.96	1.00	0.94	0.29	0.87	0.02	0.03	0.02
32.90	0.19	0.18	0.81	0.90	0.93	0.99	0.93	0.57	0.63	0.14	0.09	0.02
33.00			0.49	0.87	0.92	0.94	0.97		0.33	0.02	0.03	0.01
45.00												
47.90												
57.90												
71.80	0.20	0.59	0.81	0.37	0.92	1.00	0.98		0.74	0.50	0.09	0.03
73.80												
79.35												
82.35	0.09	0.09	0.80	0.92	0.96	0.99	0.96	0.59	0.73	0.02	0.05	0.04
83.15	0.08	0.09	0.62	0.90	0.98	0.98	0.98	0.18	0.91	0.01	0.07	0.03
84.00			0.65	0.98	0.96	0.99	0.95	0.09	0.94	0.02	0.04	0.01
86.10	0.01	0.02	0.91	0.98	0.96	1.00	0.97	0.11	0.94	0.01	0.01	0.01
103.00	0.04	0.07	0.60	0.91	0.99	0.98	0.90	0.01	0.37	0.09	0.06	0.01
109.20			0.23	0.94	1.02	0.97	0.95	0.11	0.38	0.00	0.04	0.00
124.15												
126.50	0.13	0.13	0.97	0.83	0.98	1.00	0.74	0.79		0.03	0.15	0.06
127.00	0.01	0.09	0.78	0.83	0.81	0.98		0.05	0.40	0.13	0.07	0.15
134.80												
137.00	0.04	0.11	0.52	0.87	0.81	0.89	0.97	0.64	0.36	0.06	0.10	0.03
138.20	0.01	0.16	0.26	0.53	0.83	0.96	0.98		0.14	0.10	0.10	0.00
138.55	0.01		0.15	0.52	0.87	0.99	0.99		0.23	0.15	0.01	0.01
138.90			0.86		0.86	1.00	0.98			0.19	0.00	
139.25	0.17	0.65	0.93	0.95	0.93	1.00	0.96	0.92		0.11	0.21	0.04
139.35	0.04		0.88	0.94	0.94	1.00	0.97		0.73	0.02	0.07	0.01
141.00												
141.25	0.04	0.02	0.27	0.91	0.31	1.00	0.99	0.35	0.40	0.09	0.07	0.01
141.75	0.22	0.11	0.96	0.94	0.93	1.00	0.72	0.52	0.92	0.06	0.09	0.04
141.85	0.06	0.16	0.80	0.71	0.71	1.00	0.99	0.31	0.62	0.01	0.03	0.02
142.95			0.81	0.93	0.98	1.00	0.92	0.43	0.59	0.05	0.03	0.03
144.30	0.06		0.77	0.96	0.88	1.00	0.94	0.05	0.69	0.01	0.08	0.01
144.90												
150.30			0.62	0.96	0.84	1.00	0.96	0.01	0.41	0.00	0.03	

Sample depth (m)	Mg_{pyrite} (ppm)	V_{pyrite}	Mn_{pyrite}	Co_{pyrite}	Ni_{pyrite}	Cu_{pyrite}	Zn_{pyrite}	As_{pyrite}	Se_{pyrite}	Sr_{pyrite}	Mo_{pyrite}	Ag_{pyrite}	Cd_{pyrite}	Sb_{pyrite}	Ba_{pyrite}	Pb_{pyrite}	Th_{pyrite}	U_{pyrite}
30.20																		
32.50	164	1.0	7	70	303	246	89	1776	39	13	7	8	0.1	152	18	37	0.22	0.05
32.90	205	4.1	49	19	242	187	1037	714	43	141	9	9	5.6	167	53	67	1.04	0.11
33.00	97	1.5	6	6	159	276	54	162	26	1	65	9	0.5	60	0	21	0	0
45.00																		
47.90																		
57.90																		
71.80	186	1.4	246	8	19	78		17064	58	7	15	1.1	3.7	29		67	5.82	0.25
73.80																		
79.35																		
82.35	362	1.9	7	29	285	145	757	1365	0	84	11	10.0	8.8	253	97	67	0.57	0.07
83.15	252	2.4	3	37	187	282	15	783	30	35	13	13.9	0.1	287	15	48	0.43	0.06
84.00	82	1.4	7	159	845	342	0	771	6	2	29	6.7	0.3	71	7	29	0	0
86.10	87	0.2	3	181	781	267	703	4665	0	10	12	20.3	2.3	505	8	126	0.12	0.04
103.00	43	3.2	45	9	195	335	1296	1432	25	16	48	7.1	49.1	578	1	59	0.38	0.04
109.20	4	2.9	2	11	313	186	4	853	32	2	31	7.8	1.3	538	9	12	0	0
124.15																		
126.50	224	2.0	19	0	9	39	0	1964	38	26	4	0.4	0.1	121	38	79	0.07	0.15
127.00	541	0.5	36	2	54	19	9	715	37	5	0	0.2	0.7	20	2	70	0.24	0.03
134.80																		
137.00	199	1.0	15	2	48	20	5	50	57	16	35	0.4	0.1	5	69	7	0.59	0.04
138.20	93	0.9	25	1	12	21	0.1	133	54	1	235	3.2	0.3	10	0	6	0.67	0.04
138.55	63	0.1	38	1	9	15	2	171	73	3	462	0.3	0.7	4	0	3	0	0.02
138.90	0	0.0	59	0	0	8	181	1869	0	0	76	0	2.4	0	0	29	0	0
139.25	117	0.8	31	0	9	25	0	274	0	33	21	0.4	0.2	3	105	63	0.76	0.18
139.35	89	0.3	6	2	23	17	9	4117	19	11	58	0.02	0.4	6	0	41	0.00	0.03
141.00																		
141.25	104	1.2	36	4	115	4	10	7	26	17	57	0.1	0.1	0	18	4	0.09	0.02
141.75	579	1.9	43	34	97	69	0	135	0	32	6	0.7	0.03	7	20	165	0.33	0.13
141.85	218	0.6	4	4	12	8	0	55	9	3	154	0.1	0.1	3	7	26	0.34	0.03
142.95	195	0.6	57	4	53	178	0	128	0	6	34	1.2	0.4	19	10	17	0.00	0.00
144.30	74	3.3	4	20	306	140	0	516	14	27	40	5.0	2.2	334	2	48	0.00	0.05
144.90																		
150.30	0	1.2	1	6	273	128	0	790	0	4	67	10.8	2.5	315	1	26	0.00	0.00

Table 10. Results of the Steinbruch Schmidt section analysis.

Bank number	Sample depth (m)	Na_2O (%)	MgO (%)	Al_2O_3 (%)	SiO_2 (%)	P_2O_5 (%)	CaO (%)	K_2O (%)	TiO_2 (%)	MnO (%)	Fe_2O_3 (%)	V (ppm)	Cr (ppm)	Ni (ppm)	Co (ppm)	Zr (ppm)	Ba (ppm)	Cu (ppm)	Zn (ppm)	As (ppm)	Ag (ppm)	Pb (ppm)	Corg (%)	S (%)	Quartz (integ I)
72	0	0.05	0.59	3.10	13.45	0.07	43.8	0.76	0.16	0.07	0.71	14	40	6	2	45	49	8	13	2	2.1	<5	1.22	0.02	5067
110	0.4	0.10	0.50	2.14	9.00	0.04	47.4	0.51	0.11	0.07	0.99	16	33	8	6	26	34	31	17	13	<0.7	<5	0.99	0.01	3147
109	0.6	0.08	0.58	2.50	10.45	0.05	46.7	0.61	0.12	0.07	0.62	13	34	7	6	31	38	20	21	4	1.6	<5	0.92	0.01	3496
107	0.9	0.06	0.54	2.89	11.42	0.04	44.6	0.78	0.15	0.09	0.57	22	38	7	6	32	46	19	8	4	<0.7	6	1.23	0.01	4564
105	1.05	0.04	0.49	2.21	8.71	0.04	45.7	0.60	0.11	0.11	0.59	11	36	6	1	26	35	13	12	5	1.0	<5	1.14	0.00	2867
101	1.4	0.05	0.68	2.92	11.53	0.08	63.5	0.81	0.15	0.15	1.04	11	36	5	6	28	42	16	10	8	0.9	<5	1.25	0.00	2987
64	1.8	0.04	0.49	1.00	4.50	0.07	48.0	0.28	0.04	0.16	0.65	10	24	6	5	12	24	21	65	12	1.8	38	1.62	0.02	1437
62	2	0.04	0.51	0.72	4.26	0.06	49.6	0.14	0.03	0.21	0.30	7	28	5	1	8	<10	14	10	4	2.0	<5	1.42	0.03	1461
56	2.1	0.04	0.50	1.86	9.70	0.06	43.7	0.42	0.11	0.15	0.93	13	37	7	5	40	48	25	10	17	0.9	<5	1.06	0.11	3793
55	2.2	0.04	0.52	1.99	9.04	0.04	43.9	0.50	0.11	0.06	1.80	14	37	10	6	35	63	19	16	14	1.1	7	1.48	1.21	3781
53	2.4	0.04	0.45	2.01	8.93	0.04	45.3	0.48	0.12	0.04	0.71	11	34	7	5	36	47	60	12	9	2.1	<5	0.90	0.01	3492
45	3.2	0.05	0.57	1.84	8.66	0.05	47.4	0.41	0.11	0.03	0.45	9	36	6	6	37	36	20	15	3	<0.7	<5	1.12	0.02	3038
43	3.4	0.05	0.49	1.88	9.17	0.04	47.2	0.39	0.10	0.07	0.46	8	38	6	2	29	37	13	15	3	0.7	<5	0.93	0.02	3476
37	3.7	0.04	0.48	1.67	8.16	0.07	49.2	0.36	0.09	0.05	0.42	7	41	7	3	27	33	25	10	5	1.0	<5	3.78	0.01	2928
33	3.9	0.04	0.58	1.40	6.99	0.05	51.1	0.30	0.07	0.04	1.39	11	33	10	6	23	<10	32	31	13	<0.7	<5	1.14	0.02	2550
28B	4.2	0.05	0.50	1.18	6.22	0.25	51.5	0.25	0.05	0.07	0.60	13	31	6	6	14	22	24	7	7	1.4	<5	1.54	0.03	2399
26	4.4	0.05	0.55	1.31	5.56	0.05	48.2	0.34	0.05	0.05	0.72	15	36	7	8	18	13	48	16	8	0.9	<5	1.68	0.03	1831
24	4.6	0.03	0.43	0.67	4.63	0.05	50.9	0.16	0.03	0.06	0.44	16	26	7	4	11	<10	50	7	4	1.3	8	2.99	0.04	1586
23	4.7	0.10	1.09	10.88	31.13	0.18	9.0	3.22	0.52	0.19	4.57	313	77	85	56	151	279	235	40	19	4.2	22	1.47	0.39	15539
22	4.8	0.06	0.56	2.03	8.18	0.07	47.6	0.54	0.09	0.14	1.06	18	39	11	15	21	34	149	12	11	1.5	6	1.95	0.06	2738
19	5	0.05	0.50	2.25	11.01	0.04	46.8	0.53	0.14	0.11	0.56	13	42	7	9	49	44	18	16	7	<0.7	5	1.03	0.02	4984
14	5.2	0.06	0.42	2.33	11.39	0.05	44.2	0.56	0.15	0.09	2.18	13	42	13	9	48	51	33	20	20	<0.7	<5	0.95	0.02	5251
12B	5.3	0.07	0.47	2.09	9.62	0.04	47.0	0.50	0.12	0.10	0.52	13	37	8	10	39	37	19	12	7	<0.7	<5	1.08	0.01	4051
12	5.4	0.06	0.49	2.77	13.21	0.05	44.0	0.67	0.18	0.11	0.77	14	46	10	13	57	62	26	17	8	<0.7	<5	1.03	0.02	6445

Table 11. Results of the Coumiac (Stratotype) section analysis.

Bank number	Sample depth (m)	Na_2O (%)	MgO (%)	Al_2O_3 (%)	SiO_2 (%)	P_2O_5 (%)	CaO (%)	K_2O (%)	TiO_2 (%)	MnO (%)	Fe_2O_3 (%)	V (ppm)	Cr (ppm)	Ni (ppm)	Co (ppm)	Zr (ppm)	Ba (ppm)	Cu (ppm)	Zn (ppm)	As (ppm)	Ag (ppm)	Pb (ppm)	Corg (%)	S (%)	Quartz (integ I)
34AB	0	0.023	0.48	1.33	3.77	0.10	51.0	0.33	0.09	0.32	1.74	20	17	14	8	15	49	13	14	18	<0.7	<5	0.55	0.01	978
32G	1.2	0.015	0.18	1.40	3.79	0.15	52.2	0.34	0.08	0.24	0.58	19	21	10	14	15	84	176	24	33	<0.7	6	0.39	0.00	903
32B	2.25	0.007	0.54	0.57	1.18	0.05	54.1	0.14	0.04	0.16	0.36	16	13	7	9	9	<10	22	15	5	0.8	<5	0.48	0.01	363
32A	2.35	0.007	0.39	0.44	1.01	0.04	54.6	0.09	0.03	0.28	0.26	11	10	6	11	6	<10	26	20	7	1.3	<5	0.32	0.01	0
31G	2.45		0.46	0.11	0.53	0.04	54.6	0.03	0.02	0.13	0.47	23	6	16	19	4	<10	10	24	26	0.8	<5	1.01	0.03	0
31E1	2.8	0.013	0.50	0.79	2.50	0.11	52.0	0.19	0.06	0.22	1.97	13	14	11	6	12	22	23	33	7	<0.7	<5	0.20	0.01	857
30B	3.4	0.005	0.47	0.57	2.09	0.10	53.7	0.14	0.05	0.18	0.54	5	11	7	7	12	<10	11	17	5	0.8	<5	0.29	0.01	911
28AB	4.25	0.008	0.46	0.57	1.84	0.08	53.8	0.15	0.04	0.14	0.49	7	15	7	3	9	<10	11	19	20	<0.7	<5	0.49	0.01	786
26D	4.55	0.006	0.47	0.75	2.48	0.15	53.3	0.18	0.06	0.19	0.49	5	12	7	6	14	27	12	19	8	0.8	<5	0.38	0.01	813
25B	5.3	0.014	0.43	0.52	1.08	0.07	54.2	0.09	0.04	0.15	0.50	0	12	7	7	7	<10	11	20	5	<0.7	<5	0.28	0.01	0
24D	5.8	0.012	0.48	0.35	0.48	0.04	54.8	0.03	0.02	0.10	0.60	13	10	4	3	6	<10	406	57	3	1.5	6	0.29	0.01	0
24B	5.9	0.003	0.35	0.94	1.79	0.08	53.5	0.17	0.05	0.16	0.51	96	39	4	4	6	<10	20	21	12	<0.7	<5	0.01	0.01	0
24A	6	0.004	0.33	0.42	0.79	0.18	54.1	0.08	0.03	0.15	1.24	68	23	10	5	9	<10	20	18	42	<0.7	<5	0.42	0.02	0
20	7.7		0.40	0.62	2.61	0.06	53.1	0.16	0.05	0.20	1.21	6	17	10	4	13	<10	11	25	24	<0.7	<5	0.54	0.01	1131
18	9.4	0.008	0.43	0.66	2.96	0.06	53.0	0.18	0.05	0.35	0.74	8	10	10	9	10	84	32	15	115	<0.7	7	0.53	0.01	1164
16	10.6	0.008	0.56	0.84	3.21	0.07	52.5	0.24	0.07	0.39	0.54	12	17	19	13	15	71	19	20	130	<0.7	<5	0.56	0.06	1227
13	12.4	0.004	0.47	0.54	3.68	0.05	53.2	0.13	0.05	0.09	0.29	0	13	2	1	12	15	23	22	81	<0.7	9	0.56	0.01	1374
11	13.6	0.030	0.62	1.37	6.70	0.06	50.1	0.34	0.09	0.11	0.69	2	17	3	5	18	23	15	18	323	<0.7	10	0.64	0.01	2299
10	14.6	0.003	0.43	0.78	6.71	0.03	50.7	0.22	0.06	0.19	0.70	6	15	4	7	11	<10	17	19	394	<0.7	<5	0.54	0.03	2996

Table 12. Results of the La Serre trench C section analysis.

Bank number	Sample depth (m)	Na_2O (%)	MgO (%)	Al_2O_3 (%)	SiO_2 (%)	P_2O_5 (%)	CaO (%)	K_2O (%)	TiO_2 (%)	MnO (%)	Fe_2O_3 (%)	V (ppm)	Cr (ppm)	Ni (ppm)	Co (ppm)	Zr (ppm)	Ba (ppm)	Cu (ppm)	Zn (ppm)	As (ppm)	Ag (ppm)	Pb (ppm)	Corg (%)	S (%)	Quartz (integ I)
16B	0	0.02	1.75	1.52	4.52	0.04	48.0	0.33	0.10	0.04	0.51	111	28	39	5	26	121	55	97	<5	<0.7	<5	4.34	0.12	1281
15D	0.6	0.03	1.18	1.83	5.82	0.09	45.9	0.40	0.11	0.04	0.66	504	26	55	7	30	160	49	84	8	1.7	<5	5.74	0.25	1905
15B	1.9	0.02	1.03	0.62	2.07	0.07	50.9	0.21	0.05	0.04	0.32	175	17	26	6	15	27	21	33	<5	<0.7	<5	3.75	0.17	606
14H	2.8	0.02	1.26	0.96	3.05	0.14	49.0	0.35	0.07	0.05	0.37	282	30	40	6	17	117	46	82	5	<0.7	<5	4.44	0.23	633
14F2	3.1	0.01	0.90	0.49	1.84	0.33	51.0	0.22	0.04	0.04	0.37	59	18	14	3	9	341	22	21	3	0.7	<5	3.92	0.08	379
14F1	3.2		0.70	0.23	1.07	0.46	52.4	0.11	0.03	0.06	0.37	28	12	11	5	8	116	219	32	5	<0.7	6.1	2.98	0.21	279
14D	3.4	0.01	0.66	0.23	0.99	0.07	52.6	0.10	0.02	0.05	0.35	25	11	12	6	6	182	18	15	<5	<0.7	7.5	3.23	0.16	0
14B	3.9	0.01	0.77	0.57	2.31	0.06	50.9	0.22	0.05	0.13	0.59	65	14	22	10								3.18	0.13	700
13A	4.6	0.01	0.50	0.52	2.77	0.05	52.6	0.21	0.05	0.23	0.29	22	13	7	9	9	27	9	32	4	<0.7	<5	0.50	0.13	912
12B	4.9	0.01	0.41	0.52	2.79	0.06	53.0	0.20	0.04	0.17	0.27	26	5	6	3	9	148	14	68	<5	<0.7	6.8	0.24	0.03	928
12A	5.05	0.01	0.45	0.42	2.50	0.06	53.1	0.16	0.04	0.18	0.24	17	13	5	8	9	66	11	41	<5	0.9	<5	0.00	0.04	754
11	5.9	0.01	0.50	0.50	2.94	0.05	52.3	0.23	0.05	0.31	0.42	12	12	19	11	10	160	15	17	11	<0.7	8.1	0.46	0.12	1095
10	6.4	0.02	0.51	0.46	2.25	0.08	53.0	0.18	0.04	0.18	0.21	53	17	6	5	7	173	15	73	5	1.2	<5	0.77	0.03	832
9	7.5	0.01	0.35	0.06	1.24	0.03	54.0	0.02	0.02	0.08	0.10	8	10	2	4	3	95	<7	11	<5	<0.7	<5	0.69	0.03	718
8	7.8	0.02	0.47	0.19	2.43	0.05	52.9	0.09	0.02	0.05	0.22	28	8	4	4	7	324	157	28	5	<0.7	<5	1.56	0.04	1088

In der Reihe "Karlsruher Geochemische Hefte" (ISSN 0943-8599) sind erschienen:

Band 1: U. Kramar (1993)
Methoden zur Interpretation von Daten der geochemischen Bachsedimentprospektion am Beispiel der Sierra de San Carlos/ Tamaulipas Mexiko

Band 2: Z. Berner (1993)
S-Isotopengeochemie in der KTB - Vorbohrung und Beziehungen zu den Spuren-elementmustern der Pyrite

Band 3: J.-D. Eckhardt (1993)
Geochemische Untersuchungen an jungen Sedimenten von der Galapagos-Mikroplatte: Hydrothermale und stratigraphisch signifikante Signale

Band 4: B. Bergfeldt (1994)
Lösungs- und Austauschprozesse in der ungesättigten Bodenwasserzone und Auswirkungen auf das Grundwasser

Band 5: M. Hodel (1994)
Untersuchungen zur Festlegung und Mobilisierung der Elemente As, Cd, Ni und Pb an ausgewählten Festphasen unter besonderer Berücksichtigung des Einflusses von Huminstoffen.

Band 6: T. Bergfeldt (1995)
Untersuchungen der Arsen- und Schwermetallmobilität in Bergbauhalden und kontaminierten Böden im Gebiet des Mittleren Schwarzwaldes.

Band 7: M. Manz (1995)
Umweltbelastungen durch Arsen und Schwermetalle in Böden, Halden, Pflanzen und Schlacken ehemaliger Bergbaugebiete des Mittleren und Südlichen Schwarzwaldes.

Band 8: J. Ritter (1995)
Genese der Mineralisation Herrmanngang im Albtalgranit (SE-Schwarzwald) und Wechselwirkungen mit dem Nebengestein.

Band 9: J. Castro (1995)
Umweltauswirkungen des Bergbaus im semiariden Gebiet von Santa Maria de la Paz, Mexiko.

Band 10: T. Rüde (1996)
Beiträge zur Geochemie des Arsens.

Band 11: J. Schäfer (1998)
Einträge und Kontaminationspfade Kfz-emittierter Platin-Gruppen-Elemente (PGE) in verschiedenen Umweltkompartimenten.

Band 12: M. A. Leosson (1999)
A Contribution to the Sulphur Isotope Geochemistry of the Upper Continental Crust: The KTB Main Hole - A Case Study

Band 13: B. A. Kappes (2000)
Mobilisierbarkeit von Schwermetallen und Arsen durch saure Grubenabwässer in Bergbaualtlasten der Ag-Pb-Zn-Lagerstätte in Wiesloch

Band 14: H. Philipp (2000)
The behaviour of platinum-group elements in petrogenetic processes:
A case study from the seaward-dipping reflector sequence (SDRS), Southeast Greenland volcanic rifted margin

Band 15: E. Walpersdorf (2000)
Nähr- und Spurenelementdynamik im Sediment/Wasser-Kontaktbereich nach einer Seekreideaufspülung - Pilotstudie Arendsee -

Band 16: R. H. Kölbl (2000)
Models of hydrothermal plumes by submarine diffuse venting in a coastal area: A case study for Milos, South Aegean Volcanic Arc, Greece

Band 17: U. Heiser (2000)
Calcium-rich Rhodochrosite layers in Sediments of the Gotland Deep, Baltic Sea, as Indicators for Seawater Inflow

In der Fortsetzungsreihe "Karlsruher Mineralogische und Geochemische Hefte" (ISSN 1618-2677) sind bisher erschienen:

Band 18: S. Norra (2001)
Umweltgeochemische Signale urbaner Systeme am Beispiel von Böden, Pflanzen, und Stäuben in Karlsruhe

Band 19: M. von Wagner, Alexander Salichow, Doris Stüben (2001)
Geochemische Reinigung kleiner Fließgewässer mit Mangankiesen, einem Abfallsprodukt aus Wasserwerken (GReiFMan)

Band 20: U. Berg (2002)
Die Kalzitapplikation als Restaurierungsmaßnahme für eutrophe Seen – ihre Optimierung und Bewertung

Band 21: Ch. Menzel (2002)
Bestimmung und Verteilung aquatischer PGE-Spezies in urbanen Systemen

Band 22: P. Graf (2002)
Meta-Kaolinit als latent-hydraulische Komponente in Kalkmörtel

Band 23: D. Buqezi-Ahmeti (2003)
Die Fluidgehalte der Mantel-Xenolithe des Alkaligesteins-Komplexes der Persani-Berge, Ostkarpaten, Rumänien: Untersuchungen an Fluid-Einschlüssen

Band 24: B. Scheibner (2003)
Das geochemische Verhalten der Platingruppenelemente bei der Entstehung und Differenzierung der Magmen der Kerguelen-Flutbasaltprovinz (Indischer Ozean)

Ab Band 25 erscheinen die Karlsruher Mineralogischen und Geochemischen Hefte im Karlsruher Universitätsverlag online unter der Internetadresse

http://www.uvka.de/univerlag/institut.php?fakultaet=1

Auf Wunsch sind beim Karlsruher Universitätsverlag gedruckte Exemplare erhältlich („print on demand“).

Band 25: A. Stögbauer (2005)
Schwefelisotopenfraktionierung in abwasserbelasteten Sedimenten - Biogeochemische Umsetzungen und deren Auswirkung auf den Schwermetallhaushalt

Band 26: X. Xie (2005)
Assessment of an ultramicroelectrode array (UMEA) sensor for the determination of trace concentrations of heavy metals in water

Band 27: F. Friedrich (2005)
Spectroscopic investigations of delaminated and intercalated phyllosilicates

Band 28: L. Niemann (2005)
Die Reaktionskinetik des Gipsabbindens: Makroskopische Reaktionsraten und Mechanismen in molekularem Maßstab

Band 29: F. Wagner (2005)
Prozessverständnis einer Naturkatastrophe: eine geo- und hydrochemische Untersuchung der regionalen Arsen-Anreicherung im Grundwasser West-Bengalens (Indien)

Band 30: F. Pujol (2005)
Chemostratigraphy of some key European Frasnian-Famennian boundary sections (Germany, Poland, France)